"Growth folds above propagating normal faults"

Coleman, A.J., Duffy, O.B. and Jackson, C. A.-L.

All data presented in this preprint can be found here:
https://figshare.com/s/c6663901f6ca8c6f6fe4

Growth folds above propagating normal faults

Alexander J. Coleman[1]*, Oliver B. Duffy[2] and Christopher A.-L. Jackson[1]

[1]*Basins Research Group (BRG), Department of Earth Science and Engineering, Imperial College, Prince Consort Road, London SW7 2BP, UK*

[2]*Bureau of Economic Geology, The University of Texas at Austin, University Station, Box X, Austin, Texas 78713-7508, USA*

*Corresponding author's e-mail: a.coleman14@imperial.ac.uk

Keywords

Fault-propagation fold, forced fold, normal fault, fault-related fold, rifting, extension, salt-influenced rift

Abstract

Growth folds developed above the upper tips of propagating normal faults are ubiquitous in extensional settings, especially during the early phases of extension and in salt-rich basins. As growth folds develop as slip accumulates on the underlying normal fault, the geometry and size of the fold changes, reflecting the dip, throw and displacement rate of the underlying normal fault and the thickness and rheology of the overlying cover. This has a marked impact on basin physiography and thus, the architecture and distribution of synkinematic strata but also the geometry and density of secondary deformation. This study analyses a large dataset of fault-propagation and forced folds in nature and models to: (i) characterise their diagnostic features; (ii) investigate the controls on their geometry, size and differences; and (iii) describe how they grow with increasing extensional strain. The examined dataset demonstrates that larger growth folds are associated with larger fault throws, thicker and weaker cover, whereas small throws, thin and strong brittle cover generates smaller folds. We show that the geometry and size of growth folds vary through time; the width of the fold is established relatively early during fold growth, whereas the fold amplitude increases gradually and incrementally with fault throw. The fold width and amplitude become increasingly similar during fold evolution, until they are breached by the underlying normal fault. We also derive a number of parametric equations that are potentially powerful tools in estimating unknown fold geometry and size in profile by utilising other known structural and stratigraphic parameters for both salt-free and salt-rich settings. As forced folds are typically found in salt-rich basins, forced fold geometry is often affected by across- and along-strike salt flow, so that these folds have typically larger fold amplitudes and widths compared to fault-propagation folds for the same fault throw. In addition, we discuss how fault growth models (i.e. constant-length vs. isolated) may impact the three-dimensional evolution of growth folds. This work also highlights that growth folds are likely more common than they have previously been credited for. Although weak and ductile cover strata and low strain rates promote growth folding, the dataset illustrates that growth folds may occur in brittle, strong cover and in regions with high strain rates. However, the underlying controls on fold occurrence remain tentative. This review has implications for hydrocarbon trapping and reservoir distribution, structural restoration and estimating strain in salt-rich and salt-free extensional settings.

1. Introduction

Fault-related folds are ubiquitous in extensional settings (Fig. 1; Appendix A) and strongly control basin physiography through time. One of the most common fault-related folds, particularly during the early phases of extension are 'growth folds' (Fig. 2) (e.g. Gawthorpe and Leeder, 2000; Jackson and Lewis, 2016). Growth folds develop above the vertical tips of upward-propagating normal faults and may be classified as either: 'fault-propagation folds' or 'forced folds'. Where deformation is predominantly faulted at depth but gradually transitions upwards into a distributed zone of folding, we use the term 'fault-propagation folding' (Fig. 2A; after Withjack et al., 2002; cf. Withjack et al., 1990; Gawthorpe et al., 1997) . Where the deformation at depth is faulted but transitions abruptly to folding at shallow levels, we use the term 'forced folding' (Fig. 2B; sensu Stearns, 1978; cf. Withjack and Callaway, 2000; Withjack et al., 2002).

Fault-propagation and forced folds grow as slip accumulates on the underlying fault at depth, with concomitant changes in the geometry and size of the folds. This has a marked impact on the architecture and distribution of synkinematic sediments (e.g. Gawthorpe et al., 1997; Lewis et al., 2015), as well as the styles of secondary deformation as strain is accommodated within the fold (e.g. Ameen, 1988; Ameen, 1990; Cosgrove and Ameen, 1999; Sharp et al., 2000a; Jackson et al., 2006; Tavani et al., 2018). Furthermore, the geometry and evolution of growth folds has implications for how and where hydrocarbons are trapped (e.g. Mitra, 1990), where synkinematic strata may be deposited during sea level changes (e.g. Lewis et al., 2015), for fluid flow in normal fault zones (e.g. Wibberley et al., 2008; Tavani et al., 2018), determining strain in sedimentary and volcanic basins (e.g. Morley, 1996; Coleman et al., 2017) (e.g. Morley, 1996; Coleman et al., 2017), and for interpreting fault length for earthquake hazard evaluation (e.g. Allmendinger and Shaw, 2000; Blakeslee and Kattenhorn, 2013).

Despite the importance of growth folds, the relationship between the geometry and size of a fold as it evolves remains poorly-understood. Whilst physical and numerical models have shed light on these relationships (e.g. Withjack et al., 1990; Hardy and McClay, 1999; Finch et al., 2004), documenting a parametric relationship between structural- (e.g. fault throw, fault dip, etc.) and stratigraphic (e.g. cover thickness, rheology, etc.) -related factors, they are rarely quantitatively compared to natural examples. Furthermore, several questions regarding growth folds remain unanswered: how does the geometry and size of growth folds change with ongoing fault slip? Do fault-propagation and forced folds grow differently, and if so, why? And what controls the occurrence of growth folds?

To understand and answer these questions, this study firstly reviews the wealth of recent literature that has advanced our understanding of these folds, including two key aspects: how growth folds affect synkinematic strata, and how strain is accommodated within growth folds. We then quantitatively analyse a large dataset of c. 420 natural examples from > 150 sedimentary and volcanic basins, and c. 250 physical and c. 180 numerical models to investigate: (i) the controls on the geometry and size of growth folds, (ii) the differences between fault-propagation and forced folds, and (iii) their occurrence in extensional settings. To the best of our knowledge, this is the largest known global compilation of growth fold parameter measurements. We then place these examples into a dynamic context to investigate how fault-propagation and forced folds grow with increasing slip in two- and three-dimensions. In addition, we construct a data-driven interpretation method to aid the identification of growth folds, so that they are not confused with other fault-related folds e.g. frictional drag, inversion and drape folds (Fig. 1). We also derive a number of parametric equations that are potentially powerful tools in estimating unknown fold parameters by utilising other known structural and stratigraphic parameters. Finally, we discuss the implications of our results for hydrocarbon systems and structural restorations in sedimentary and volcanic basins.

2. How is the development of growth folds preserved in the stratigraphic record?

Growth folds developed above the tips of upward-propagating normal faults have a marked impact on the geomorphic development of extensional basins, and thus, the architecture and distribution of synkinematic strata (e.g. Jackson and Leeder, 1994; Maurin and Niviere, 1999; Corfield and Sharp, 2000; Sharp et al., 2000b; Corfield et al., 2001; Ford et al., 2007; Lewis et al., 2015). Synkinematic strata therefore provide important information on the geometry and growth of these folds, such as the amplitude and width through time (cf. Gawthorpe et al., 1997; Corfield et al., 2001; Patton, 2004; Lewis et al., 2015).

As fault-propagation and forced folds grow above the tips of blind normal faults, strata typically thin towards the fold crest and thicken basinwards (Gawthorpe et al., 1997; Gawthorpe and Hardy, 2002; Patton, 2004; Lewis et al., 2015; Fig. 3A). Pronounced unconformities develop towards the fold, whereas off-structure, these same unconformities pass basinward into conformable sections (Sharp et al., 2000b; Patton, 2004). The geometry and occurrence of these unconformities are principally controlled by the interplay of eustasy (sea level) and the structural relief related to growth folding. These in turn, affect the architecture and distribution of synkinematic sediments (Burbank et al., 1996; Gupta et al., 1999; Corfield et al., 2001; Lewis et al., 2015).

During sea level rise, if the rate of fold amplification is less than the rate of rising sea level, a synkinematic growth wedge will cover both limbs of the fold. When the rate of fold amplification is greater than the sea level rise rate, the upthrown fold limb may be sub-aerially exposed, and strata will onlap onto the dipping fold limb. This forms an off-structure wedge (Gawthorpe et al., 1997; Gupta et al., 1999; Lewis et al., 2015).

During sea level fall, if the subsidence related to growth folding is slower than the rate of falling sea level, no synkinematic deposition takes place. Where the growth fold is sub-aerially exposed, the folded prekinematic strata may be eroded (Gawthorpe et al., 1997; Patton, 2004; Lewis et al., 2015). If synkinematic strata do not cover the entirety of the fold and/or erosion takes place, information about the fold geometry (and its growth) are not preserved in the rock record. This partially explains why the growth folds and the structural style of early rifts, particularly in continental settings, is poorly constrained (cf. Gawthorpe and Leeder, 2000).

Sea level changes during growth folding not only affect the architecture of synkinematic units but also, control whether the synkinematic units are mud- or sand-dominated. Lewis et al. (2015) speculated two end-member scenarios: (i) growth folding during sea level rise (Fig. 4A), and (ii) growth folding during sea level fall (Fig. 4B). In the first scenario (Fig. 4A), fold growth is restricted to periods of sea level rise so that wedge-shaped mudstone-dominated strata onlap and thin onto the fold. Sand-dominated strata are deposited immediately after fold amplification, are tabular and have a sharp contact with underlying mudstone-dominated unit (Lewis et al., 2015). In the second scenario, (Fig. 4B), fold growth is restricted to periods of sea level fall, so that wedge-shaped sand-dominated synkinematic strata onlap and thin onto the fold. Mudstone-dominated strata are deposited immediately following fold growth, are isopachous and have a sharp contact with the underlying sandstone-dominated units (Lewis et al., 2015).

Growth folds developed in basins with rheological heterogeneities, such as thick salt, may have significantly different geometries and evolve differently from those that form in largely homogeneous and brittle strata. During early extension, salt may inhibit the propagation of sub-salt, basement-involved faults, mechanically decoupling them from, but being kinematically responsible for, forced folds in the supra-salt strata (e.g. Withjack and Callaway, 2000; Ford et al., 2007; Lewis et al., 2013; Ge et al., 2016; Jackson and Lewis, 2016; Coleman et al., 2017). The size and geometry of these supra-salt forced folds is dependent, at least in part, on the throw of the sub-salt fault along-strike. Fold size is largest towards the fault centre where sub-salt throw is greatest and smallest at the fault tips (Fig. 1A in Corfield and Sharp, 2000; cf. Fig. 11 in Sharp et al., 2000b).

As the forced fold grows with increasing sub-salt throw, salt flows along-strike below the supra-salt strata towards the location of maximum throw (Richardson et al., 2005). Supra-salt synkinematic depocentres are created in the hangingwall of the sub-salt faults, but because of the forced folding and salt swell, they are offset from and thin towards the fault trace (Fig. 5A). As the sub-salt faults grow and their tips propagate laterally (cf. Jackson et al., 2017), not only does the along-strike extent of forced folding lengthen but the sub-salt faults may interact with neighbouring sub-salt faults (Fig. 5B). The linkage of the sub-salt faults may lead to changes in the position of the throw maxima along-strike stimulating further salt flow towards the new throw maximum. This draws more salt into the space beneath the supra-salt strata, forming a larger salt swell (Richardson et al., 2005). Synkinematic depocentres associated with each of the forced folds and their associated fault segments will subsequently merge to create a single, large depocentre (Fig. 5C). The newly formed, synkinematic sediments within the large depocentre will then thin over the crest of the forced fold and salt swell (Richardson et al., 2005; cf. Fig. 3A). Additional across-strike salt flow may further complicate stacking patterns within synkinematic strata (cf. Duffy et al., 2013; Warsitzka et al., 2015) and may even mask changes in sea level and accommodation, independent of regional extension (Duffy et al., 2013).

During the latter stages of regional extension, in either salt-rich or salt-free settings, growth folds may be breached as the upward propagating fault tip breaks-surface. At this point, a hangingwall depocentre may form next to the fault and strata may thicken into it (e.g. Gawthorpe et al., 1997; Corfield and Sharp, 2000; Sharp et al., 2000a; Kane et al., 2010; Duffy et al., 2013; Fig. 3B). Fold breaching may not occur along the full length of the fault contemporaneously, and instead, unbreached folds of different sizes and geometries may be located along-strike from breached folds (Fig. 3) (e.g. Gawthorpe et al., 1997; Gupta et al., 1999; Corfield and Sharp, 2000; Sharp et al., 2000b; Corfield et al., 2001; Khalil and McClay, 2002; Willsey et al., 2002; White and Crider, 2006; Lewis et al., 2013; Lewis et al., 2015; Khalil and McClay, 2016). Furthermore, the architecture and distribution of synkinematic strata may vary significantly along-strike within the same extensional basin (Gawthorpe et al., 1997; Corfield and Sharp, 2000; Richardson et al., 2005; Lewis et al., 2015).

3. How is strain accommodated within growth folds?

The distribution of strain in extensional basins controls where faults and folds develop and thus, the location of synkinematic depocentres and secondary deformation. Growth folds, particularly during early extension, accommodate a significant proportion of extensional strain, and as these folds grow, there will be associated changes in the style and distribution of fracture and fault populations (Fig. 6) (e.g. Sharp et al., 2000a; Tavani et al., 2018).

Initially, as a growth fold forms above a propagating normal fault (herein termed ‘master fault’), secondary normal and reverse faults form in the cover (e.g. Fig. 7 in Koopman et al., 1987; Fig. 13 in Harvey and Stewart, 1998; Fig. 7 in Withjack and Callaway, 2000; Fig. 13 in Jackson et al., 2006; Fig. 11A in Tavani et al., 2018). These secondary faults may nucleate at the uppermost tip of the master fault and propagate upwards (e.g. Withjack et al., 1990; Mitra, 1993; Paul and Mitra, 2015), or nucleate in the folded cover and propagate downwards (Parfitt and Peacock, 2001; Peacock and Parfitt, 2002; Martel and Langley, 2006; White and Crider, 2006) forming sigmoidal geometries with normal offsets at their base, and reverse offsets at their top (Sharp et al., 2000a; Sharp et al., 2000b; Jackson et al., 2006; Paul and Mitra, 2015; Fig. 6D).

As the fold amplifies, secondary faults are rotated, translated and become inactive as the dipping fold limb steepens. To accommodate further strain within the fold, new secondary faults form (e.g. Horsfield, 1977; Mitra and Islam, 1994; Patton et al., 1998; Berg and Skar, 2005; Jackson et al., 2006; Tavani and Granado, 2014; Paul and Mitra, 2015; Tavani et al., 2018) which often offset earlier fault generations until they too become inactive and become offset, either by latter faults or the propagating master fault (e.g. Matthews III and Work, 1978; Palmquist, 1978; Patton et al., 1998; Sharp et al., 2000a; Berg and Skar, 2005; Fodor et al., 2005; Egholm et al., 2007).

The location of, density of and net slip on the secondary faults through time is directly related to the along-strike curvature of the growth fold and the underlying master fault. The greater the along-strike curvature, the denser the population of secondary faults in the immediate hangingwall (Sharp et al., 2000a). The width of this secondary fault zone, normal to the fold hinge, is dependent on the geometry of the growth fold and thus, the slip and dip of the underlying master fault; gently-dipping faults produce broader folds and wider zones of fracturing compared to steeply-dipping faults (Horsfield, 1977; Withjack et al., 1990; Willsey et al., 2002; Paul and Mitra, 2015). In addition to secondary faulting, boudinage, sigmoidal veins and foliation textures may develop to accommodate flexural slip along bedding planes (Fig. 11 in Gross et al., 1997; Fig. 10 in Lynch et al., 1998; Sharp et al., 2000b; Fig. 6A). Where flexural slip cannot take place, fracturing and faulting increases (cf. Couples and Lewis, 1999; Fig. 6B - C).

During the latter stages of fold growth, the dipping fold limb may become very steep and gravity-induced thin-skinned faults may develop (cf. Stewart et al., 1997; Stewart, 1999; Stewart and Argent, 2000). Where detachments are present, such as salt or shale, these thin-skinned faults may either detach (e.g. Fig. 3 in Withjack et al., 1989; Morley and Guerin, 1996; Sharp et al., 2000b; Withjack and Callaway, 2000; Fig. 9B in Jackson et al., 2006) or become layer-bound (e.g. Fig. 4 in Gross et al., 1997; cf. Couples et al., 1998; Fig. 10 in Lynch et al., 1998; cf. Couples and Lewis, 1999; Fig. 9 in Keller and Lynch, 1999; cf. Soliva et al., 2005; Fig. 9C in Jackson et al., 2006; Fig. 9B in Tavani et al., 2018). As larger amounts of strain are localised onto the detachment surfaces, the ductile units may become stretched and thin (cf. 'tectonic thinning' after Brown, 1988). If the detachment on the footwall thins sufficiently, secondary normal faults in the cover above the detachment may link with the master fault at depth (Fig. 6C – D). Furthermore, the growth fold may become breached (Koyi et al., 1993;

Koyi et al., 1995; Stewart et al., 1996; Pascoe et al., 1999; Withjack and Callaway, 2000; Dooley et al., 2003).

4. What are the controls on the geometry and size of growth folds?

The geometry, size and occurrence of growth folds above propagating normal faults is widely understood to be controlled by the interplay of structural factors (related to fault character) and stratigraphic factors (related to the rheology and thickness of the cover) (Fig. 7). Critically however, the relative importance of each of these structural and stratigraphic factors upon the geometry and size of a growth fold is not well-constrained. This is largely because: (i) we only observe the *final* geometry of growth folds in nature; (ii) there are few natural examples of growth folds in nature with high-resolution growth strata that permit the geometric evolution of the fold to be constrained; (iii) a large number of different factors control fold geometry through time; and (iv) it is difficult to quantify some of these factors e.g. the strata may not be preserved, or the parameters themselves may change through time. Examples of changing parameters through time include but are not limited to, the detachment thickness and the proportion of rheologically strong vs. weak strata.

Structural factors are associated with the kinematic and geometric evolution of the underlying fault, including the dip, throw, and shape of the fault, and the fault tip propagation and displacement rate. Stratigraphic factors are associated with the mechanical behaviour, thickness and rheology of the strata, including the confining pressure (depth of burial), differential compaction, and rheological heterogeneity. The effect of each controlling factor on the fold size and fold-shape-factor (the ratio of fold amplitude-to-width; FSF) is summarised in Fig. 7. When the fold-shape-factor is greater than 1 (FSF > 1), the fold width is larger than its amplitude. Where the fold-shape-factor is equal to 1 (FSF ~ 1), the fold width and amplitude are the same.

Where the fold-shape-factor is less than 1 (FSF < 1), the fold width is smaller than the fold amplitude.

In this section, we review how each structural and stratigraphic factor influences the two-dimensional (2D) fold geometry and size as the throw on the underlying fault increases.

4.1. Influence of structural factors on the geometry and size of growth folds

Prior studies have shown that structural factors strongly control the 2D geometry and size of growing folds. Here, we summarise how the dip, throw and displacement rate of the fault, affects fold geometry and size (Fig. 7A – C).

As a fault propagates towards the surface, fault dip plays an increasingly important role in fold geometry (e.g. Horsfield, 1977; Tsuneishi, 1978; Vendeville, 1987; Richard, 1989; Withjack et al., 1990; Koyi et al., 1993; Howard and John, 1997). Gently-dipping faults form wide folds (high FSFs) with gently-dipping fold limbs, while steeply-dipping faults form narrow folds (low FSFs) with steeply-dipping fold limbs (Fig. 7A). As there is a larger amount of rock material in front of the propagating fault tip for gently-dipping faults compared to steeply-dipping faults, all else being equal, a steeply-dipping fault will be break-surface earlier than a gently-dipping fault (Fig. 8). Where the fault dip changes with depth, complex growth fold geometries may develop. For example, where there are ramp flats, forced folds may form at multiple stratigraphic levels (Stewart et al., 1997; Lewis et al., 2013; Gabrielsen et al., 2016; Vasquez et al., 2018).

Fault throw, in contrast to fault dip, controls not only the fold geometry but also its size. As throw increases, so does the fold amplitude and width and thus, the FSF changes (e.g. Fig. 4 in Horsfield, 1977; Fig. 5 in Ameen, 1988; Fig. 4 in Withjack et al., 1990). Large throws are associated with large folds with low FSFs, while small throws are associated with small folds with high FSFs (e.g. Horsfield, 1977; Patton et al., 1998; Fig. 7B). If the throw becomes too large, eventually the fold will be unable to accommodate any further strain, and the fold will become breached as the fault breaks-surface (e.g. Fig. 7 in Withjack and Callaway, 2000; cf. Fig. 3B). Once breached, folding ceases.

Similar to fault throw, the displacement rate of the fault, which is intimately linked to the propagation rate of the upper fault tip not only has the potential to control the shape, size and even the occurrence potential for a fold (e.g. Allmendinger, 1998; Withjack and Callaway, 2000; Cardozo et al., 2003; Finch et al., 2004; Jin and Groshong, 2006; Ford et al., 2007; Hardy and Allmendinger, 2011; Carola et al., 2013; Tavani and Granado, 2014; Deckers, 2015; Wilson et al., 2015). Slowly-propagating faults form wide folds with high FSFs as they take a longer to breach the cover, hence more folding occurs (e.g. Fig. 11A in Withjack and Callaway, 2000; low propagation rates are required in the Rhine Graben to form forced folds - Ford et al., 2007). Rapidly-propagating faults in contrast, form narrow folds with low FSFs and in some cases, may propagate so quickly through their cover that folds do not develop (Fig. 7C) (e.g. Fig. 10 vs. 11 in Withjack and Callaway, 2000).

Applying this logic, growth folds are more likely to occur in basins where the upper tip propagation rate of individual faults is slow and rare in basins with rapidly-propagating faults. For example, we may hypothesise that rapidly-extending basins (cf. Nicol et al., 1997; Meyer et al., 2002; Mueller, 2017) will express rapid fault-propagation rates, therefore restricting the development of growth folds. Meanwhile, slowly-extending basins may be prone to slower tip propagation rates and thus, more growth folding. Alternatively, mechanical barriers to fault propagation, such as shale or salt (e.g. Morley and Guerin, 1996; Maurin and Niviere, 1999; Duffy et al., 2013; Jackson and Lewis, 2016; Coleman et al., 2017), may produce slowly-propagating faults. However, this hypothesis remains untested.

We may also expect the prevalence of growth folds will vary temporally and spatially within an extensional fault array. For example, during rift initiation, where regional strain is distributed over a large number of isolated faults, each with relatively low fault-propagation rates, growth folds may be common across the rift. Whereas during rift climax, where regional strain is localised onto a few, well-connected large faults but also towards the rift axis (Cowie, 1998; Gupta et al., 1998; Cowie et al., 2000; Gawthorpe and Leeder, 2000; Cowie et al., 2005), growth folds may be expected to develop in the strain shadows of larger faults or abandoned faults away from the strain locus, perhaps towards the rift margins. Although this too, remains poorly constrained.

4.2. Influence of stratigraphic factors on the geometry and size of growth folds

Stratigraphic factors also exert significant controls on the geometry and size of growth folds. Here, we summarise the influence of the rheology and thickness of the cover, the detachment thickness and the confining pressure (depth of burial) on fold growth with increasing slip on the underlying fault (Fig. 7D – G).

As a fault tip propagates upwards, it may encounter ductile as well as brittle lithologies in its cover. These rheological variations in the cover have a profound impact upon the growth folding at the upper tip. Cover comprising ductile rocks such as salt of overpressured shale typically produce wider folds (high FSFs) than those in brittle sequences (low FSFs) (Withjack et al., 1990; Withjack and Callaway, 2000; Finch et al., 2004; Fig. 7D). As rheologically-weak strata tend to inhibit the upward propagation of a fault (e.g. Nicol et al., 1996; Couples and Lewis, 1999; Corfield and Sharp, 2000; Wilkins and Gross, 2002; Benedicto et al., 2003; Soliva and Benedicto, 2005; Soliva et al., 2005; Lăpădat et al., 2016), folding is likely to last longer in ductile strata and may not be breached as rapidly as in brittle-cover scenarios. Thus growth folds in rheologically-weak cover may be large and well-developed, whereas growth folds developed in homogeneous, rheologically-strong cover sequences (e.g. in volcanic basins) are likely to be rare and poorly-developed. Given that rheological variations in the cover can control the geometry and size of growth folds, it follows that cover with rheological heterogeneities such as multiple salt or shale layers, may be expected to produce broader folds (high FSFs) as the fault tip becomes temporarily arrested by each of the mechanical barriers. However, these hypotheses remain untested.

In addition to the rheology, the thickness of the cover also has been shown to control fold geometry and shape (Fig. 7E). Where the cover is thin, lesser degrees of folding are expected as the propagating fault takes a shorter time to breach the fold compared to when the cover is thick (e.g. Allmendinger, 1998). Furthermore, physical (Withjack and Callaway, 2000) and numerical models show thin cover typically produces narrow, poorly-developed folds (i.e. low FSFs) whereas thick cover is associated with wide, well-developed folds (i.e. high FSFs). Although these findings are commonly shown in models, it is yet to be found if these concepts hold in natural systems.

Detachment thickness also affects fold geometry and size (Fig. 7F). Cover with very thin detachments do not significantly inhibit fault tip propagation, thus growth folds developed in such systems tend to be narrow, poorly-developed and with low FSFs. In contrast, thick detachments generate wide, well-developed folds with high FSFs, as detachments buffer against underlying fault displacement and tip propagation (Richard, 1991; Vendeville et al., 1995; Withjack and Callaway, 2000; Stewart, 2007; Deckers, 2015; Lăpădat et al., 2016; Hardy, 2018). This prediction, largely derived from physical models (except Hardy, 2018), has never been tested in nature.

The final stratigraphic factor that influences fold geometry is confining pressure (Fig. 7G) (e.g. Friedman et al., 1976; Weinberg, 1979; Bartlett et al., 1981; Koyi et al., 1993; Patton et al., 1998; Schöpfer et al., 2007). As a growth fold is buried and the confining pressure increases, the rocks within the cover progressively compact and the rheology changes. Patton et al. (1998), in their Fig. 7, showed that the same cover lithology under different confining pressures can lead to significant changes in the fold width. Shallowly-buried folds at low confining pressures are typically narrower (low FSFs) than deeply buried folds at high confining pressures (high FSFs). This occurs as the bulk ductility of the cover and zone of microfracturing increases with higher confining pressures (Patton et al., 1998). Given that the hangingwall and footwall fault blocks lie at different depths with different confining pressures, the rheology of the cover may be different across the fault. For example, across-fault differential compaction may alter the bedding dips in the fold. In the shallowly-buried footwall where compaction is less, the dips are genter, whereas in the deeply-buried hangingwall, compaction is greatest and the dips are steeper (Jin et al., 2009). Furthermore, differential compaction and burial depth will also influence fold shape (e.g. Skuce, 1996; Færseth and Lien, 2002).

4.3. Unanswered questions

Having reviewed how each of the structural and stratigraphic factors affects growth fold geometry, a number of unanswered questions remain: (i) how do growth folds evolve with increasing fault throw?; (ii) what are the differences, if any, between the growth of fault-propagation and forced folds?; (iii) what controls the occurrence of growth folds?; and (iv) which factors exert the greatest control on growth fold geometry and size? To answer these questions, we analysed published examples of growth folds in nature and models to quantify relationships between parameters of the fault, fold and cover to investigate and subsequently predict how, where and why growth folds evolve. These predictions allow us to infer the geometric and kinematic characteristics of growth folds in areas lacking high-resolution growth strata or poor exposure/seismic imaging.

5. Fold, fault and cover parameters

Several geometrical parameters (as defined in Fig. 2), have been measured from published-cross-sections. In cross-section, the amplitude and width are determined by the vertical and horizontal distances between the ‘toe’ and ‘head’ of the fold, respectively. The toe is defined as the point at which a marker bed meets the regional datum on the hangingwall of a normal fault. The head is defined as the point where a marker bed drops below the regional datum on the footwall of a normal fault. As previously mentioned, the fold-shape-factor (FSF) is the ratio of the amplitude-to-width and is used to quantitatively compare fault-propagation and forced folds, irrespective of their scale. High values of FSF indicate the fold is far wider than it is tall, whereas low values of FSF indicate the fold has a larger amplitude than its width. The prekinematic thickness is the stratigraphic thickness of the largely tabular, isopachous strata deposited prior to extension. For forced folds, the detachment thickness is the vertical thickness of the detachment layer which separates folded strata above and faulted strata below. Where applicable, the cover-detachment (C:D) ratio is used to quantitatively compare forced folds, irrespective of their scale. High C:D ratios indicate the prekinematic cover is thicker than the detachment thickness, whereas low C:D ratios indicate that the detachment thickness is thicker than the prekinematic cover thickness. Fault dip is measured from the underlying master fault. Fault throw is the vertical change in elevation of a prekinematic marker bed across a fault; for forced folds, throw is measured immediately below the detachment.

6. How are the geometries and sizes of growth folds affected by structural and stratigraphic parameters?

Quantitative comparative analysis of parameters measured from published cross-sections oriented perpendicular to the underlying master fault was carried out for c. 600 fault-propagation folds (Fig. 9; Appendix B) and c. 300 forced folds (Fig. 10; Appendix C). The resulting global dataset characterises fault-propagation and forced folds from extensional settings (see Appendices D – E for all measured data). Without growth strata, the kinematic evolution of these growth folds is difficult to constrain. However, by compiling this database of fault-propagation and forced folds of different sizes and shapes, and at different stages of development (Table 1), we can assess the dynamics of these folds and predict the parameters and geometry for folds that are poorly-imaged in seismic reflection data or less well-preserved in the field.

For each fold, the geometrical parameters described in Fig. 2 were recorded. Measurements of the geometrical parameters in models and natural examples all have uncertainties, however, only high confidence examples have been used for the statistical analysis and the associated uncertainties have been noted (see Appendix F for the full details).

6.1. Regression analysis

To understand the genesis and development of growth folds, a quantitative study has been undertaken based on published literature. This extensive data compilation features >150 different localities and >800 examples, each with its own unique tectonic parameters (e.g. strain rate, lithology, tectonic setting) allowing us to compare geometrical characteristics in volcanic and sedimentary extensional systems and isolate the primary controls on the geometric and kinematic evolution of growth folds in two-dimensions.

Relationships between these parameters are investigated in a series of cross plots (Figs. 11 – 12), which show best-fit lines generated by least-square regression methods for moderate-strong correlations (coefficient of determination, R^2 = 0.5 – 0.8, = 0.8 – 1.0, respectively). Equations describing best-fit lines between parameter pairs showing a moderate-strong correlation are shown in Table 2. Best-fit lines have been plotted using linear, power-law and 2nd degree polynomial functions. The function that shows the best-fit to the data, characterised by the highest R^2 value, has generally been selected for each parameter pair. The only exceptions are where polynomial functions that give best-fit lines with minima that are poorly constrained by data control and are geologically unreasonable. In these select cases, the second best-fit function has been chosen.

Two types of relationships between parameters are observed. The first type comprises positive and negative correlations between parameters from related domains (e.g. fold amplitude vs. fold-shape-factor). The second type comprises positive and negative correlations between parameters from different dimensional domains that were not derived from each other (e.g. amplitude vs. prekinematic thickness). The second type of relationship is more meaningful, as it highlights potential links between parameters that are not directly related. The presence of several moderate – strong correlations between these parameters is remarkable in its own right, as it indicates that growth folds at different scales, in different extensional settings and with varying lithological heterogeneity can be described quantitatively by our regression equations. These equations are potentially powerful tools that enable estimation of unknown parameters by utilising other known parameters extracted from folds.

6.1.1. Fault-propagation folds

Natural fault-propagation folds show moderate-to-strong correlations between: (1) fault throw and fold amplitude, (2) fault throw and fold width, (3) prekinematic thickness and fold amplitude, (4) prekinematic thickness and fold width, (5) fold amplitude and width (Table 1; Figs. 11A - E). These correlations suggest that the fault throw and thickness of the prekinematic strata cover control the size of the fold, and thus, large throws generate large fault-propagation fold amplitudes and widths.

Physical models show that fault throw and fold amplitude are moderately correlated for physical models of fault-propagation folds (Table 1; Fig. 11F), similar to natural examples. This suggests that fault throw is the principal control on fold amplitude.

Numerical models show strong correlations between: (1) fault throw and fold amplitude, (2) fault throw and fold width, (3) prekinematic thickness and fold amplitude, (4) prekinematic thickness and fold width, and (5) fold amplitude and fold width. In other words, these correlations suggest that large fault throws and thick prekinematic cover generate large folds with large amplitudes which are also wide (Table 1; Fig. 11H – L), similar to the natural examples but largely different from the physical models.

6.1.2. Forced folds

Natural examples of forced folds show moderate-to-strong correlations for: (1) fault throw and fold amplitude, (2) fault throw and fold width, (3) prekinematic thickness and fold amplitude, (4) prekinematic thickness and fold width and (5) fold amplitude and fold width, similar to fault-propagation folds (Table 1; Figs. 12A – B, E - G). In addition, forced folds also shown moderate-to-strong correlations for (6) detachment thickness and fold amplitude, and (7) detachment thickness and fold width (Figs. 12C - D). These correlations suggest that large fault throws, a thick prekinematic cover and a thicker detachment produce larger folds.

Physical models of forced folds lack moderate-to-strong correlations between fault, fold and stratigraphic geometrical parameters. This suggests that no single measured fault- or stratigraphic- related parameter controls the amplitude and width of the forced fold, at least for all examples in physical model. To the best of our knowledge, only Hardy (2018) has modelled forced folds numerically so quantitative analysis given the small sample size would not be appropriate. Trishear models, which have on occasion been used to investigate forced folds (Ford et al., 2007), have also not been included in our analysis.

6.2. Principal Component Analysis (PCA)

Physical models suggest that structural and stratigraphic factors control the geometry and size of evolving growth folds, but the lack of moderate-to-strong correlations for physical models in our regression analyses suggest this may not be the case (Table 2; Figs. 11 – 12). To investigate whether the quantitative relationships identified in the regression analyses are reasonable, not only for models but also in nature, and whether data scatter is obscuring trends between structural and stratigraphic factors, principal component analysis (PCA) has also been used. PCA simplifies the complexity of high-dimensional multi-variate data, such as our growth fold dataset (Appendices D – E), while retaining trends and patterns (e.g. Jolliffe, 1993; Jolliffe, 2002; Ringnér, 2008; Abdi and Williams, 2010; Josse and Husson, 2016; Lever et al., 2017). In other words, PCA allows us to identify possible relationships between growth fold parameters which are non-linear, or at least, very complex. See Appendices G – H for further details.

To identify whether the measured growth fold parameters may be related, we apply PCA to examples of fault-propagation and forced folds in nature, physical models and numerical models in turn. We then interpret the results and suggest which parameters may control the two-dimensional fold size and shape.

6.2.1. Fault-propagation folds

In natural examples of fault-propagation folds, the first three PCs account for 85% of total data variation (Fig. 13A). The first PC comprises the amplitude and width of the fold, the thickness of the strata and the underlying fault throw, whereas the second and third PCs describe the dip of the fault and the fold-shape-factor. The percentage of total variation accounted for by each of the first PCs are 52%, 21% and 12%, respectively. In other words, our analysis indicates that the thickness of the prekinematic cover and fault throw likely control the fold amplitude and width, whereas fault dip controls the geometry of the fold.

In physical models, principal components 1 – 3 account for 78% of the data variance (Fig. 13B). PC1 comprises the prekinematic thickness and fold size parameters, PC2 comprises of fold shape and fault dip and throw, and PC3 comprises prekinematic thickness, fold shape and fault throw. The percentage of total variation accounted for by each of the first PCs are 38%, 24% and 16%, respectively. These results indicate that the thickness of the prekinematic cover controls fold amplitude and width, whereas the dip and throw of the fault controls the width and the overall geometry of the fold.

In numerical models, the first three principal components account for 93% of the data variance (Fig. 13C). The percentage of total variation accounted for by each of the first PCs are 63%, 19% and 11%, respectively. PC1 describes fault throw and dip, prekinematic thickness, and fold size. PC2 describes fold shape, width and fault dip. PC3 is associated with fault dip only. Furthermore, the dip and throw of the underlying fault and thickness of the prekinematic cover control the fold size, whereas the fault dip controls the fold width and the overall shape of the fold.

6.2.2. Forced folds

Similar to the fault-propagation folds, PCA may also provide insights into related parameters in examples of forced folds in nature and from physical models. In natural examples, the first three principal components account for 74% of total data variation (Fig. 14A). The first PC comprises the fold amplitude, width, the thickness of the cover and the fault throw, whereas the second PC describes the fold shape and fold width, and the dip of the fault. The third PC comprises of the fold amplitude and width, and the cover thickness. The percentage of total variation accounted for by each of the first PCs are 36%, 23% and 15%, respectively. In other words, our analysis indicates that the fault throw and the cover thickness controls the fold size, whereas the dip of the fault controls the width of the fold and thus, the overall shape.

In physical models, principal components 1 – 3 account for 71% of the total data variance (Fig. 14B). The percentage of total variation accounted for by each of the first PCs are 30%, 23% and 18%, respectively. The first PC comprises of the cover thickness, fold shape and fold width, whereas the second PC comprises of the fold amplitude and width, and fault throw. The third PC consists of the dip of the fault, the thickness of the cover and the proportion of ductile lithologies in the cover. In other words, the thickness of the cover and the fault throw control the shape and the size of the forced fold. The dip of the fault, in contrast to the natural examples, is not a major factor on fold shape or size. To the best of our knowledge, only Hardy (2018) has modelled forced folds numerically. In select cases (e.g. Ford et al., 2007), trishear models have also been used to reconstruct forced fold evolution, however, these have been excluded from the analysis.

7. Do physical and numerical models accurately represent natural growth fold characteristics?

By comparing the correlations between structural and stratigraphic parameters from our regression analysis (Figs. 11 – 12) and from our principal component analysis (Figs. 13 – 14) in nature and in models, we now investigate whether physical and numerical models accurately describe growth folds in nature.

In physical models, the strength and relative importance of structural and stratigraphic factors on fold geometry varies substantially and there is a high amount of scatter and weak correlations between fault-fold parameters (Table 2). For example, only fault throw and fold amplitude are moderately correlated for physical models of fault-propagation folds (Fig. 11F), while there are no moderate-to-strong correlations for physical models of forced folds. This could be due to the extensive range of material strengths for the cover (e.g. sand, wet clay, gypsum powder, limestone), detachment (e.g. silicon, asphalt, wax, oil, clay), and the temporal and spatial scaling used in the models (see Koyi, 1997; Panien et al., 2006; Schreurs et al., 2006; Schellart and Strak, 2016, for a discussion on the variability associated with physical modelling approaches).

When an individual model of a growth fold is taken in isolation, it show similar correlations between structural and stratigraphic factors and fold geometry as in nature. For example, fold amplitude increases with throw for individual models for fault-propagation (Fig. 15A) and forced folds (Fig. 15B). However, when all models are analysed together, the correlations are weaker or apparently, non-existent due to the large data variance (Fig. 15). Thus, for a physical model to be an appropriate analogue to a natural example, the rheologic, stratigraphic and structural parameters must be broadly equivalent; not all physical models will be appropriate for comparing the geometry and size of natural examples, especially their evolution through time.

Kinematic models, that is those where rock properties are not incorporated in the model (e.g. Erslev, 1991; Hardy and Ford, 1997; Cardozo et al., 2011), and mechanical models where rock properties are incorporated (e.g. Finch et al., 2004; Hardy and Finch, 2006; Egholm et al., 2007; Hardy and Finch, 2007; Figs. 11F – L), produce very similar geometrical relationships to fault-propagation folds in nature (Figs. 11A – E). The similar correlations identified for both kinematic and mechanical models, and natural examples of fault-propagation folds suggest that cover rheology is not as important as fault throw and the cover thickness in determining fold shape and size. In addition, the correlations between structural and stratigraphic factors in numerical models and nature (e.g. fault throw vs. fold amplitude, prekinematic thickness vs fold amplitude, etc.) suggest that the final geometry of a growth fold may be accurately predicted by a model (cf. Cardozo et al., 2011). However, the two-dimensional geometric and kinematic evolution of growth folds in nature remains poorly-constrained, especially in areas lacking high-resolution growth strata.

8. How are growth folds predicted to grow?

Having established the two-dimensional geometrical relationships between the geometry of the growth fold and underlying propagating normal fault and the thickness of the cover, we now investigate how fault-propagation and forced folds grow with increasing displacement on the underlying fault. Given that we can only measure the final, present-day geometry of natural folds, we are unable to know how these folds grew with increasing extensional strain. Physical and numerical models therefore provide a snapshot of the growth fold geometry at different fault displacements with increasing extensional strain (cf. Hardy and McClay, 1999; Ford et al., 2007; Cardozo et al., 2011). In this section, we use published models of growth folds above upward propagating normal faults to investigate how each of the controlling factors (Fig. 7) affects two-dimensional fold geometry and size through time, and with increasing fault throw in 2D (Figs. 16 – 19). In all cases, only a single controlling factor is changed i.e., throw is plotted against amplitude and the fold-shape-factor for each variable.

Weak or rheologically heterogeneous cover (Figs. 16A; 17A; 18A; 18E), higher confining pressures (i.e. greater burial depths; Fig. 16C), increased detachment content (Fig. 18E; 19A), thick cover thicknesses (Figs. 17D; 18D), with gently-dipping faults (Figs. 16B; 17C; 18C; 19B), low fault propagation tip rates (Fig. 17B) and low regional strain rates and displacement rates (Fig. 18B) produce wide folds in physical (Ameen, 1988; Richard, 1989; Withjack et al., 1990; Withjack and Callaway, 2000; Miller and Mitra, 2011) and numerical models (Allmendinger, 1998; Hardy and McClay, 1999; Finch et al., 2004; Hardy, 2018). In all cases, folds initially have relatively high FSF values as final fold widths are established very early during fold growth and remain largely constant throughout. In contrast, fold amplitude increases gradually as throw accrues on the underlying normal fault. Therefore, the initial (and largest) FSF that can be developed is controlled by the structural and stratigraphic factors that control fold width. As the fold grows and amplitude slowly increases as throw accrues on the underlying fault, the FSF gradually decreases (Figs. 16 – 19).

In addition to the geometrical evolution of growth folds through time, models permit an insight into the structural and stratigraphic factors that affect the duration of folding and explicitly what factors control fold breaching. Folds with weak cover (Figs. 16A; 17A; 18A; cf. Fig. 19A), low strain rates (Fig. 18B), low fault propagation rates (Fig. 17B), higher confining pressures (i.e. greater burial depths; Fig. 16C), and gentle fault dips (Figs. 16B; 17C; 18C; 19B) inhibit the breaching of growth folds above the upper tips of propagating normal faults (Ameen, 1988;

Richard, 1989; Withjack et al., 1990; Allmendinger, 1998; Hardy and McClay, 1999; Withjack and Callaway, 2000; Finch et al., 2004; Miller and Mitra, 2011).

9. Discussion

9.1. How do fault-propagation and forced folds grow?

A growth fold pathway is the track that an evolving fault-propagation or forced fold takes as it amplifies and widens on Fig. 20. The growth fold pathways provide important insights into fold growth and allows us to predict the 2D geometry and size of growth folds through time. When the fold amplitude and width are plotted for all growth folds, we observe a relationship between the two, suggesting that fold amplitude and width grow together with increasing displacement on the underlying fault – Path 1 on Fig. 20A. However, it is striking that in the physical, mechanical and kinematic models (cf. Ameen, 1988; Richard, 1989; Withjack et al., 1990; Patton et al., 1998; Hardy and McClay, 1999; Withjack and Callaway, 2000; Finch et al., 2004; Miller and Mitra, 2011; Figs. 16 - 19), this is not the case. In these models we observe how the fold width and amplitude develop at different times and different rates during fold evolution, producing an initially high FSF that gradually declines with fold growth (see the dashed lines on Figs. 8, 16 – 19). In other words, the final fold width is established relatively early during fold growth, when the fold amplitude (and fault throw) is small. As the fold continues to grow with increasing fault throw, the fold amplitude then increases whereas the fold width remains largely constant – Path 2 on Fig. 20A. These growth fold pathways help explain how natural examples of fault-propagation and forced folds may geometrically and kinematically evolve in extensional settings. Furthermore, when seismic imaging or exposure is poor (cf. Botter et al., 2014), high-resolution growth strata are not available (such as during sub-aerial continental rifting - Gawthorpe and Leeder, 2000; Patton, 2004), or there is not an appropriate physical or numerical model, these pathways may be used to make quantitative estimates for fold geometry and size through time in 2D.

So far, we have only discussed the 2D geometry and evolution of fault-propagation and forced folds, but in reality, growth folds change shape and size along- and across-strike and are dependent upon the growth of the underlying master fault, which varies in three-dimensions (Fig. 21). If the fault length and throw accumulate gradually and synchronously (Fig. 21A; 'isolated fault model' – e.g. Walsh and Watterson, 1988; Dawers and Anders, 1995; Fig. 4A in Jackson et al., 2017a), the along-strike width of the growth folds may be expected to increase progressively through time. Alternatively, if faults rapidly establish their along-strike length before accumulating displacement ('constant-length fault model' - cf. Childs et al., 1995; Meyer et al., 2002; Walsh et al., 2003; Jackson and Rotevatn, 2013; Tvedt et al., 2016; Fig. 4B in Jackson et al., 2017a), the along-strike width of the fold may be very large for a small amount of throw (Fig. 21B). Regardless of the fault growth model (i.e. isolated vs constant-length), the fold may be breached when the fault slip is large enough or the propagation rate of the upper fault tip increases sufficiently. This increase in displacement could be due regional extension rate (cf. Nicol et al., 1997; Hardy and McClay, 1999; Meyer et al., 2002; Mueller, 2017), or as strain becomes focused onto larger, well-connected faults during the latter stages of extension (e.g. Gawthorpe and Leeder, 2000; Cowie et al., 2005; Finch and Gawthorpe, 2017).

9.2. Differences between fault-propagation and forced fold growth

Given that fault-propagation and forced folds have different shapes and sizes for a given throw on the underlying fault, their growth pathways may be different. For example, forced folds have larger amplitudes (Fig. 22A) and widths (Fig. 22B) for a given fault throw than fault-propagation folds. This is likely due to the across- and along-strike salt flow. As a forced fold grows, salt may move from the hangingwall into the footwall during extension (Koyi et al., 1993; Burliga et al., 2012) or sediment loading (e.g. the Cormorant structure, Jeanne d'Arc Basin - Withjack and Callaway, 2000; cf. Warsitzka et al., 2015; Warsitzka et al., 2017), causing the fold amplitude to increase ('salt inflation' in Fig. 20B) relative to a fault-propagation fold that has experienced the same fault throw. In addition, the fold amplitude may increase very rapidly compared to fold width, and more rapidly than a fault-propagation fold. Alternatively, salt may flow laterally away from a pre-existing sub-salt step in the basement ('detachment withdrawal' on Fig. 20B), creating a 'withdrawal drape fold' (Fig. 16 in Withjack and Callaway, 2000; cf. Fig. 1). As salt is evacuated from beneath the supra-salt strata in the hangingwall, the amplitude of the fold may rapidly increase compared to width, appearing geometrically similar and growing very similarly to a forced fold (Path 2 on Fig. 20).

Forced folds tend to have larger fold amplitudes and widths compared to fault-propagation folds (Figs. 22C - D) for the same total cover thickness (i.e. the thickness of the detachment and the prekinematic cover). Richard (1989) and Hardy (2018) showed that as the thickness of the detachment is increased relative to the prekinematic thickness i.e. the detachment content of the cover increases, growth folds are wider for a given fold amplitude and fault throw (Figs. 18E; 19A). This behaviour might be because as the overall cover is weakened (by the introduction of ductile material), extensional strain may be distributed over a wider area (cf. Fig. 7D).

9.3. What controls the occurrence of growth folds?

Why do growth folds occur in some basins but not others? Prior studies (e.g. Corfield and Sharp, 2000; Ford et al., 2007) have highlighted two key factors that may induce growth folding: (i) the presence of weak lithologies or mechanical heterogeneities in the cover, and (ii) low displacement (and low upper tip fault propagation) rates. Here, we discuss these factors in turn, drawing upon key examples from our growth fold dataset, to critically assess whether these factors may control growth fold occurrence.

Folding is expected to be more common in relatively rheologically-weak cover, as the strain is not only distributed over a wide area but also these rheological heterogeneities inhibit upward fault propagation (cf. Couples and Lewis, 1998; Withjack and Callaway, 2000; Finch et al., 2004; Ford et al., 2007; Roche et al., 2012; Jackson and Lewis, 2016; Hardy, 2018). In contrast, folding may be expected to be absent in relatively rheologically-strong cover as strain is focused in the vicinity of the fault, permitting rapid propagation and leaving little time for folding (cf. Withjack and Callaway, 2000; Finch et al., 2004; Hardy and Finch, 2007; Hardy, 2011). Rheological strong and brittle volcanic sequences may therefore be expected to lack growth folds (e.g. Fig. 2 in Hardy, 2013), however, this is not always the case. For example, growth folds are documented in the flanks of Kilauea, Hawaii (Kattenhorn et al., 2000; Parfitt and Peacock, 2001; Peacock and Parfitt, 2002; Holland et al., 2006; Martel and Langley, 2006; Kaven and Martel, 2007; Podolsky and Roberts, 2008), the Modoc Plateau, USA (White and Crider, 2006; Blakeslee and Kattenhorn, 2013; Crider, 2015; Kattenhorn et al., 2016), and the Reykjanes Peninsula, Iceland (Bull et al., 2003; Grant and Kattenhorn, 2004; Bull et al., 2005; Trippanera et al., 2015) suggesting that cover rheology is *not* the principal control on growth fold occurrence, although it may affect their geometry and size (Fig. 7D). Although it is possible intra-basaltic heterogeneity e.g. paleosols, volcaniclastics, rubble horizons, mineralisation, pre-existing fractures may weaken the cover rheology (cf. Finch et al., 2004; e.g. Walker et al., 2012; Walker et al., 2013; Bubeck et al., 2018; Smart and Ferrill, 2018) and thus, permit folding. Although growth folds are seemingly more widespread in basins with rheological heterogeneity, such as salt or thick shale (cf. Jackson et al., 2006; Jackson and Lewis, 2016; Coleman et al., 2017), they clearly also occur in predominantly brittle successions (cf.

Gawthorpe et al., 1997; Willsey et al., 2002) in largely homogeneous crust (cf. Gawthorpe and Leeder, 2000).

Growth fold occurrence has also been linked to the interplay of the propagation rate and displacement rates of the upper tips of normal faults, that may in part, be related to the rheology of the cover (Hardy and McClay, 1999; Finch et al., 2004; Jackson et al., 2006). We can therefore speculate that relatively high propagation rates are less likely to cause growth folding as rapidly-propagating fault tips breach the surface early during fold growth. Rapidly-propagating faults may be expected in regions with high strain rates (cf. Nicol et al., 1997; Meyer et al., 2002; Mueller, 2017), during rift climax (cf. Cowie, 1998; Cowie et al., 2000; Gawthorpe and Leeder, 2000; Cowie et al., 2005), towards the rift axis (Cowie et al., 2005), or within fault arrays with relatively few faults (Walsh et al., 2003; Wilson et al., 2013; Nixon et al., 2014). However, do growth folds develop in these areas? Are they more widespread than perhaps, they are given credit for?

In the flanks of Kilauea, Hawaii (e.g. Macdonald, 1957; Duffield, 1975; Kattenhorn et al., 2000; Parfitt and Peacock, 2001; Martel and Langley, 2006; Kaven and Martel, 2007; Podolsky and Roberts, 2008; Bubeck et al., 2018) and in the eastern Gulf of Corinth (e.g. Vita-Finzi and King, 1985), fault-propagation folds are forming at the present-day despite very high regional extension rates (Kilauea Volcano - 9 – 12 cm/yr from Owen et al., 1995; Gulf of Corinth - 5 – 15 mm/yr from Bell et al., 2011). Similarly, ancient growth folds have formed under different extension rates. In the Halten Terrace, km-scale growth folds formed over <60 Myr time period (Corfield and Sharp, 2000; Corfield et al., 2001; Marsh et al., 2010; Coleman et al., 2017), while in the Gulf of Suez, similarly-sized growth folds formed over 4 Myr (Sharp et al., 2000a; Sharp et al., 2000b). Even though salt is present in the Halten Terrace, which may have inhibited the upward propagation of fault tips to the surface, this variability highlights that regional extension rate does not seem to control the occurrence of growth folds. Instead, growth fold occurrence is likely dependent on the propagation and displacement rates on individual faults which is likely to vary spatially and temporally within extensional fault arrays, as speculated by Withjack and Callaway (2000; in the Jeanne d'Arc Basin), Willsey et al. (2002), Ford et al. (2007) and Bubeck et al. (2018).

During rift initiation, strain is distributed over many small, isolated faults with low slip and propagation rates (Cowie, 1998; Gupta et al., 1998; Cowie et al., 2000; Cowie et al., 2005), promoting the development of growth folding (cf. Gawthorpe and Leeder, 2000). However, as these small faults interact and link during rift climax, slip is transferred onto increasingly large, well-connected faults (Cowie, 1998; Cowie et al., 2000; Gawthorpe and Leeder, 2000) that may rapidly propagate through the cover. Rapid fault propagation may not only breach pre-existing growth folds but may also inhibit the formation of new growth folds at their upper tips, so that they may not develop at all (cf. Bubeck et al., 2018). Furthermore, growth folds may develop in some locations with similar cover rheology and similar throws, but not others (e.g. Faroe Islands - Walker et al., 2012; Walker et al., 2013; e.g. presence of growth folds in the western, but not eastern Koa'e Fault System, Kilauea, Hawaii - Bubeck et al., 2018). In contrast, growth folds above isolated small faults in the stress shadows of these larger faults may be preserved. Examples may include the isolated faults in the vicinity of the Strathspey-Brent-Statfjord fault system of the Northern North Sea (McLeod et al., 2000), the Nopolo Structure of the Gulf of California (Willsey et al., 2002), or the El Qaa fault block of the Gulf of Suez (Lewis et al., 2015). In addition, as strain becomes focused onto larger faults, particularly towards the rift axis (Cowie et al., 2005), growth folds may preferentially develop at the rift margins (e.g. Laubscher, 1982). In the Gulf of Corinth, strain has become increasingly focused towards the rift margins (Nixon et al., 2016), opposed to the rift axis, but fault-propagation folds may still be found at the margin (Hemelsdaël and Ford, 2014).

Finally, individual faults as part of a large network (i.e. distributed deformation) may propagate at a slower rate compared to faults within a small fault network, where the strain is localised onto fewer faults (Walsh et al., 2003; Putz-Perrier and Sanderson, 2009; Wilson et al., 2013; Nixon et al., 2014). Although this is likely the case, as shown in physical models with one basement fault and high strain rates (e.g. Withjack and Callaway, 2000; Miller and Mitra, 2011; Paul and Mitra, 2015), few attempts (e.g. Ford et al., 2007) have been made to measure the displacement rates of individual faults. In addition, the displacement rates (and possibly, the propagation rates) may be greatest towards the centre of fault arrays but lower towards the tips (Cowie and Roberts, 2001; Papanikolaou and Roberts, 2007). Furthermore, growth folds may be expected to be rarer or at least breached (cf. Parfitt and Peacock, 2001; Grant and Kattenhorn, 2004; Martel and Langley, 2006; White and Crider, 2006; Tavani et al., 2013; Tavani and Granado, 2014) towards fault array centres.

We do not claim here to know why growth folds occur in particular locations more readily than others, but this data compilation suggests that growth folds are far more prevalent than they have been credited for. Perhaps, growth folds occur in every basin worldwide, but instead, their small size (especially where folds are poorly-developed under high fault tip propagation rates; cf. Bubeck et al., 2018) and the lack of high-resolution synkinematic strata, particularly during early extension, make it difficult to identify them.

9.4. What controls the geometry and size of growth folds?

Natural examples of fault-propagation and forced folds show similar relationships between fold size and geometry, and the properties of the underlying fault and cover. This suggests that the structural and stratigraphic factors controlling fault-propagation and forced folds are largely similar. The only exception is the thickness of the detachment in forced folds, which by definition, require an abrupt transition from faulting to folding (cf. Withjack et al., 2002). We find that fault throw, and the thickness of the cover are the major controls on fault-propagation and forced fold geometry and size (Figs. 11 – 12), and although cover rheology and fault dip undoubtedly control fold geometry and size, as shown in physical (Figs. 7; 16; 18) and numerical models (Fig. 17; 19), their role is masked by the dataset scatter (as in Fig. 15). Here, we discuss in mechanical terms why the identified correlations may exist between growth fold parameters, and which parameters exert the greatest influence of fold size and shape.

Our analysis suggests that large fault throws and thicker prekinematic cover for fault-propagation and forced folds generates large fold amplitudes and widths, as suggested by Horsfield (1977), Withjack et al. (1990), Withjack and Callaway (2000), and Miller and Mitra (2011). As the fault throw increases, intuitively the amplitude of the folded cover increases too as the hangingwall block is displaced downwards relative to the footwall, and the cover is increasingly folded (Fig. 22A). Furthermore, the fault throw is the principal control on fold amplitude and explains why the values are very similar for the majority of growth folds. These results are corroborated by Lăpădat et al. (2016), in their Fig. 13C and D. Once the fold is breached, fold amplitude is independent of the fault throw (Appendix D – E), also documented by Lăpădat et al. (2016).

As the fault throw (and the fold amplitude) increases, the width also increases (Fig. 22B), similar to Conneally et al. (2017) in their Fig. 6C, 13C and 16. However, as discussed earlier, we suspect that the width is largely set during the initial stages of growth folding (cf. Path 2 on Fig. 20) and although it may increase slightly as throw is accrued on the underlying fault, the width may be instead dependent on the rheology (or flexural rigidity) of the cover, or the dip of the underlying fault (Figs. 7A; 7C).

The thickness of the prekinematic cover strongly affects fold growth. Thicker cover generates larger amplitude and width folds (Figs. 7E; 17D; 19D; 22C - D). We interpret that as the cover thickness increases, there is a larger amount of rock in front of the propagating fault tip. By increasing the thickness of the cover, the duration of folding will increase, permitting the growth of large folds with large throws.

We showed that as the cover rheology strength weakens, the fold becomes much wider for a given throw (Figs. 7D; 16A; 17A). This likely reflects that strain is accommodated in narrow zones near the fault tip in strong cover, but this same strain is far more distributed in weak cover. Similarly, gently-dipping faults distribute strain over a wider area compared to steeply-dipping faults, and thus, the dip of the fault will also control the fold width (Figs. 7A; 8). Given that both the rheology of the cover and dip of the fault strongly control fold width, they also strongly control the fold shape, corroborating results from Patton (2004). This is especially the case during the initial stages of folding, since the fold amplitude will be initially low (as fault throw is small), but the final width is established very early (cf. Path 2 on Fig. 20).

In addition to the aforementioned structural and stratigraphic factors, forced fold geometry and size is also affected by the thickness of the detachment (Figs. 7F; 12C - D). We suggest that detachments significantly weaken the overall strength of the cover and therefore, thicker detachments may distribute extensional strain over a broader area and increase the fold width. Given that the fold width is larger for a forced fold compared to a fault-propagation fold (Fig. 22B), thicker detachments also increase the fold-shape-factor for a given amount of fault throw. This is similar to increasing the ductile portion of the cover, where folds have similar amplitudes for a given fault throw, but the width of the fold increases as the detachment content increases (Figs. 18E; 19A; Richard, 1989; Hardy, 2018).

As the detachment thickness also increases the total cover thickness, and thus, the amount of rock in front of the propagating fault tip, the folding duration also increases. A forced fold therefore has longer to grow before becoming breached by the underlying fault. This allows forced folds to reach larger amplitudes and widths compared to fault-propagation folds, and not become breached despite large fault throws. Ductile flow of the detachment, due to salt expulsion (cf. Fig. 5 in Koyi et al., 1993; Figs. 5 - 6 in Burliga et al., 2012; Figs. 5 - 6 in Warsitzka et al., 2015; Fig. 10 in Warsitzka et al., 2017), may also increase the amplitude of the forced fold. In some cases, the amplitude of the forced fold may be larger than the throw on the underlying fault (Fig. 22A).

Changes in structural and stratigraphic parameters are commonplace in extensional settings and thus, growth fold evolution may differ significantly between fault segments in different intra-rift settings (e.g. the rift margin vs. rift axis, transfer zones vs fault segment centres etc.) and in particular, between salt-free and salt-rich basins. We present conceptual models for how growth folds may vary between salt-free and salt-rich basins (Fig. 23), with particular emphasis on their 3D geometry and size in relation to the dip, throw and displacement rate of master faults, the rheology, thickness, and rheological heterogeneity of the cover. These concepts are testable using natural examples, physical and numerical models, which may fill in gaps in our understanding in how growth folds develop through time and their occurrence.

9.5. Implications for hydrocarbons and structural restoration

We have shown that positive correlations exist between fault, fold and stratigraphic parameters. This means it is now possible to quantify: the fold amplitude (and structural relief) for growth folds for a given amount of throw on the underlying fault, the fold width during fold growth, and the fold shape during fold evolution once one or more growth fold- and/or fault-related parameters (cf. Fig. 2) have been constrained. These have potentially important implications (Fig. 24), as understanding the likely shape and size of a growth fold through time is critical for determining palaeo- and present-day spill points for hydrocarbons in fold hinges (Mitra, 1990; Withjack et al., 1990; Withjack and Callaway, 2000; Tavani et al., 2018), as well as understanding the architecture and width over which synkinematic hydrocarbon reservoirs and seals may thin (Corfield et al., 2001; Patton, 2004; Lewis et al., 2015). This is especially useful in areas where synkinematic growth strata are below seismic resolution.

Fault-propagation and forced folds provide a rare opportunity to target vertically-stacked hydrocarbon plays (Fig. 24). Beneath the growth fold, hydrocarbons may become trapped in the underlying fault blocks (e.g. Uphoff, 2005). Within the growth fold, hydrocarbons may become trapped within the fold crest (e.g. Hibernia-Nautilus and Cormorant fields – Tankard and Welsink, 1987; Withjack and Callaway, 2000; Smørbukk Sør Field - Corfield and Sharp, 2000; Corfield et al., 2001), within the heavily-fractured prekinematic cover or compartmentalised by secondary normal and reverse faults (Fig. 24). These secondary faults may either detach onto a detachment or link with the underlying master fault (Fig. 24B). The former creates fault-related traps, whereas the latter may allow hydrocarbons to leak from deeper to shallower levels (cf. Heggland, 1998; Ostanin et al., 2013; Mohammedyasin et al., 2016; Fig. 10D in Tavani et al., 2018) and may create fault-bound compartments in the cover (e.g. Mikkel, Midgard, Heidrun and Smørbukk fields of the Halten Terrace - Koch and Heum, 1995; Corfield and Sharp, 2000). Above the growth fold, synkinematic reservoirs may thin over the fold (Fig. 24A – B; e.g. the Garn and Melke Fm of the Halten Terrace; Koch and Heum, 1995; Corfield and Sharp, 2000; Corfield et al., 2001; cf. Lewis et al., 2013; Lewis et al., 2015). Fold-related relief may also affect transverse drainage patterns and control the distribution of fluvial (e.g. the Åre and Tofte formations of the Halten Terrace; Koch and Heum, 1995; cf. Burbank et al., 1996; Bernal et al., 2018) or turbidite reservoirs (cf. Grecula et al., 2003).

Additional plays may also be found in the detachment, such stringers (cf. van Gent et al., 2011; Fig. 24B).

Our results also have implications for the structural restoration of growth folds. For structural restoration to be valid, the kinematics and mode of deformation need to be identified (Lingrey and Vidal-Royo, 2015). In growth folds, the method for structural restoration method in section depends on the rheology of the cover, the mechanical heterogeneity, and the amount of strain. In salt-free basins (Fig. 23 – top), deformation associated with fault-propagation folds is focused in a broadly triangular zone emanating from the propagating fault tip upwards into the cover. Here, the lengths and thicknesses of individual beds are not maintained, but by assuming the area of the strata are the same, trishear methodologies (cf. Erslev, 1991; Hardy and Ford, 1997; Allmendinger, 1998) may be used for restoration (e.g. Khalil and McClay, 2002; Jackson et al., 2006; Ford et al., 2007; Jin et al., 2009). However, caution is often applied as the geological significance of the parameters associated with trishear are poorly understood (Hardy and Ford, 1997; Cardozo et al., 2011; Hardy and Allmendinger, 2011). In salt-rich basins (Fig. 23 – bottom), salt may permit layer-parallel slip so that strain is not accommodated at the fault tip but instead outboard from the structure. Furthermore, the cover may not be stretched (cf. 'tectonic thinning' after Brown, 1988) and instead be faulted (cf. 'detachment slide' after Brown, 1988). Salt may also facilitate slip between the cover and the basement (cf. Johnson and Johnson, 2002) or out-of-plane flow (e.g. Rowan and Kligfield, 1989; Rowan and Ratliff, 2012), which is not permitted in trishear and may produce a different fold geometry (cf. Johnson and Johnson, 2002). Fault block restoration and flexural slip may therefore be most appropriate for salt-rich settings as bed lengths and orthogonal thicknesses may be preserved, at least at moderate strains (cf. Lingrey and Vidal-Royo, 2015). If the salt becomes immobile or welded during growth folding, layer-parallel slip and out-of-plane salt flow may cease and thus, trishear methods may be more appropriate. This has implications for extension estimates, particularly in settings where growth folds are common, as the amount of extensional strain and mechanism responsible may be difficult to discern (Coleman et al., 2017). This also means that the most appropriate technique for restoring growth folds may change with fold growth, so how may we select the most appropriate? And how can the geometry and size of a growth fold be inferred?

High-resolution growth strata or inferences from scaled models may be used to constrain fold geometry through time and thus aid restoration, however, synkinematic strata may not always be preserved (cf. Gawthorpe and Leeder, 2000; Patton, 2004) and model analogues may not be appropriate (cf. Fig. 15). Our results provide an additional independent constraint on growth fold geometry and size for structural and stratigraphic parameters that may be easily measured. Inevitably an iterative approach is required to isolate the most appropriate structural restoration solutions for growth folds in in salt-free and salt-rich settings. However, by constraining these solutions with growth strata, inferences from models and our parametric equations (Table 2), our understanding of the geometry, size and development of growth folds in nature may improve significantly.

10. Conclusions

- Growth folds are very common in sedimentary and volcanic basins, and perhaps more prevalent than they have been historically given credit for. Not only do they form as transient features during the early stages of salt-free rifting and persist throughout most of salt-rich rifting, but they also occur in a wide range of settings, including those with high regional strain rates that were previously interpreted to be unlikely to host these folds. They also occur in relatively brittle (e.g. volcanic sequences in Iceland and Hawaii) and ductile cover sequences (e.g. salt or shale-rich sequences). Furthermore, rheology alone is unlikely to be the principal control on growth fold occurrence. Instead, we speculate that the propagation rate of individual faults may vary within an area and may control the distribution of growth folds.

- Fault-propagation and forced folds rapidly attain their near-final width relatively early during fold growth before they amplify. The rate of fold amplification is likely a function of the throw on the underlying normal fault. Their shape therefore changes throughout fold growth, evolving from a relatively broad, low amplitude fold to a fold where the amplitude and width are largely similar. Furthermore, the fold-shape-factor of a growth typically decreases with time.
- During extension or sediment loading, salt expulsion in the hangingwall and/or the development of salt pillows in the footwall for example, may lead to increased fold amplitudes and widths for forced folds. Forced folds may therefore grow very differently to and be geometrically distinct from fault-propagation folds.
- Growth folds are also dependent on the character of the underlying normal fault. As the fault grows in three-dimensions, so does the overlying growth fold. If the fault length and throw accumulate gradually and synchronously, growth folds may be expected to widen along-strike gradually. If faults rapidly establish their along-strike length before accumulating displacement, the along-strike width of the fold may be very large for a small amount of throw.
- By comparing correlations of measured fold parameters between fault-propagation and forced folds, we show that:
    - For a given throw, the amplitude and width of a forced fold is larger than that of a fault-propagation fold.
    - For a given fold width, the amplitude of a forced fold is generally larger than that of a fault-propagation fold.

    - For a given prekinematic thickness, the width of a forced fold is greater than that of a fault-propagation fold.
- We also derive a number of parametric equations that are potentially powerful tools in estimating unknown fold geometry and size in profile by utilising other known structural and stratigraphic parameters. However, their robustness will need to be tested with further examples.
- Physical models effectively capture the geometrical features of natural examples of fault-propagation and forced folds, although their structural and stratigraphic parameters are not well correlated, in contrast to natural examples where moderate to strong correlations are present. However, an individual physical model, when analysed independently of other models shows similar parameter correlations to natural examples (e.g. fault throw vs. fold amplitude). Overall, comparisons between physical models and natural examples should be used with care, especially if used to infer the geometrical evolution of growth folds.
- Numerical models show similar correlations between stratigraphic and structural parameters to natural examples. However, numerical models, especially those where mechanical properties of rock units are not incorporated (i.e. kinematic models), cannot accurately describe the small-scale deformation observed in nature or physical models. Kinematic models however, do match the final geometry of growth folds in physical models and in nature, allowing the evolving fold geometry to be inferred. This is particularly useful in areas lacking synkinematic sediments.

Acknowledgements

We thank Stephen Watkins for his valuable suggestions, observations and advice on fault-related folding in extensional settings, and Thilo Wrona for his help regarding multi-variate data analysis. We also extend our thanks to the Basins Research Group (BRG), particularly Thomas Phillips, for additional discussions and their guidance throughout. John Cosgrove and Atle Rotevatn are thanked for their comments and feedback on an earlier version of the manuscript.

11. References

Abdi, H., and Williams, L. J., 2010, Principal component analysis: Wiley interdisciplinary reviews: computational statistics, v. 2, no. 4, p. 433-459.

Allmendinger, R. W., 1998, Inverse and forward numerical modeling of trishear fault-propagation folds: Tectonics, v. 17, no. 4, p. 640-656.

Allmendinger, R. W., and Shaw, J. H., 2000, Estimation of fault propagation distance from fold shape: Implications for earthquake hazard assessment: Geology, v. 28, no. 12, p. 1099-1102.

Ameen, M., 1990, Macrofaulting in the Purbeck-Isle of Wight monocline: Proceedings of the Geologists' Association, v. 101, no. 1, p. 31-46.

Ameen, M. S., 1988, Folding of layered cover due to dip-slip basement faulting: Imperial College London (University of London).

Bartlett, W., Friedman, M., and Logan, J., 1981, Experimental folding and faulting of rocks under confining pressure Part IX. Wrench faults in limestone layers: Tectonophysics, v. 79, no. 3-4, p. 255-277.

Bell, R. E., McNeill, L. C., Henstock, T. J., and Bull, J. M., 2011, Comparing extension on multiple time and depth scales in the Corinth Rift, Central Greece: Geophysical Journal International, v. 186, no. 2, p. 463-470.

Benedicto, A., Schultz, R., and Soliva, R., 2003, Layer thickness and the shape of faults: Geophysical Research Letters, v. 30, no. 20.

Berg, S. S., and Skar, T., 2005, Controls on damage zone asymmetry of a normal fault zone: outcrop analyses of a segment of the Moab fault, SE Utah: Journal of Structural Geology, v. 27, no. 10, p. 1803-1822.

Bernal, A., Hardy, S., and Gawthorpe, R., 2018, Three-Dimensional Growth of Flexural Slip Fault-Bend and Fault-Propagation Folds and Their Geomorphic Expression: Geosciences, v. 8, no. 4, p. 110.

Blakeslee, M. W., and Kattenhorn, S. A., 2013, Revised earthquake hazard of the Hat Creek fault, northern California: A case example of a normal fault dissecting variable-age basaltic lavas: Geosphere, v. 9, no. 5, p. 1397-1409.

Botter, C., Cardozo, N., Hardy, S., Lecomte, I., and Escalona, A., 2014, From mechanical modeling to seismic imaging of faults: A synthetic workflow to study the impact of faults on seismic: Marine and Petroleum Geology, v. 57, p. 187-207.

Brown, W. G., 1988, Deformational style of Laramide uplifts in the Wyoming foreland: Interaction of the Rocky Mountain foreland and the Cordilleran thrust belt: Geological Society of America Memoir, v. 171, p. 1-25.

Bubeck, A., Walker, R. J., Imber, J., and MacLeod, C. J., 2018, Normal fault growth in layered basaltic rocks: The role of strain rate in fault evolution: Journal of Structural Geology, v. 115, p. 103-120.

Bull, J. M., Minshull, T. A., Mitchell, N. C., Thors, K., Dix, J. K., and Best, A. I., 2003, Fault and magmatic interaction within Iceland's western rift over the last 9 kyr: Geophysical Journal International, v. 154, no. 1, p. F1-F8.

Bull, J. M., Minshull, T. A., Mitchell, N. C., Dix, J. K., and Hardardottir, J., 2005, Magmatic and tectonic history of Iceland's western rift zone at Lake Thingvallavatn: Geological Society of America Bulletin, v. 117, no. 11, p. 1451.

Burbank, D., Meigs, A., and Brozović, N., 1996, Interactions of growing folds and coeval depositional systems: Basin Research, v. 8, no. 3, p. 199-223.

Burliga, S., Koyi, H. A., and Chemia, Z., 2012, Analogue and numerical modelling of salt supply to a diapiric structure rising above an active basement fault: Geological Society, London, Special Publications, v. 363, no. 1, p. 395-408.

Cardozo, N., Bhalla, K., Zehnder, A. T., and Allmendinger, R. W., 2003, Mechanical models of fault propagation folds and comparison to the trishear kinematic model: Journal of Structural Geology, v. 25, no. 1, p. 1-18.

Cardozo, N., Jackson, C. A.-L., and Whipp, P. S., 2011, Determining the uniqueness of best-fit trishear models: Journal of Structural Geology, v. 33, no. 6, p. 1063-1078.

Carola, E., Tavani, S., Ferrer, O., Granado, P., Quintà, A., Butillé, M., and Muñoz, J. A., 2013, Along-strike extrusion at the transition between thin- and thick-skinned domains in the Pyrenean Orogen (northern Spain): Geological Society, London, Special Publications, v. 377, no. 1, p. 119-140.

Childs, C., Watterson, J., and Walsh, J. J., 1995, Fault overlap zones within developing normal fault systems: Journal of the Geological Society, v. 152, no. 3, p. 535-549.

Coleman, A. J., Jackson, C. A.-L., and Duffy, O. B., 2017, Balancing sub- and supra-salt strain in salt-influenced rifts: Implications for extension estimates: Journal of Structural Geology, v. 102, p. 208-225.

Conneally, J., Childs, C., and Nicol, A., 2017, Monocline formation during growth of segmented faults in the Taranaki Basin, offshore New Zealand: Tectonophysics, v. 721, p. 310-321.

Corfield, S., and Sharp, I., 2000, Structural style and stratigraphic architecture of fault propagation folding in extensional settings: a seismic example from the Smørbukk area, Halten Terrace, Mid-Norway: Basin Research, v. 12, no. 3-4, p. 329-341.

Corfield, S., Sharp, I., Häger, K.-O., Dreyer, T., and Underhill, J., 2001, An integrated study of the garn and melke formations (middle to upper jurassic) of the smorbukk area, halten terrace, mid-norway, *in* Ole, J. M., and Tom, D., eds., Norwegian Petroleum Society Special Publications, Volume Volume 10, Elsevier, p. 199-210.

Cosgrove, J. W., and Ameen, M. S., 1999, A comparison of the geometry, spatial organization and fracture patterns associated with forced folds and buckle folds: Geological Society, London, Special Publications, v. 169, no. 1, p. 7-21.

Couples, G. D., and Lewis, H., 1998, Lateral variations of strain in experimental forced folds: Tectonophysics, v. 295, no. 1, p. 79-91.

Couples, G. D., Lewis, H., and Tanner, P. G., 1998, Strain partitioning during flexural-slip folding: Geological Society, London, Special Publications, v. 127, no. 1, p. 149-165.

Couples, G. D., and Lewis, H., 1999, Effects of interlayer slip in model forced folds: Geological Society, London, Special Publications, v. 169, no. 1, p. 129-144.

Cowie, P., Gupta, S., and Dawers, N., 2000, Implications of fault array evolution for synrift depocentre development: insights from a numerical fault growth model: Basin Research, v. 12, no. 3-4, p. 241-261.

Cowie, P. A., 1998, A healing–reloading feedback control on the growth rate of seismogenic faults: Journal of Structural Geology, v. 20, no. 8, p. 1075-1087.

Cowie, P. A., and Roberts, G. P., 2001, Constraining slip rates and spacings for active normal faults: Journal of Structural Geology, v. 23, no. 12, p. 1901-1915.

Cowie, P. A., Underhill, J. R., Behn, M. D., Lin, J., and Gill, C. E., 2005, Spatio-temporal evolution of strain accumulation derived from multi-scale observations of Late Jurassic rifting in the northern North Sea: A critical test of models for lithospheric extension: Earth and Planetary Science Letters, v. 234, no. 3–4, p. 401-419.

Crider, J. G., 2015, The initiation of brittle faults in crystalline rock: Journal of Structural Geology, v. 77, p. 159-174.

Dawers, N. H., and Anders, M. H., 1995, Displacement-length scaling and fault linkage: Journal of Structural Geology, v. 17, no. 5, p. 607-614.

Deckers, J., 2015, Decoupled extensional faulting and forced folding in the southern part of the Roer Valley Graben, Belgium: Journal of Structural Geology, v. 81, p. 125-134.

Dooley, T., McClay, K., and Pascoe, R., 2003, 3D analogue models of variable displacement extensional faults: applications to the Revfallet Fault system, offshore mid-Norway: Geological Society, London, Special Publications, v. 212, no. 1, p. 151-167.

Duffield, W. A., 1975, Structure and origin of the Koae fault system, Kilauea volcano, Hawaii, US Government Printing Office.

Duffy, O. B., Gawthorpe, R. L., Docherty, M., and Brocklehurst, S. H., 2013, Mobile evaporite controls on the structural style and evolution of rift basins: Danish Central Graben, North Sea: Basin Research, v. 25, no. 3, p. 310-330.

Egholm, D. L., Sandiford, M., Clausen, O. R., and Nielsen, S. B., 2007, A new strategy for discrete element numerical models: 2. Sandbox applications: Journal of Geophysical Research: Solid Earth, v. 112, no. 1-12.

Erslev, E. A., 1991, Trishear fault-propagation folding: Geology, v. 19, no. 6, p. 617.

Færseth, R. B., and Lien, T., 2002, Cretaceous evolution in the Norwegian Sea—a period characterized by tectonic quiescence: Marine and Petroleum Geology, v. 19, no. 8, p. 1005-1027.

Finch, E., Hardy, S., and Gawthorpe, R., 2004, Discrete-element modelling of extensional fault-propagation folding above rigid basement fault blocks: Basin Research, v. 16, no. 4, p. 467-488.

Finch, E., and Gawthorpe, R., 2017, Growth and interaction of normal faults and fault network evolution in rifts: insights from three-dimensional discrete element modelling: Geological Society, London, Special Publications, v. 439, p. SP439. 423.

Fodor, L., Turki, S., Dalub, H., and Al Gerbi, A., 2005, Fault-related folds and along-dip segmentation of breaching faults: syn-diagenetic deformation in the south-western Sirt basin, Libya: Terra Nova, v. 17, no. 2, p. 121-128.

Ford, M., Le Carlier de Veslud, C., and Bourgeois, O., 2007, Kinematic and geometric analysis of fault-related folds in a rift setting: The Dannemarie basin, Upper Rhine Graben, France: Journal of Structural Geology, v. 29, no. 11, p. 1811-1830.

Friedman, M., Handin, J., Logan, J., Min, K., and Stearns, D., 1976, Experimental folding of rocks under confining pressure: Part III. Faulted drape folds in multilithologic layered specimens: Geological Society of America Bulletin, v. 87, no. 7, p. 1049-1066.

Gabrielsen, R. H., Sokoutis, D., Willingshofer, E., and Faleide, J. I., 2016, Fault linkage across weak layers during extension: an experimental approach with reference to the Hoop Fault Complex of the SW Barents Sea: Petroleum Geoscience.

Gawthorpe, R. L., Sharp, I., Underhill, J. R., and Gupta, S., 1997, Linked sequence stratigraphic and structural evolution of propagating normal faults: Geology, v. 25, no. 9, p. 795.

Gawthorpe, R. L., and Leeder, M. R., 2000, Tectono-sedimentary evolution of active extensional basins: Basin Research, v. 12, no. 3-4, p. 195-218.

Gawthorpe, R. L., and Hardy, S., 2002, Extensional fault-propagation folding and base-level change as controls on growth-strata geometries: Sedimentary Geology, v. 146, no. 1, p. 47-56.

Ge, Z., Gawthorpe, R. L., Rotevatn, A., and Thomas, M. B., 2016, Impact of normal faulting and pre-rift salt tectonics on the structural style of salt-influenced rifts: The Late Jurassic Norwegian Central Graben, North Sea: Basin Research, p. n/a-n/a.

Grant, J. V., and Kattenhorn, S. A., 2004, Evolution of vertical faults at an extensional plate boundary, southwest Iceland: Journal of Structural Geology, v. 26, no. 3, p. 537-557.

Grecula, M., Flint, S., Potts, G., Wickens, D., and Johnson, S., 2003, Partial ponding of turbidite systems in a basin with subtle growth-fold topography: Laingsburg-Karoo, South Africa: Journal of Sedimentary Research, v. 73, no. 4, p. 603-620.

Gross, M. R., Becker, A., and Gutiérrez-Alonso, G., 1997, Transfer of displacement from multiple slip zones to a major detachment in an extensional regime: Example from the Dead Sea rift, Israel: Geological Society of America Bulletin, v. 109, no. 8, p. 1021-1035.

Gupta, S., Cowie, P. A., Dawers, N. H., and Underhill, J. R., 1998, A mechanism to explain rift-basin subsidence and stratigraphic patterns through fault-array evolution: Geology, v. 26, no. 7, p. 595-598.

Gupta, S., Underhill, J., Sharp, I., and Gawthorpe, R., 1999, Role of fault interactions in controlling synrift sediment dispersal patterns: Miocene, Abu Alaqa Group, Suez Rift, Sinai, Egypt: Basin Research, v. 11, no. 2, p. 167-189.

Hardy, S., and Ford, M., 1997, Numerical modeling of trishear fault propagation folding: Tectonics, v. 16, no. 5, p. 841-854.

Hardy, S., and McClay, K., 1999, Kinematic modelling of extensional fault-propagation folding: Journal of Structural Geology, v. 21, no. 7, p. 695-702.

Hardy, S., and Finch, E., 2006, Discrete element modelling of the influence of cover strength on basement-involved fault-propagation folding: Tectonophysics, v. 415, no. 1-4, p. 225-238.

Hardy, S., and Finch, E., 2007, Mechanical stratigraphy and the transition from trishear to kink-band fault-propagation fold forms above blind basement thrust faults: A discrete-element study: Marine and Petroleum Geology, v. 24, no. 2, p. 75-90.

Hardy, S., 2011, Cover deformation above steep, basement normal faults: Insights from 2D discrete element modeling: Marine and Petroleum Geology, v. 28, no. 5, p. 966-972.

Hardy, S., and Allmendinger, R. W., 2011, Trishear: A review of kinematics, mechanics, and applications, *in* McClay, K., ed., Thrust fault-related folding, AAPG Memoir 94, AAPG, p. 95-119.

Hardy, S., 2013, Propagation of blind normal faults to the surface in basaltic sequences: Insights from 2D discrete element modelling: Marine and Petroleum Geology, v. 48, no. 0, p. 149-159.

Hardy, S., 2018, Coupling a frictional-cohesive cover and a viscous substrate in a discrete element model: First results of application to thick- and thin-skinned extensional tectonics: Marine and Petroleum Geology, v. 97, p. 32-44.

Harvey, M. J., and Stewart, S. A., 1998, Influence of salt on the structural evolution of the Channel Basin: Geological Society, London, Special Publications, v. 133, no. 1, p. 241-266.

Heggland, R., 1998, Gas seepage as an indicator of deeper prospective reservoirs. A study based on exploration 3D seismic data: Marine and Petroleum Geology, v. 15, no. 1, p. 1-9.

Hemelsdaël, R., and Ford, M., 2014, Relay zone evolution: a history of repeated fault propagation and linkage, central Corinth rift, Greece: Basin Research, v. 28, p. 34-56.

Holland, M., Urai, J. L., and Martel, S., 2006, The internal structure of fault zones in basaltic sequences: Earth and Planetary Science Letters, v. 248, no. 1, p. 301-315.

Horsfield, W., 1977, An experimental approach to basement-controlled faulting: Geologie en Mijnbouw, v. 56, no. 4, p. 363-370.

Howard, K. A., and John, B. E., 1997, Fault-related folding during extension: Plunging basement-cored folds in the Basin and Range: Geology, v. 25, no. 3, p. 223-226.

Jackson, C. A.-L., Gawthorpe, R. L., and Sharp, I. R., 2006, Style and sequence of deformation during extensional fault-propagation folding: examples from the Hammam Faraun and El-Qaa fault blocks, Suez Rift, Egypt: Journal of Structural Geology, v. 28, no. 3, p. 519-535.

Jackson, C. A.-L., and Rotevatn, A., 2013, 3D seismic analysis of the structure and evolution of a salt-influenced normal fault zone: A test of competing fault growth models: Journal of Structural Geology, v. 54, p. 215-234.

Jackson, C. A.-L., Bell, R. E., Rotevatn, A., and Tvedt, A. B. M., 2017, Techniques to determine the kinematics of synsedimentary normal faults and implications for fault growth models: Geological Society, London, Special Publications, v. 439.

Jackson, C. A. L., and Lewis, M. M., 2016, Structural style and evolution of a salt-influenced rift basin margin; the impact of variations in salt composition and the role of polyphase extension: Basin Research, v. 28, no. 1, p. 81-102.

Jackson, J., and Leeder, M., 1994, Drainage systems and the development of normal faults: an example from Pleasant Valley, Nevada: Journal of Structural Geology, v. 16, no. 8, p. 1041-1059.

Jin, G., and Groshong, R. H., 2006, Trishear kinematic modeling of extensional fault-propagation folding: Journal of Structural Geology, v. 28, no. 1, p. 170-183.

Jin, G., Groshong, R. H., and Pashin, J. C., 2009, Growth trishear model and its application to the Gilbertown graben system, southwest Alabama: Journal of Structural Geology, v. 31, no. 9, p. 926-940.

Johnson, K. M., and Johnson, A. M., 2002, Mechanical models of trishear-like folds: Journal of Structural Geology, v. 24, no. 2, p. 277-287.

Jolliffe, I. T., 1993, Principal component analysis: A beginner's guide — II. Pitfalls, myths and extensions: Weather, v. 48, no. 8, p. 246-253.

Jolliffe, I. T., 2002, Principal component analysis, New York, Springer.

Josse, J., and Husson, F., 2016, missMDA: a package for handling missing values in multivariate data analysis: Journal of Statistical Software, v. 70, no. 1, p. 1-31.

Kane, K. E., Jackson, C. A.-L., and Larsen, E., 2010, Normal fault growth and fault-related folding in a salt-influenced rift basin: South Viking Graben, offshore Norway: Journal of Structural Geology, v. 32, no. 4, p. 490-506.

Kattenhorn, S. A., Aydin, A., and Pollard, D. D., 2000, Joints at high angles to normal fault strike: an explanation using 3-D numerical models of fault-perturbed stress fields: Journal of structural Geology, v. 22, no. 1, p. 1-23.

Kattenhorn, S. A., Krantz, B., Walker, E. L., and Blakeslee, M. W., 2016, Evolution of the Hat Creek fault system, northern California.

Kaven, J. O., and Martel, S. J., 2007, Growth of surface-breaching normal faults as a three-dimensional fracturing process: Journal of Structural Geology, v. 29, no. 9, p. 1463-1476.

Keller, J. V. A., and Lynch, G., 1999, Displacement transfer and forced folding in the Maritimes basin of Nova Scotia, eastern Canada: Geological Society, London, Special Publications, v. 169, no. 1, p. 87-101.

Khalil, S., and McClay, K., 2002, Extensional fault-related folding, northwestern Red Sea, Egypt: Journal of Structural Geology, v. 24, no. 4, p. 743-762.

Khalil, S. M., and McClay, K. R., 2016, 3D geometry and kinematic evolution of extensional fault-related folds, NW Red Sea, Egypt: Geological Society, London, Special Publications, v. 439, p. 1-11.

Koch, J.-O., and Heum, O., 1995, Exploration trends of the Halten Terrace: Norwegian Petroleum Society Special Publications, v. 4, p. 235-251.

Koopman, A., Speksnijder, A., and Horsfield, W., 1987, Sandbox model studies of inversion tectonics: Tectonophysics, v. 137, no. 1-4, p. 379-388.

Koyi, H., Talbot, C. J., and Tørudbakken, B. O., 1993, Salt diapirs of the southwest Nordkapp Basin: analogue modelling: Tectonophysics, v. 228, no. 3, p. 167-187.

Koyi, H., Talbot, C. J., and Torudbakken, B., 1995, Analogue models of salt diapirs and seismic interpretation in the Nordkapp Basin, Norway: Petroleum geoscience, v. 1, no. 2, p. 185-192.

Koyi, H., 1997, Analogue modelling: from a qualitative to quantitative technique - a historical outline: Journal of Petroleum Geology, v. 20, no. 2, p. 223-238.

Lăpădat, A., Imber, J., Yielding, G., Iacopini, D., McCaffrey, K. J. W., Long, J. J., and Jones, R. R., 2016, Occurrence and development of folding related to normal faulting within a mechanically heterogeneous sedimentary sequence: a case study from Inner Moray Firth, UK: Geological Society, London, Special Publications, v. 439.

Laubscher, H., 1982, Die Sudostecke des Rheingrabens-ein kinematisches und dynamisches problem: Eclogae Geologicae Helvetiae, v. 75, no. 1, p. 101-116.

Lever, J., Krzywinski, M., and Altman, N., 2017, Points of significance: Principal component analysis: Nature Methods, v. 14, p. 641-642.

Lewis, M. M., Jackson, C. A.-L., and Gawthorpe, R. L., 2013, Salt-influenced normal fault growth and forced folding: The Stavanger Fault System, North Sea: Journal of Structural Geology, v. 54, p. 156-173.

Lewis, M. M., Jackson, C. A.-L., Gawthorpe, R. L., and Whipp, P. S., 2015, Early synrift reservoir development on the flanks of extensional forced folds: A seismic-scale outcrop analog from the Hadahid Fault System, Suez Rift, Egypt: AAPG Bulletin, no. 20,150,119.

Lingrey, S., and Vidal-Royo, O., 2015, Evaluating the quality of bed length and area balance in 2D structural restorations: Interpretation, v. 3, no. 4, p. SAA133-SAA160.

Lynch, G., Keller, J. V., and Giles, P. S., 1998, Influence of the Ainslie Detachment on the stratigraphy of the Maritimes Basin and mineralization in the Windsor Group of northern Nova Scotia, Canada: Economic Geology, v. 93, no. 6, p. 703-718.

Macdonald, G. A., 1957, Faults and monoclines on Kilauea Volcano, Hawaii: Geological Society of America Bulletin, v. 68, no. 2, p. 269-271.

Marsh, N., Imber, J., Holdsworth, R., Brockbank, P., and Ringrose, P., 2010, The structural evolution of the Halten Terrace, offshore Mid-Norway: extensional fault growth and strain localisation in a multi-layer brittle–ductile system: Basin Research, v. 22, no. 2, p. 195-214.

Martel, S. J., and Langley, J. S., 2006, Propagation of normal faults to the surface in basalt, Koae fault system, Hawaii: Journal of Structural Geology, v. 28, no. 12, p. 2123-2143.

Matthews III, V., and Work, D. F., 1978, Laramide folding associated with basement block faulting along the northeastern flank of the Front Range, Colorado: Laramide folding associated with basement block faulting in the western United States: Geological Society of America Memoir, v. 151, p. 101-124.

Maurin, J. C., and Niviere, B., 1999, Extensional forced folding and decollement of the pre-rift series along the Rhine graben and their influence on the geometry of the syn-rift sequences: Geological Society, London, Special Publications, v. 169, no. 1, p. 73-86.

McLeod, A. E., Dawers, N. H., and Underhill, J. R., 2000, The propagation and linkage of normal faults: insights from the Strathspey–Brent–Statfjord fault array, northern North Sea: Basin Research, v. 12, no. 3-4, p. 263-284.

Meyer, V., Nicol, A., Childs, C., Walsh, J., and Watterson, J., 2002, Progressive localisation of strain during the evolution of a normal fault population: Journal of Structural Geology, v. 24, no. 8, p. 1215-1231.

Miller, J. F., and Mitra, S., 2011, Deformation and secondary faulting associated with basement-involved compressional and extensional structures: AAPG bulletin, v. 95, no. 4, p. 675-689.

Mitra, S., 1990, Fault-propagation folds: geometry, kinematic evolution, and hydrocarbon Traps: AAPG Bulletin, v. 74, no. 6, p. 921-945.

Mitra, S., 1993, Geometry and kinematic evolution of inversion structures: AAPG Bulletin, v. 77, no. 7, p. 1159-1191.

Mitra, S., and Islam, Q. T., 1994, Experimental (clay) models of inversion structures: Tectonophysics, v. 230, no. 3, p. 211-222.

Mohammedyasin, S. M., Lippard, S. J., Omosanya, K. O., Johansen, S. E., and Harishidayat, D., 2016, Deep-seated faults and hydrocarbon leakage in the Snøhvit Gas Field, Hammerfest Basin, Southwestern Barents Sea: Marine and Petroleum Geology, v. 77, p. 160-178.

Morley, C., 1996, Discussion of potential errors in fault heave methods for extension estimates in rifts, with particular reference to fractal fault populations and inherited fabrics: Geological Society, London, Special Publications, v. 99, no. 1, p. 117-134.

Morley, C., and Guerin, G., 1996, Comparison of gravity-driven deformation styles and behavior associated with mobile shales and salt: Tectonics, v. 15, no. 6, p. 1154-1170.

Mueller, K., 2017, Variation in slip rates on active faults: Natural growth or stress transients?: Geology, v. 45, no. 3, p. 287-288.

Nicol, A., Watterson, J., Walsh, J., and Childs, C., 1996, The shapes, major axis orientations and displacement patterns of fault surfaces: Journal of Structural Geology, v. 18, no. 2-3, p. 235-248.

Nicol, A., Walsh, J., Watterson, J., and Underhill, J., 1997, Displacement rates of normal faults: Nature, v. 390, no. 6656, p. 157.

Nixon, C. W., Bull, J. M., and Sanderson, D. J., 2014, Localized vs distributed deformation associated with the linkage history of an active normal fault, Whakatane Graben, New Zealand: Journal of Structural Geology, v. 69, p. 266-280.

Nixon, C. W., McNeill, L. C., Bull, J. M., Bell, R. E., Gawthorpe, R. L., Henstock, T. J., Christodoulou, D., Ford, M., Taylor, B., Sakellariou, D., Ferentinos, G., Papatheodorou, G., Leeder, M. R., Collier, R. E. L., Goodliffe, A. M., Sachpazi, M., and Kranis, H., 2016, Rapid spatiotemporal variations in rift structure during development of the Corinth Rift, central Greece: Tectonics, v. 35, no. 5, p. 1225-1248.

Ostanin, I., Anka, Z., di Primio, R., and Bernal, A., 2013, Hydrocarbon plumbing systems above the Snøhvit gas field: structural control and implications for thermogenic methane leakage in the Hammerfest Basin, SW Barents Sea: Marine and Petroleum Geology, v. 43, p. 127-146.

Owen, S., Segall, P., Freymueller, J., Mikijus, A., Denlinger, R., Árnadóttir, T., Sako, M., and Bürgmann, R., 1995, Rapid Deformation of the South Flank of Kilauea Volcano, Hawaii: Science, v. 267, no. 5202, p. 1328-1332.

Palmquist, J. C., 1978, Laramide structures and basement block faulting: Two examples from the Big Horn Mountains, Wyoming, *in* Matthews, I. I. I. V., ed., Laramide Folding Associated with Basement Block Faulting in the Western United States, Geological Society of America.

Panien, M., Schreurs, G., and Pfiffner, A., 2006, Mechanical behaviour of granular materials used in analogue modelling: insights from grain characterisation, ring-shear tests and analogue experiments: Journal of Structural Geology, v. 28, no. 9, p. 1710-1724.

Papanikolaou, I. D., and Roberts, G. P., 2007, Geometry, kinematics and deformation rates along the active normal fault system in the southern Apennines: Implications for fault growth: Journal of Structural Geology, v. 29, no. 1, p. 166-188.

Parfitt, E. A., and Peacock, D. C. P., 2001, Faulting in the South Flank of Kilauea Volcano, Hawai'i: Journal of Volcanology and Geothermal Research, v. 106, no. 3–4, p. 265-284.

Pascoe, R., Hooper, R., Storhaug, K., and Harper, H., 1999, Evolution of extensional styles at the southern termination of the Nordland Ridge, Mid-Norway: a response to variations in coupling above Triassic salt: Petroleum Geology Conference Series, v. 5, p. 83-90.

Patton, T. L., Logan, J. M., and Friedman, M., 1998, Experimentally generated normal faults in single-layer and multilayer limestone specimens at confining pressure: Tectonophysics, v. 295, no. 1, p. 53-77.

Patton, T. L., 2004, Numerical models of growth-sediment development above an active monocline: Basin Research, v. 16, p. 25-39.

Paul, D., and Mitra, S., 2015, Fault patterns associated with extensional fault-propagation folding: Marine and Petroleum Geology, v. 67, p. 120-143.

Peacock, D. C. P., and Parfitt, E. A., 2002, Active relay ramps and normal fault propagation on Kilauea Volcano, Hawaii: Journal of Structural Geology, v. 24, no. 4, p. 729-742.

Podolsky, D. M., and Roberts, G. P., 2008, Growth of the volcano-flank Koa'e fault system, Hawaii: Journal of Structural Geology, v. 30, no. 10, p. 1254-1263.

Putz-Perrier, M. W., and Sanderson, D. J., 2009, Distribution of faults and extensional strain in fractured carbonates of the North Malta Graben: AAPG bulletin, v. 94, no. 4, p. 435-456.

Richard, P., 1989, Champs de failles au dessus d'un décrochement de socle : modélisation expérimentale: Université Rennes 1.

Richard, P., 1991, Experiments on faulting in a two-layer cover sequence overlying a reactivated basement fault with oblique-slip: Journal of Structural Geology, v. 13, no. 4, p. 459-469.

Richardson, N. J., Underhill, J. R., and Lewis, G., 2005, The role of evaporite mobility in modifying subsidence patterns during normal fault growth and linkage, Halten Terrace, Mid-Norway: Basin Research, v. 17, no. 2, p. 203-223.

Ringnér, M., 2008, What is principal component analysis?: Nature Biotechnology, v. 26, p. 303.

Roche, V., Homberg, C., and Rocher, M., 2012, Fault displacement profiles in multilayer systems: from fault restriction to fault propagation: Terra Nova, v. 24, no. 6, p. 499-504.

Rowan, M. G., and Kligfield, R., 1989, Cross section restoration and balancing as aid to seismic interpretation in extensional terranes: AAPG bulletin, v. 73, no. 8, p. 955-966.

Rowan, M. G., and Ratliff, R. A., 2012, Cross-section restoration of salt-related deformation: Best practices and potential pitfalls: Journal of Structural Geology, v. 41, p. 24-37.

Schellart, W. P., and Strak, V., 2016, A review of analogue modelling of geodynamic processes: Approaches, scaling, materials and quantification, with an application to subduction experiments: Journal of Geodynamics, v. 100, p. 7-32.

Schöpfer, M. P., Childs, C., and Walsh, J. J., 2007, Two-dimensional distinct element modeling of the structure and growth of normal faults in multilayer sequences: 2. Impact of confining pressure and strength contrast on fault zone geometry and growth: Journal of Geophysical Research: Solid Earth (1978–2012), v. 112, no. B10.

Schreurs, G., Buiter, S. J. H., Boutelier, D., Corti, G., Costa, E., Cruden, A. R., Daniel, J.-M., Hoth, S., Koyi, H. A., Kukowski, N., Lohrmann, J., Ravaglia, A., Schlische, R. W., Withjack, M. O., Yamada, Y., Cavozzi, C., Del Ventisette, C., Brady, J. A. E., Hoffmann-

Rothe, A., Mengus, J.-M., Montanari, D., and Nilforoushan, F., 2006, Analogue benchmarks of shortening and extension experiments: Geological Society, London, Special Publications, v. 253, no. 1, p. 1-27.

Sharp, I., Gawthorpe, R., Armstrong, B., and Underhill, J., 2000a, Propagation history and passive rotation of mesoscale normal faults: implications for synrift stratigraphic development: Basin Research, v. 12, no. 3-4, p. 285-305.

Sharp, I. R., Gawthorpe, R. L., Underhill, J. R., and Gupta, S., 2000b, Fault-propagation folding in extensional settings: Examples of structural style and synrift sedimentary response from the Suez rift, Sinai, Egypt: Geological Society of America Bulletin, v. 112, no. 12, p. 1877-1899.

Skuce, A. G., 1996, Forward modelling of compaction above normal faults: an example from the Sirte Basin, Libya: Geological Society, London, Special Publications, v. 99, no. 1, p. 135-146.

Smart, K. J., and Ferrill, D. A., 2018, Discrete element modeling of extensional fault-related monocline formation: Journal of Structural Geology, v. 115, p. 82-90.

Soliva, R., and Benedicto, A., 2005, Geometry, scaling relations and spacing of vertically restricted normal faults: Journal of Structural Geology, v. 27, no. 2, p. 317-325.

Soliva, R., Schultz, R. A., and Benedicto, A., 2005, Three-dimensional displacement-length scaling and maximum dimension of normal faults in layered rocks: Geophysical Research Letters, v. 32, no. 16.

Stearns, D. W., 1978, Faulting and forced folding in the Rocky Mountains foreland: Geological Society of America Memoirs, v. 151, p. 1-38.

Stewart, S., and Argent, J., 2000, Relationship between polarity of extensional fault arrays and presence of detachments: Journal of Structural Geology, v. 22, no. 6, p. 693-711.

Stewart, S., 2007, Salt tectonics in the North Sea Basin: a structural style template for seismic interpreters: Geological Society, London, Special Publications, v. 272, p. 361.

Stewart, S. A., Harvey, M. J., Otto, S. C., and Weston, P. J., 1996, Influence of salt on fault geometry: examples from the UK salt basins: Geological Society, London, Special Publications, v. 100, no. 1, p. 175-202.

Stewart, S. A., Ruffell, A. H., and Harvey, M. J., 1997, Relationship between basement-linked and gravity-driven fault systems in the UKCS salt basins: Marine and Petroleum Geology, v. 14, no. 5, p. 581-604.

Stewart, S. A., 1999, Geometry of thin-skinned tectonic systems in relation to detachment layer thickness in sedimentary basins: Tectonics, v. 18, no. 4, p. 719-732.

Tankard, A., and Welsink, H., 1987, Extensional tectonics and stratigraphy of Hibernia oil field, Grand Banks, Newfoundland: AAPG Bulletin, v. 71, no. 10, p. 1210-1232.

Tavani, S., Carola, E., Granado, P., Quintà, A., and Muñoz, J. A., 2013, Transpressive inversion of a Mesozoic extensional forced fold system with an intermediate décollement level in the Basque-Cantabrian Basin (Spain): Tectonics, v. 32, no. 2, p. 146-158.

Tavani, S., and Granado, P., 2014, Along-strike evolution of folding, stretching and breaching of supra-salt strata in the Plataforma Burgalesa extensional forced fold system (northern Spain): Basin Research, p. 1-13.

Tavani, S., Balsamo, F., and Granado, P., 2018, Petroleum system in supra-salt strata of extensional forced-folds: A case-study from the Basque-Cantabrian basin (Spain): Marine and Petroleum Geology, v. 96, p. 315 - 330.

Trippanera, D., Acocella, V., Ruch, J., and Abebe, B., 2015, Fault and graben growth along active magmatic divergent plate boundaries in Iceland and Ethiopia: Tectonics, v. 34, no. 11, p. 2318-2348.

Tsuneishi, Y., 1978, Geological and Experimental Studies on Mechanism of Block Faulting.

Tvedt, A. B. M., Rotevatn, A., and Jackson, C. A. L., 2016, Supra-salt normal fault growth during the rise and fall of a diapir: Perspectives from 3D seismic reflection data, Norwegian North Sea: Journal of Structural Geology, v. 91, p. 1-26.

Uphoff, T. L., 2005, Subsalt (pre-Jurassic) exploration play in the northern Lusitanian basin of Portugal: AAPG bulletin, v. 89, no. 6, p. 699-714.

van Gent, H., Urai, J. L., and de Keijzer, M., 2011, The internal geometry of salt structures – A first look using 3D seismic data from the Zechstein of the Netherlands: Journal of Structural Geology, v. 33, no. 3, p. 292-311.

Vasquez, L., Nalpas, T., Ballard, J.-F., De Veslud, C. L. C., Simon, B., Dauteuil, O., and Du Bernard, X., 2018, 3D geometries of normal faults in a brittle-ductile sedimentary cover: Analogue modelling: Journal of Structural Geology, v. 112, p. 29-38.

Vendeville, B., 1987, Champs de failles et tectonique en extension: Modélisation expérimentale: Université Rennes 1.

Vendeville, B. C., Ge, H., and Jackson, M. P. A., 1995, Scale models of salt tectonics during basement-involved extension: Petroleum Geoscience, v. 1, no. 2, p. 179-183.

Vita-Finzi, C., and King, G., 1985, The seismicity, geomorphology and structural evolution of the Corinth area of Greece: Philosophical Transactions of the Royal Society of London A: Mathematical, Physical and Engineering Sciences, v. 314, no. 1530, p. 379-407.

Walker, R., Holdsworth, R., Imber, J., Faulkner, D., and Armitage, P., 2013, Fault zone architecture and fluid flow in interlayered basaltic volcaniclastic-crystalline sequences: Journal of Structural Geology, v. 51, p. 92-104.

Walker, R. J., Holdsworth, R. E., Imber, J., and Ellis, D., 2012, Fault-zone evolution in layered basalt sequences: A case study from the Faroe Islands, NE Atlantic margin: Geological Society of America Bulletin, v. 124, no. 7-8, p. 1382-1393.

Walsh, J. J., and Watterson, J., 1988, Analysis of the relationship between displacements and dimensions of faults: Journal of Structural geology, v. 10, no. 3, p. 239-247.

Walsh, J. J., Childs, C., Imber, J., Manzocchi, T., Watterson, J., and Nell, P. A. R., 2003, Strain localisation and population changes during fault system growth within the Inner Moray Firth, Northern North Sea: Journal of Structural Geology, v. 25, no. 2, p. 307-315.

Warsitzka, M., Kley, J., and Kukowski, N., 2015, Analogue experiments of salt flow and pillow growth due to basement faulting and differential loading: Solid Earth, v. 6, no. 1, p. 9.

Warsitzka, M., Kley, J., Jähne-Klingberg, F., and Kukowski, N., 2017, Dynamics of prolonged salt movement in the Glückstadt Graben (NW Germany) driven by tectonic and sedimentary processes: International Journal of Earth Sciences, v. 106, no. 1, p. 131-155.

Weinberg, D. M., 1979, Experimental folding of rocks under confining pressure: Part VII. Partially scaled models of drape folds: Tectonophysics, v. 54, no. 1, p. 1-24.

White, I. R., and Crider, J. G., 2006, Extensional fault-propagation folds: mechanical models and observations from the Modoc Plateau, northeastern California: Journal of Structural Geology, v. 28, no. 7, p. 1352-1370.

Wibberley, C. A. J., Yielding, G., and Di Toro, G., 2008, Recent advances in the understanding of fault zone internal structure: a review: Geological Society, London, Special Publications, v. 299, no. 1, p. 5-33.

Wilkins, S. J., and Gross, M. R., 2002, Normal fault growth in layered rocks at Split Mountain, Utah: influence of mechanical stratigraphy on dip linkage, fault restriction and fault scaling: Journal of Structural Geology, v. 24, no. 9, p. 1413-1429.

Willsey, S. P., Umhoefer, P. J., and Hilley, G. E., 2002, Early evolution of an extensional monocline by a propagating normal fault: 3D analysis from combined field study and numerical modeling: Journal of Structural Geology, v. 24, no. 4, p. 651-669.

Wilson, P., Elliott, G. M., Gawthorpe, R. L., Jackson, C. A.-L., Michelsen, L., and Sharp, I. R., 2013, Geometry and segmentation of an evaporite-detached normal fault array: 3D seismic analysis of the southern Bremstein Fault Complex, offshore mid-Norway: Journal of Structural Geology, v. 51, p. 74-91.

Wilson, P., Elliott, G. M., Gawthorpe, R. L., Jackson, C. A.-L., Michelsen, L., and Sharp, I. R., 2015, Lateral variation in structural style along an evaporite-influenced rift fault system in the Halten Terrace, Norway: Influence of basement structure and evaporite facies: Journal of Structural Geology, v. 79, p. 110-123.

Withjack, M. O., Meisling, K. E., and Russell, L. R., 1989, Forced Folding and Basement-Detached Normal Faulting in the Haltenbanken Area, Offshore Norway: Chapter 37: North Sea and Barents Shelf, *in* Tankard, A. J., and Balkwill, H. R., eds., Extensional Tectonics and Stratigraphy of the North Atlantic Margins, AAPG Memoir 46, p. 567-575.

Withjack, M. O., Olson, J., and Peterson, E., 1990, Experimental models of extensional forced folds: AAPG Bulletin, v. 74, no. 7, p. 1038-1054.

Withjack, M. O., and Callaway, S., 2000, Active normal faulting beneath a salt layer: an experimental study of deformation patterns in the cover sequence: AAPG bulletin, v. 84, no. 5, p. 627-651.

Withjack, M. O., Schlische, R. W., and Olsen, P. E., 2002, Rift-basin structure and its influence on sedimentary systems: Society for Sedimentary Geology Special Publication, v. 73, p. 57-81.

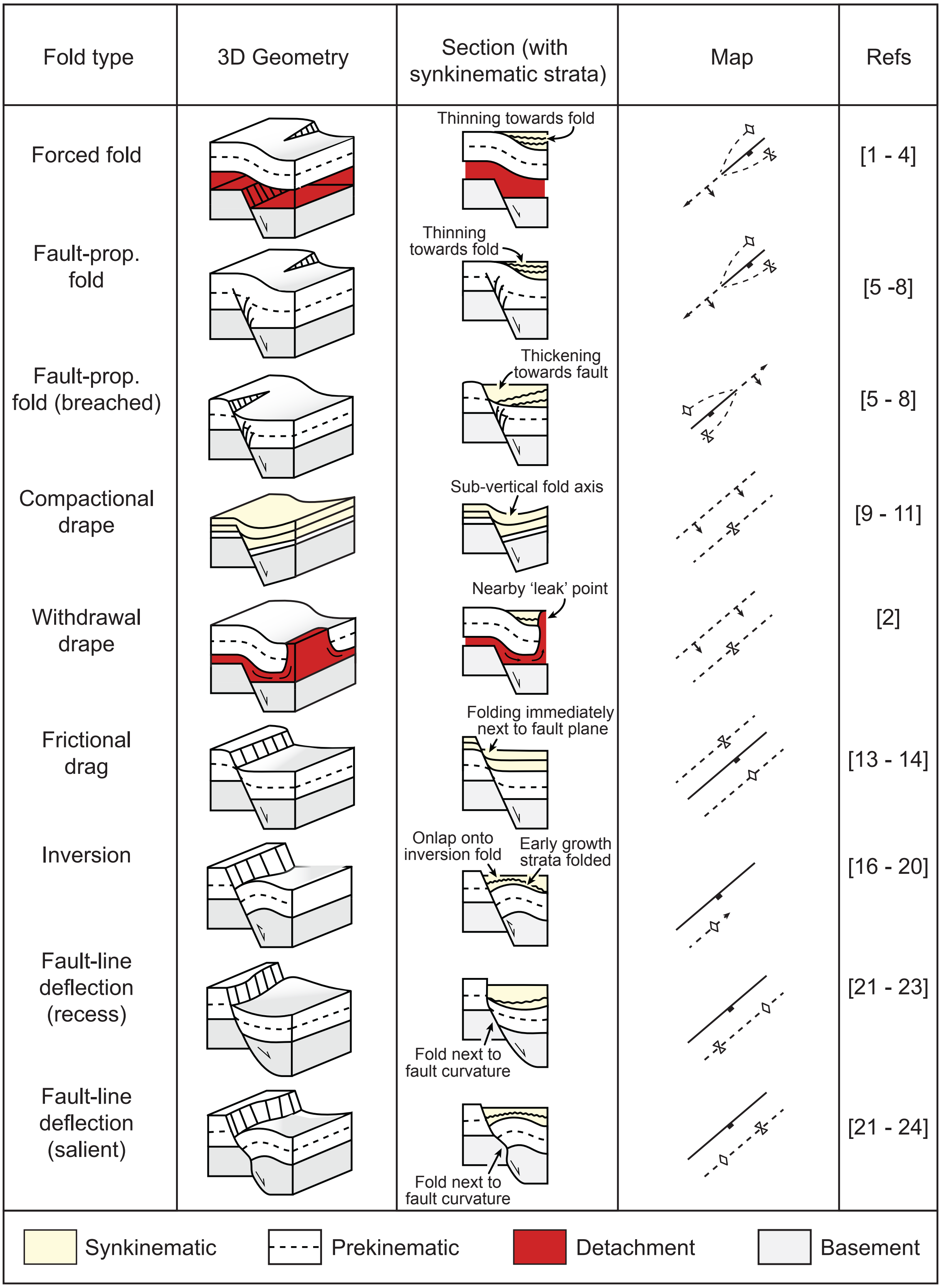
Fold type
3D Geometry
Section (with synkinematic strata)
Map
Refs
Forced fold
Thinning towards fold
[1 - 4]
Fault-prop. fold
Thinning towards fold
[5 -8]
Fault-prop. fold (breached)
Thickening towards fault
[5 - 8]
Compactional drape
Sub-vertical fold axis
[9 - 11]
Withdrawal drape
Nearby 'leak' point
[2]
Frictional drag
Folding immediately next to fault plane
[13 - 14]
Inversion
Onlap onto inversion fold
Early growth strata folded
[16 - 20]
Fault-line deflection (recess)
Fold next to fault curvature
[21 - 23]
Fault-line deflection (salient)
Fold next to fault curvature
[21 - 24]
Synkinematic
Prekinematic
Detachment
Basement

Figure 1 - Fault-related folds in extensional settings. See Appendix A for brief description of how each fold is developed. References are as follows: 1 – Laubscher, 1982; 2 – Withjack and Callaway, 2000; 3 - Ford et al., 2007; 4 – Lewis et al., 2013; 5 – Withjack et al., 1990; 6 – Gawthorpe et al., 1997; 7 – Sharp et al., 2000; 8 – Jackson et al., 2006; 9 – Thomson and Underhill, 1993; 10 - Skuce, 1996; 11- Faerseth and Lien, 2002; 12 – Billings, 1972; 13 – Resor, 2008; 14- Davis et al., 2011; 15 – Spahic et al., 2013; 16 – Badley et al., 1989; 17 – Mitra, 1993; 18 – Mitra and Islam, 1994; 19 – Turner and Williams, 2004; 20 – Jackson et al., 2013; 21 – Wheeler, 1939; 22 – Stewart and Hancock, 1991; 23 - Ehrlich and Gabrielsen, 2004; 24 – Machette et al., 1991. Synkinematic and prekinematic strata are also shown. Example detachments could include but are not limited to, salt (or evaporitic sequences) and overpressured shale.

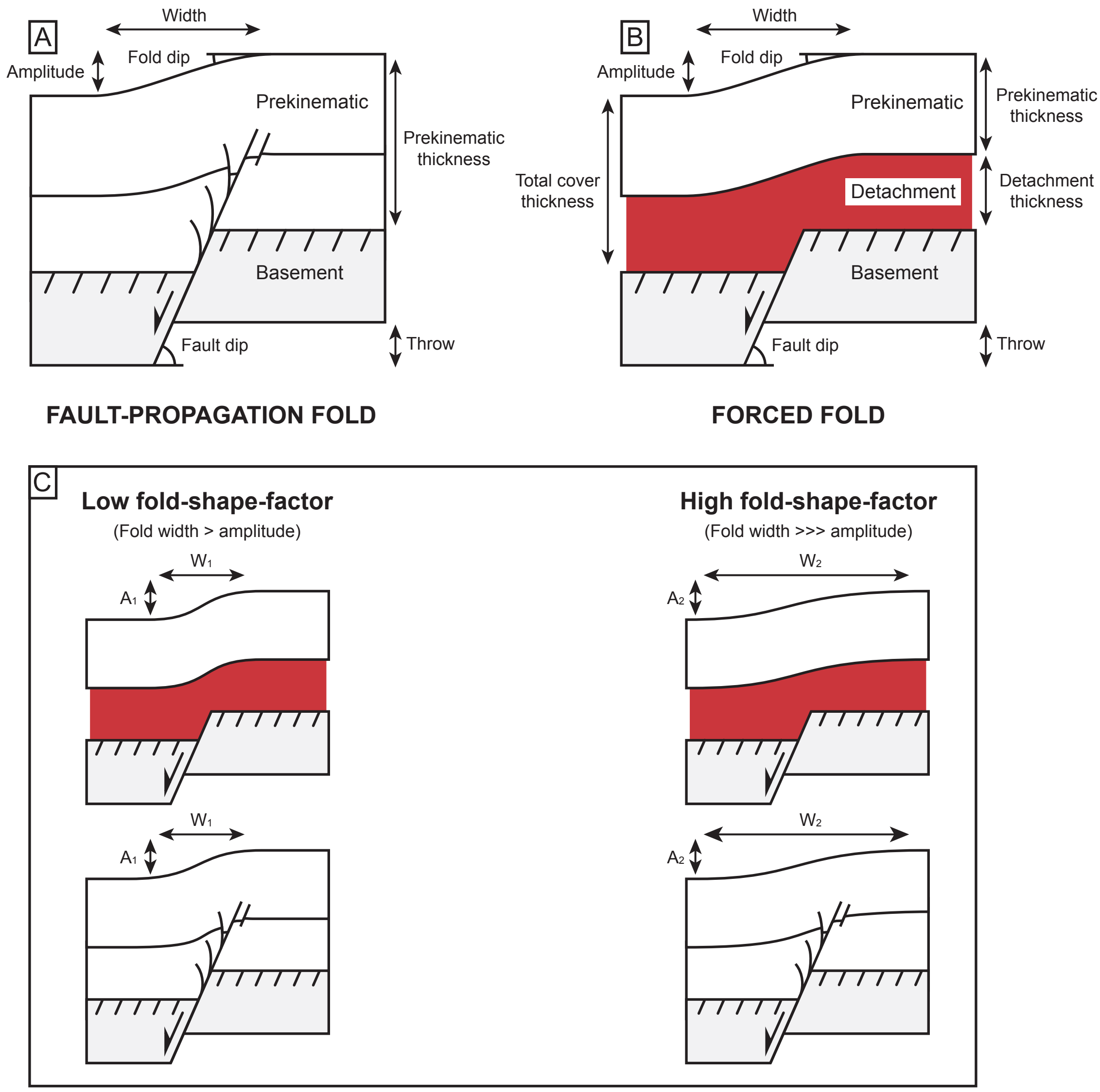

Figure 2 - Schematic, nomenclature and measured parameters for forced folds (A) and fault-propagation folds (B), showing the transition between faulting and folding. Modified after Withjack et al. (1990) and Stewart et al. (1996). Fold-shape-factor (FSF) = fold width/fold amplitude. Wide folds with small amplitudes have large FSF values, narrow folds with large amplitudes have low FSF values. Cover-detachment ratio (C:D) = prekinematic thickness/detachment thickness. Sequences with thick prekinematic strata and thin detachments have high C:D ratios. Sequences with very thin prekinematic strata and thick detachments have low C:D ratios. (C) Examples of high and low fold-shape-factor growth folds are also shown. A_1 - A_2 and W_1 - W_2 are widths and amplitudes for the different folds. Note that $A_1 = A_2$, but $W_1 < W_2$.

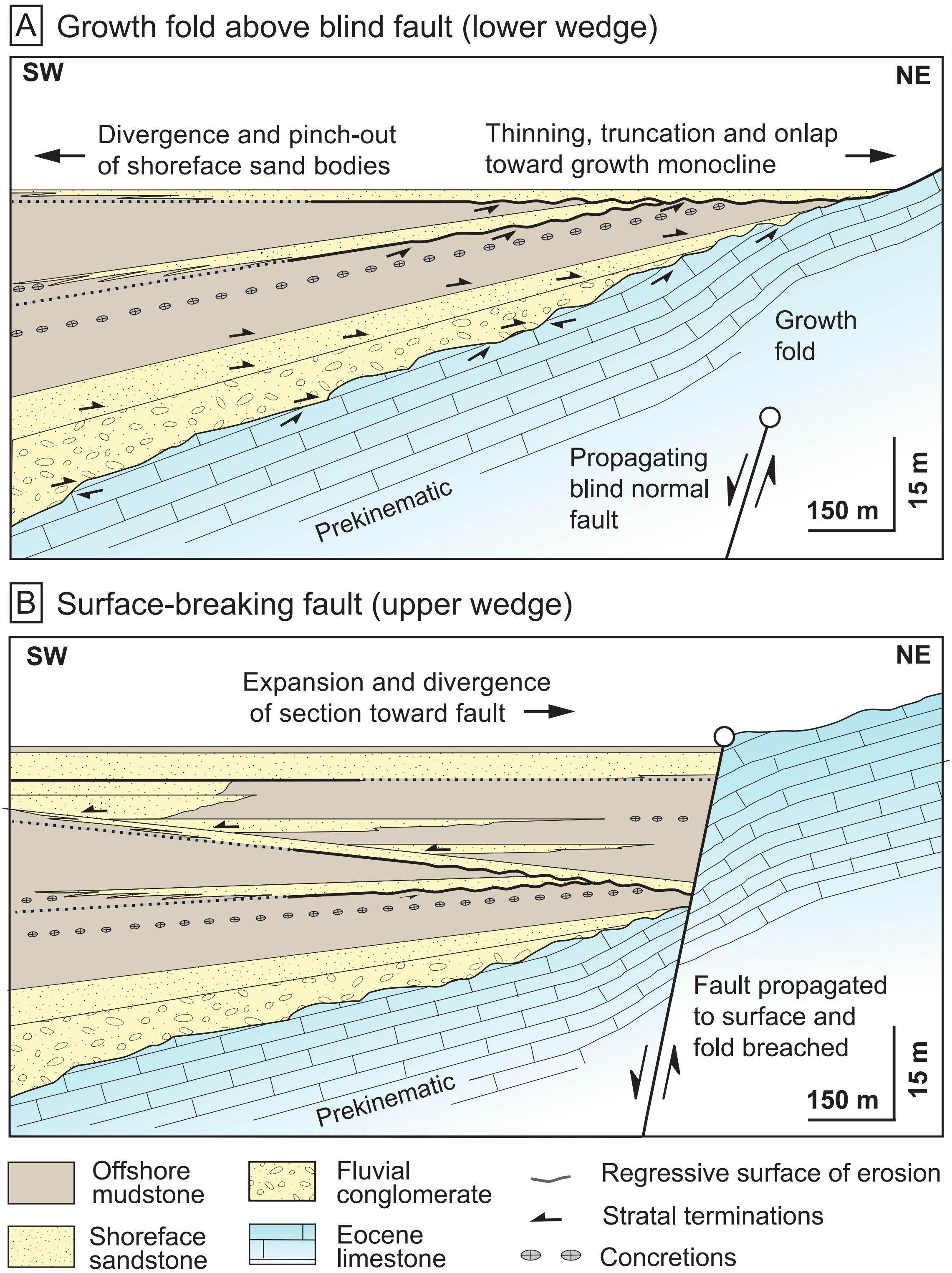
A
Growth fold above blind fault (lower wedge)
SW
NE
Divergence and pinch-out of shoreface sand bodies
Thinning, truncation and onlap toward growth monocline
Growth fold
Propagating blind normal fault
Prekinematic
150 m
15 m
B
Surface-breaking fault (upper wedge)
SW
NE
Expansion and divergence of section toward fault
Fault propagated to surface and fold breached
Prekinematic
150 m
15 m
Offshore mudstone
Shoreface sandstone
Fluvial conglomerate
Eocene limestone
Regressive surface of erosion
Stratal terminations
Concretions

Figure 3 - Tectonostratigraphic evolution of the Baba-Sidri fault zone, Gulf of Suez. (A) Synkinematic sediments onlap onto the fault-propagation fold above a blind fault tip and thickening basinwards. (B) The fold is breached by the propagating normal fault and sediments thicken towards the fault. Modified from Gawthorpe et al. 1997.

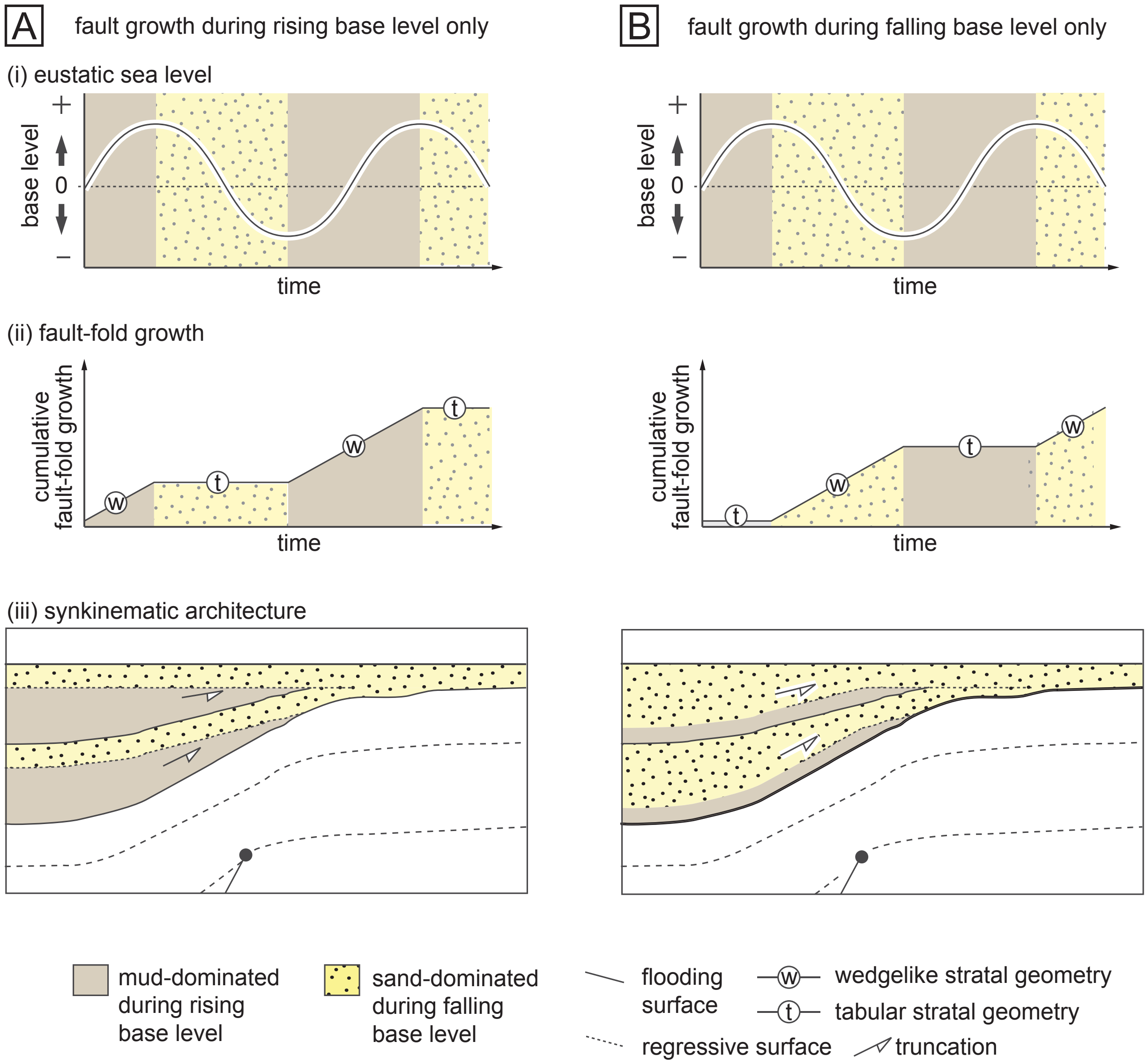

Figure 4 - How growth folds and eustasy interact to control synkinematic stratal architecture. Two end-members scenarios, depicting shallow marine shoreface sandstone deposition during falling base level (forced regression) are illustrated. (A) Surfaceward fault propagation and fold amplification during rising base level only results in basinward thickening of mudstone-dominated sediments. Shore face sands are deposited during times of tectonic quiescence, hence are tabular and truncate underlying mudstones. (B) Surfaceward fault propagation and fold amplification during falling base level results in basinward thickening of the sandstone units. Mudstones are deposited during times of tectonic quiescence, hence are tabular and are truncated near the fold crest. Unconformities near the fold may pass basinward into correlative conformities. Modified from Lewis et al. (2015).

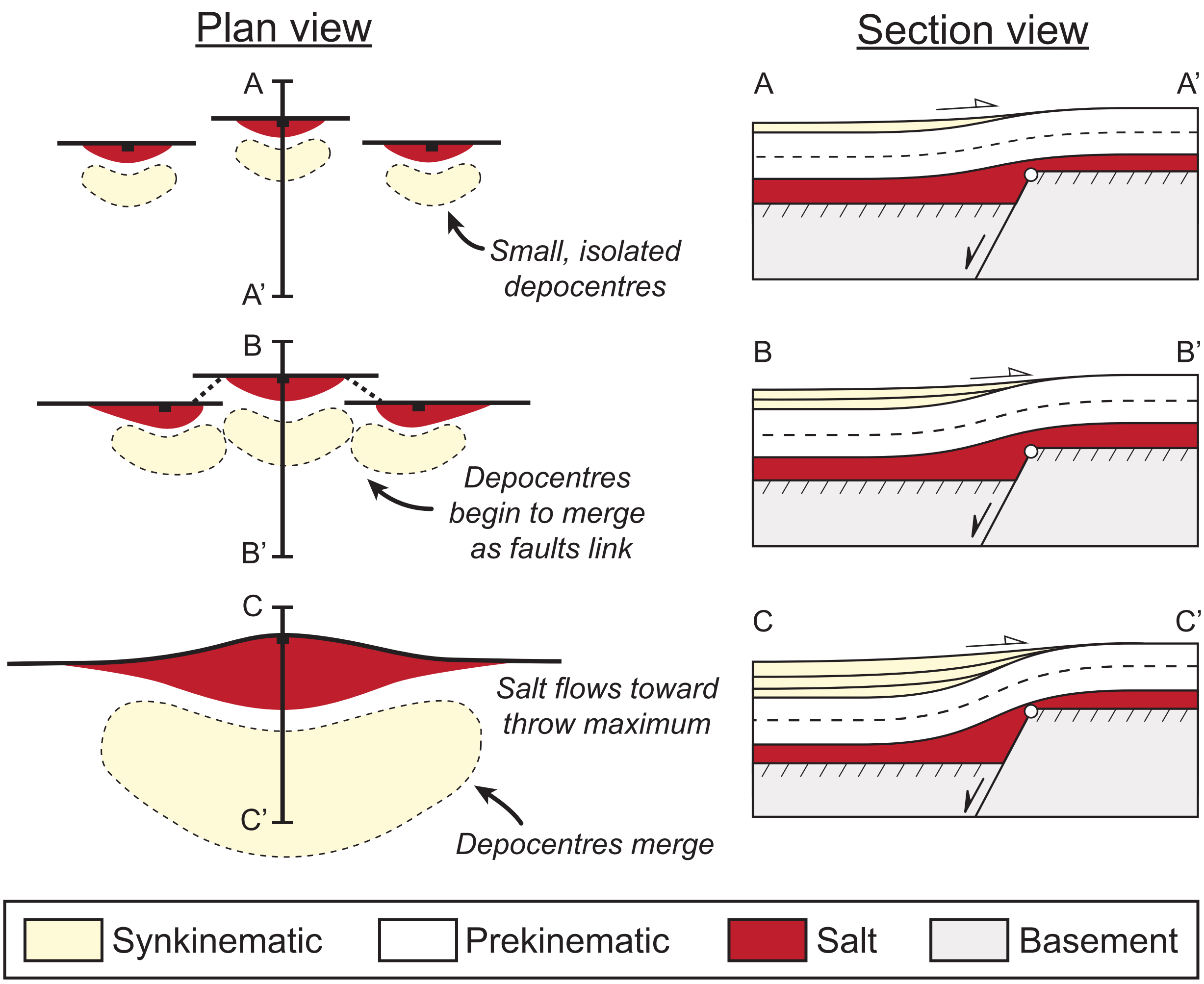

Figure 5 - Schematic diagram illustrating the evolution of salt-influenced fault-fold systems and their associated sedimentary depocentres. Modified from Richardson et al., 2005.

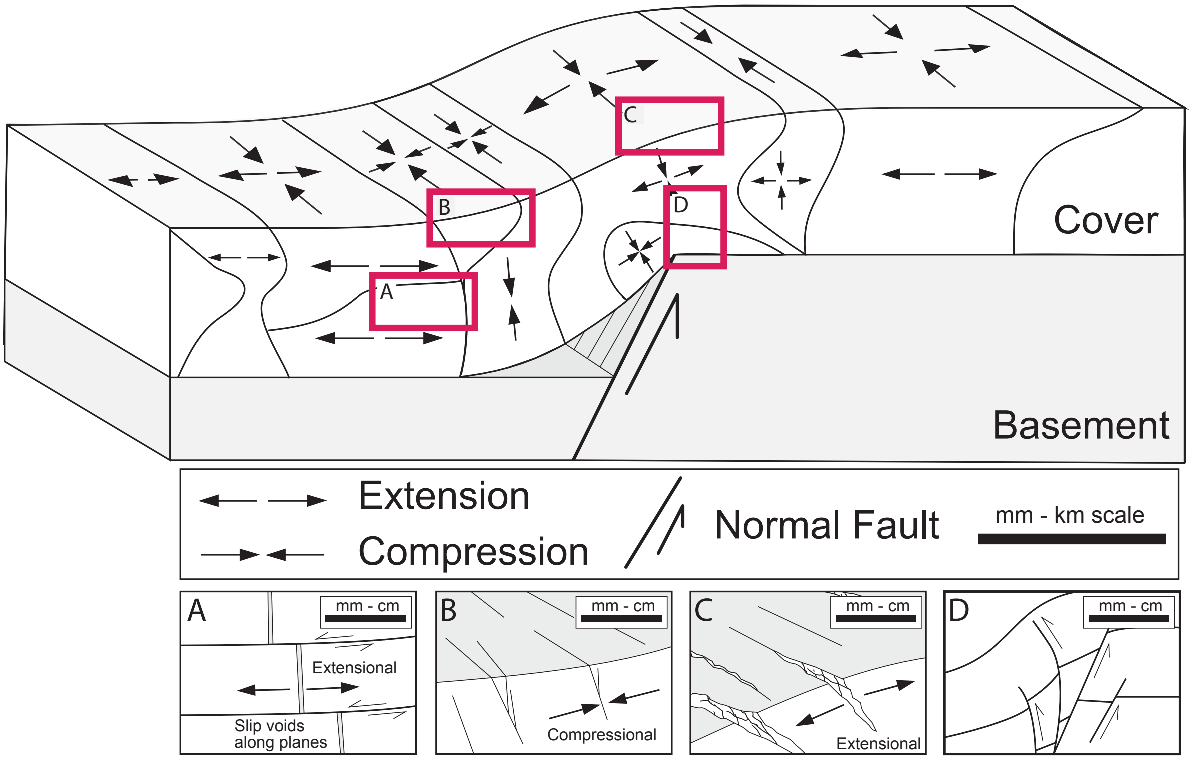

Figure 6 - Block diagram of a growth fold developed above a propagating basement normal fault. The fold has been divided into zones according to extensional or contractional strain, modified from Ameen, 1988 and Ameen, 1990. Idealised secondary deformation features are superimposed: (A) layer-parallel slip surfaces and slip voids, (B) compaction bands and closed fractures, (C) dilational fractures, and (D) secondary reverse faults. Secondary deformation inspired by observations from field studies, including the Gulf of Suez (e.g. Sharp et al., 2000a; b; Jackson et al., 2006), Brushy Canyon (e.g. Ferrill et al., 2007; Smart et al., 2010), and the Pyrenees (e.g. Tavani et al., 2018), and physical models (e.g. Withjack et al., 1990; Withjack and Callaway, 2000; Jin and Groshong, 2006; Paul and Mitra, 2015). This is not an exhaustive list of possible features, just of those traditionally reported from field studies – see text for details.

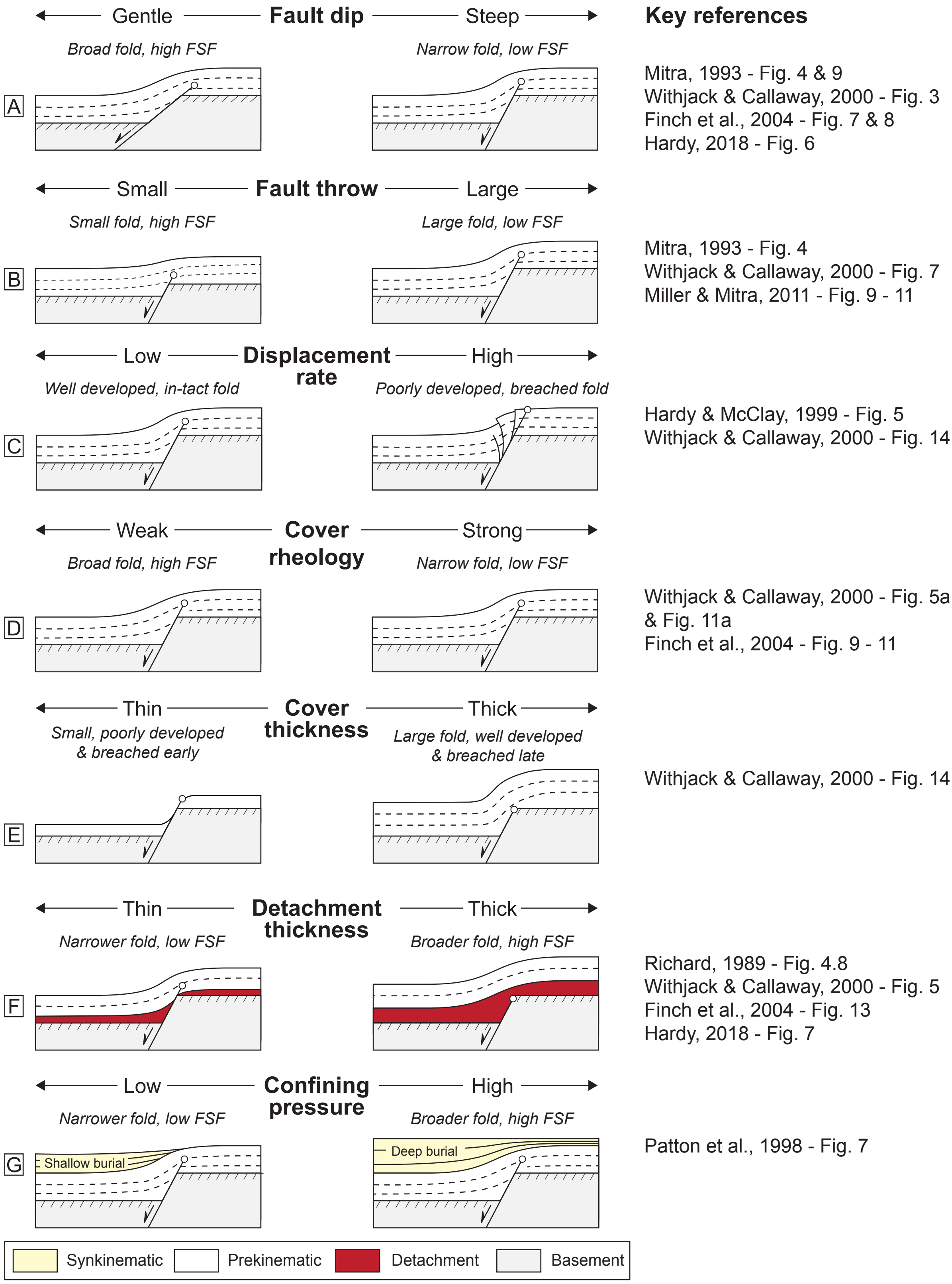

Figure 7 - Controls on growth fold shape and size as identified by physical and numerical models. Displacement rate (C), is also linked to the strain rate and propagation rate of the upper fault tip in Withjack and Callaway (2000).

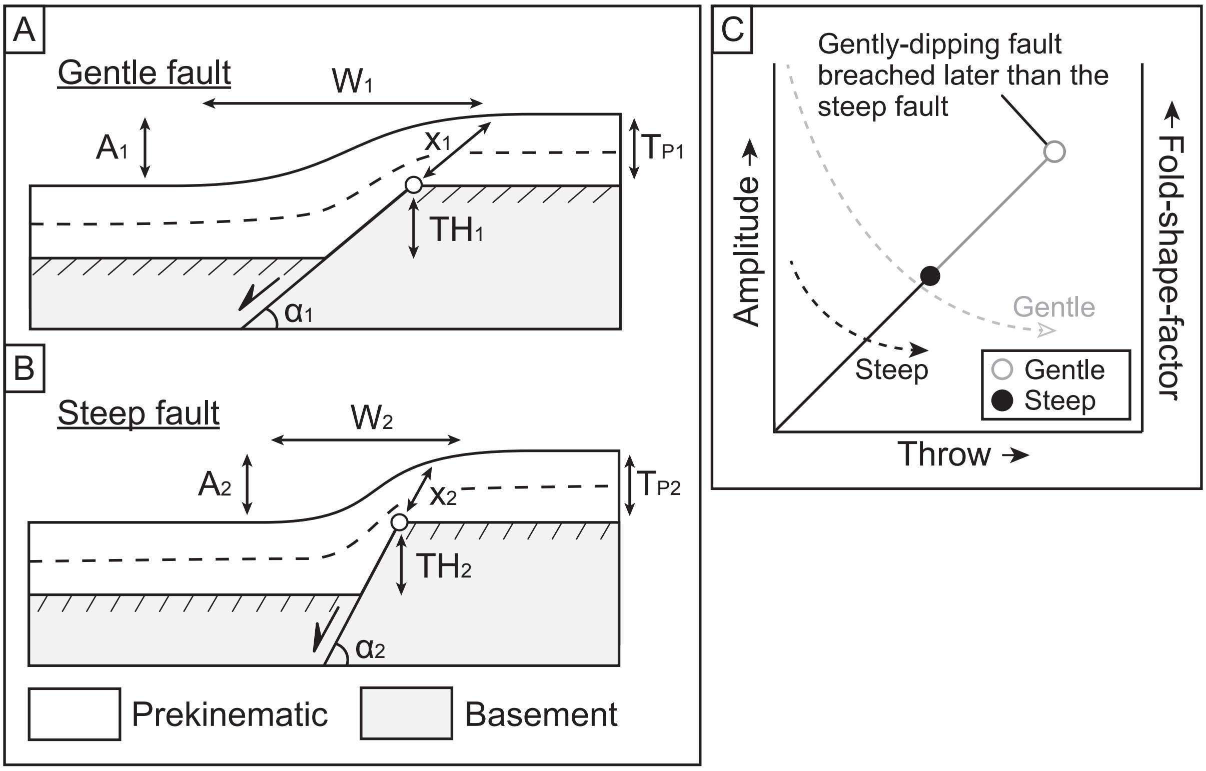

Figure 8. - Schematic showing the rapid breach of growth folds above a steeply-dipping fault (A) compared to a shallowly-dipping fault (B). The idealized geometry of the developing fold is also shown. (C) The amplitude (solid lines) for a gentle and steep fault increase with throw. Where faults breach the fold, a circle is plotted. The steeply-dipping fault breaches its associated fold more quickly than for a gently-dipping fault as there is a larger rock volume infront of the propagating upper normal fault tip i.e. $x_1 >> x_2$. The fold-shape-factor is shown by the dashed lines, and both decrease with increasing throw on the basement fault. Symbology for the parameters are also shown. Note how the fold associated with the steeply-dipping fault is breached earlier than the gently-dipping fault, and how the FSF decreases as the fold grows.

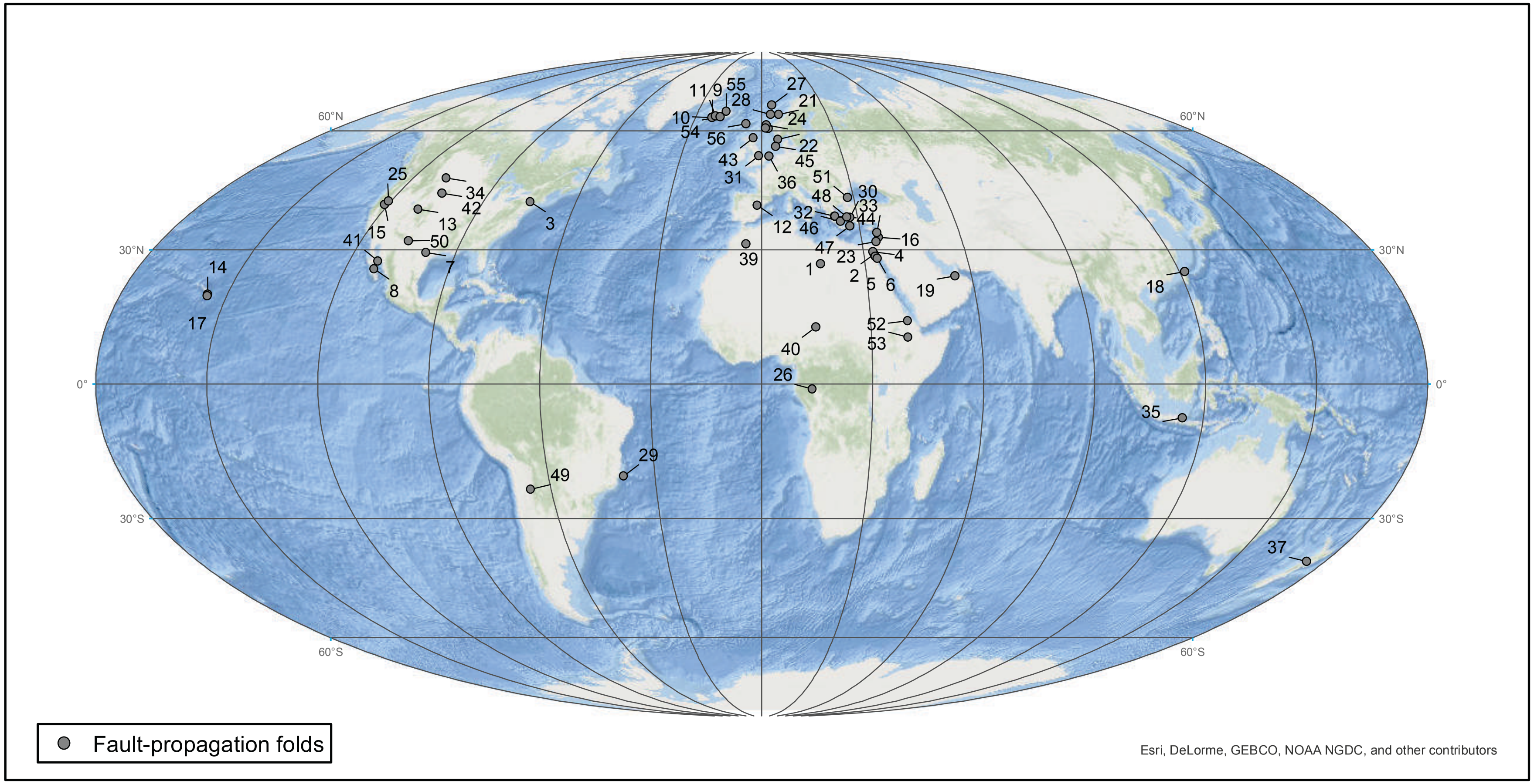

Figure 9 - Distribution of fault-propagation folds. See Appendix B for locations.

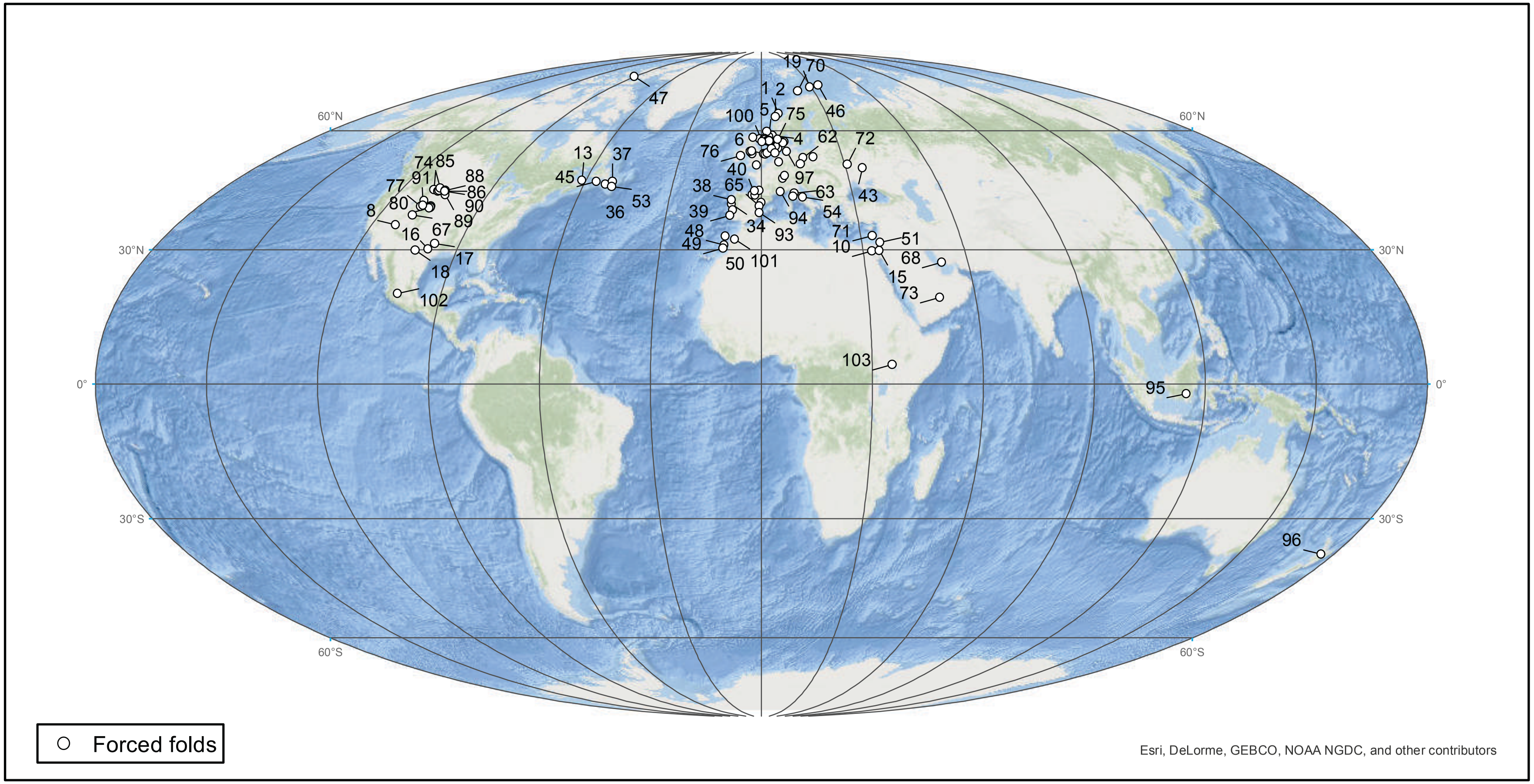

Figure 10. - Distribution of forced folds. See Appendix C for locations.

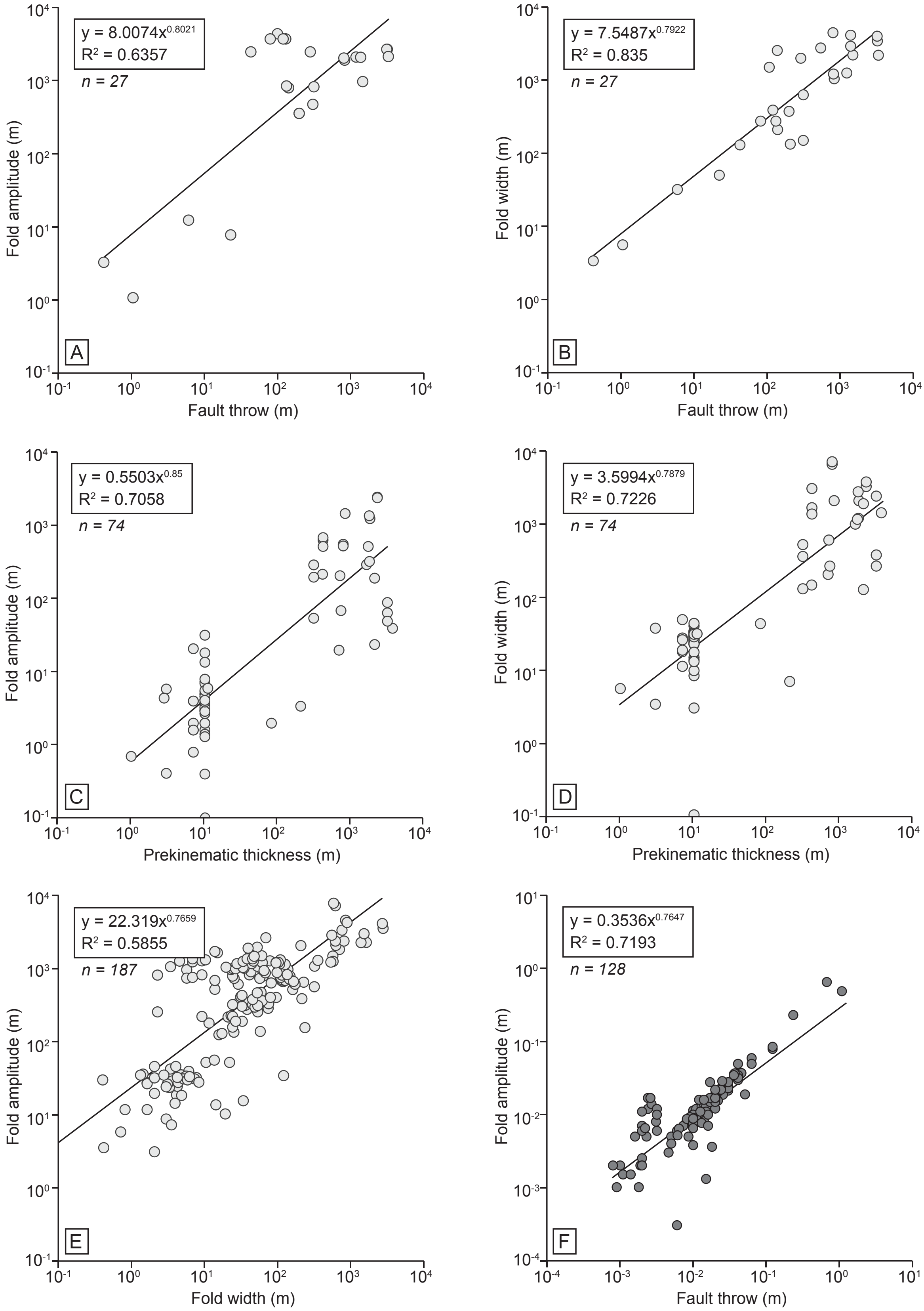

A
y = 8.0074x^0.8021
R² = 0.6357
n = 27
Fold amplitude (m)
Fault throw (m)
B
y = 7.5487x^0.7922
R² = 0.835
n = 27
Fold width (m)
Fault throw (m)
C
y = 0.5503x^0.85
R² = 0.7058
n = 74
Fold amplitude (m)
Prekinematic thickness (m)
D
y = 3.5994x^0.7879
R² = 0.7226
n = 74
Fold width (m)
Prekinematic thickness (m)
E
y = 22.319x^0.7659
R² = 0.5855
n = 187
Fold amplitude (m)
Fold width (m)
F
y = 0.3536x^0.7647
R² = 0.7193
n = 128
Fold amplitude (m)
Fault throw (m)

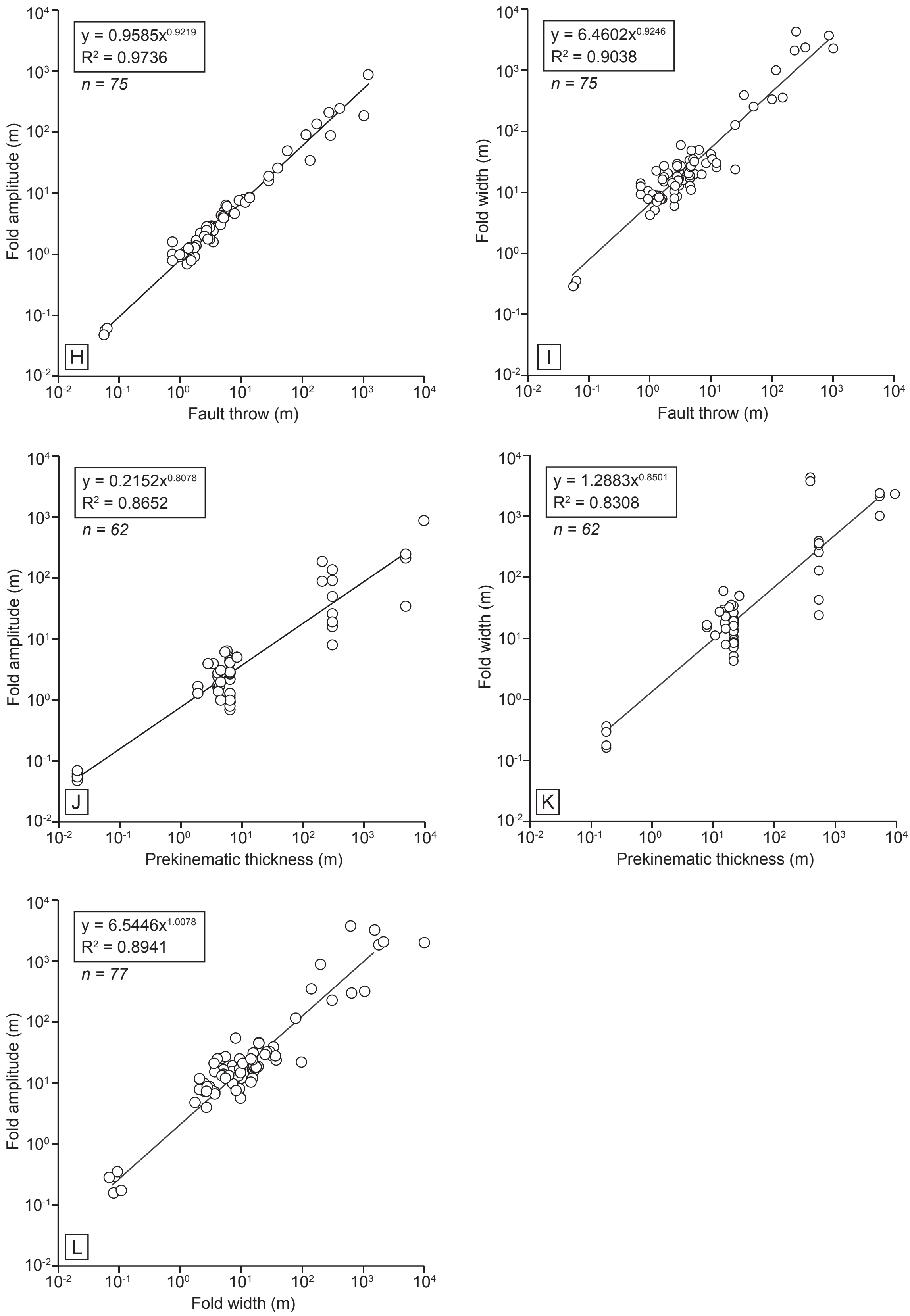
y = 0.9585x^0.9219
R² = 0.9736
n = 75
Fold amplitude (m)
Fault throw (m)
H
y = 6.4602x^0.9246
R² = 0.9038
n = 75
Fold width (m)
Fault throw (m)
I
y = 0.2152x^0.8078
R² = 0.8652
n = 62
Fold amplitude (m)
Prekinematic thickness (m)
J
y = 1.2883x^0.8501
R² = 0.8308
n = 62
Fold width (m)
Prekinematic thickness (m)
K
y = 6.5446x^1.0078
R² = 0.8941
n = 77
Fold amplitude (m)
Fold width (m)
L

Figure 11 - Moderate-to-strong correlations for fault-propagation folds in nature (A – E; light grey circles), physical models (F; dark grey circles) and numerical models (H-L; white circles). The best-fit regression, correlation coefficient (R_2) and number of observations (n) are also shown. See Table 2 for further details. See Fig. 2 for parameter descriptions.

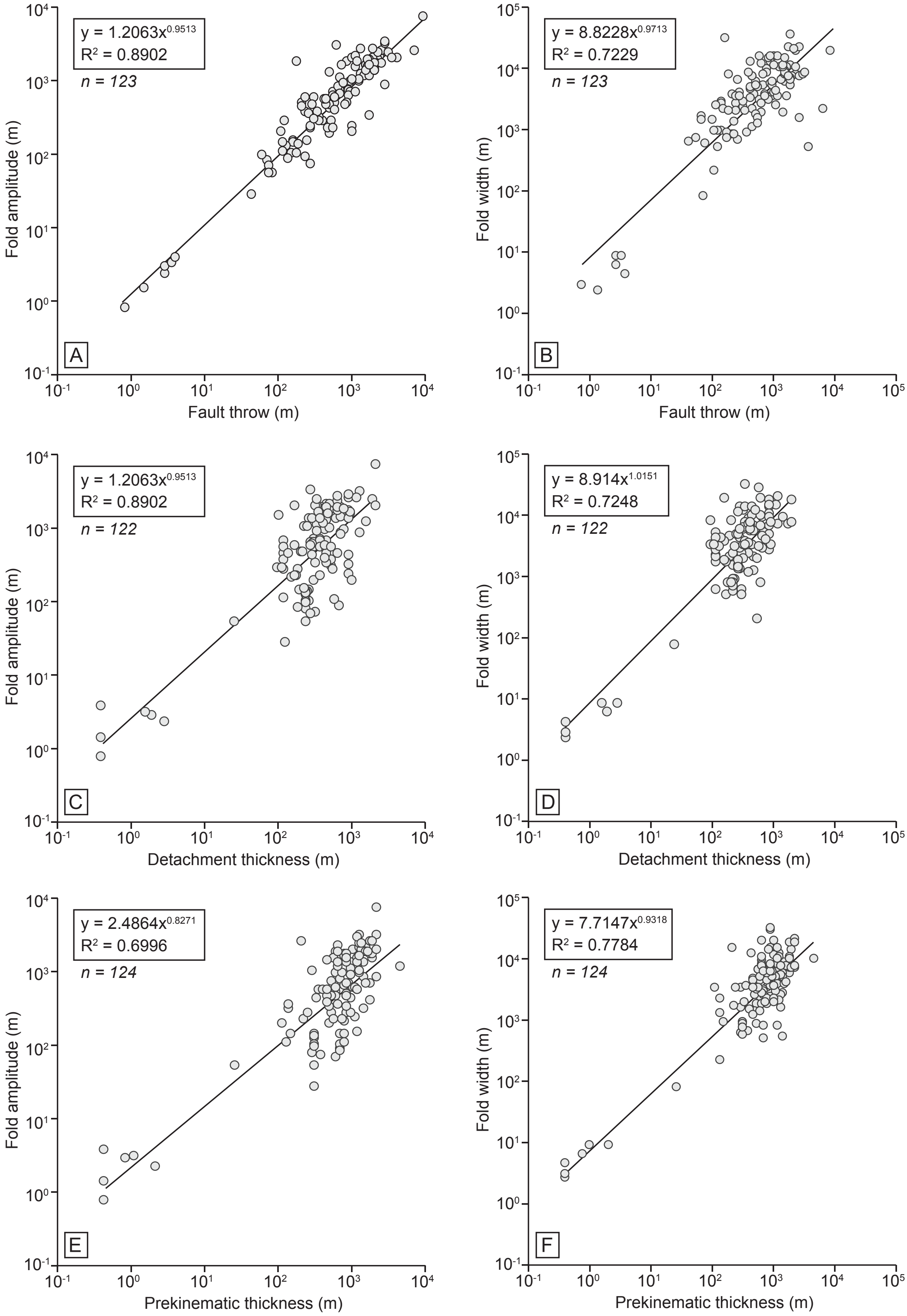
y = 1.2063x^0.9513
R^2 = 0.8902
n = 123
A
Fold amplitude (m)
Fault throw (m)
y = 8.8228x^0.9713
R^2 = 0.7229
n = 123
B
Fold width (m)
Fault throw (m)
y = 1.2063x^0.9513
R^2 = 0.8902
n = 122
C
Fold amplitude (m)
Detachment thickness (m)
y = 8.914x^1.0151
R^2 = 0.7248
n = 122
D
Fold width (m)
Detachment thickness (m)
y = 2.4864x^0.8271
R^2 = 0.6996
n = 124
E
Fold amplitude (m)
Prekinematic thickness (m)
y = 7.7147x^0.9318
R^2 = 0.7784
n = 124
F
Fold width (m)
Prekinematic thickness (m)

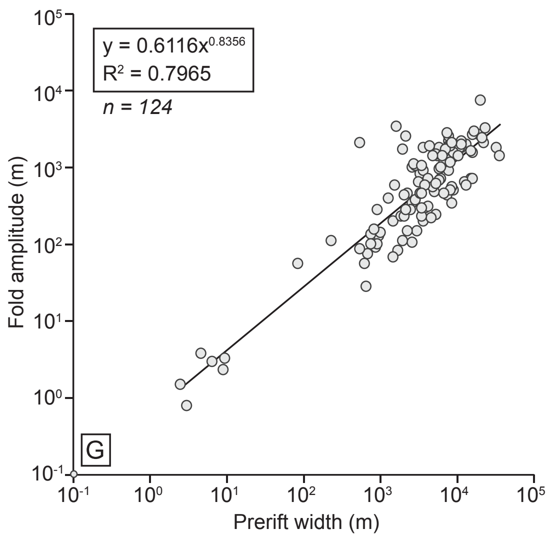

Figure 12 - Moderate-to-strong correlations for forced folds in nature (A – G; light grey circles). The best-fit regression, correlation coefficient (R_2) and number of observations (n) are also shown. Physical models lacked any moderate-to-strong correlations. See Table 2 for further details. See Fig. 2 for parameter descriptions. Analysis was not undertaken for numerical models of forced folds.

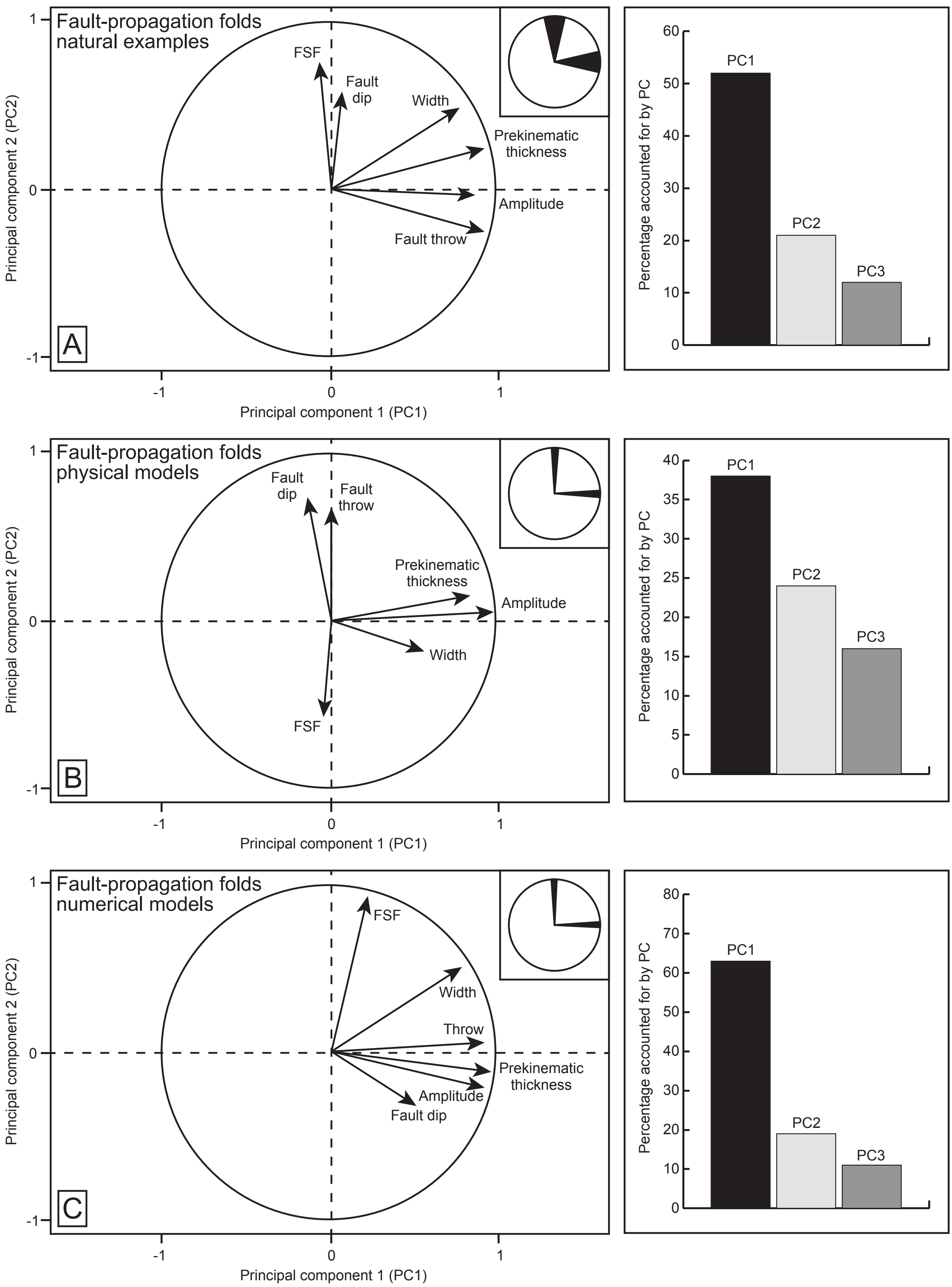

Figure 13 - Principal component analysis (PCA) for fault-propagation folds in nature (A), physical models (B) and numerical models (C). The percentage of the data variation accounted for by each principal component (PC) and uncertainty associated with missing values is shown in each case. See Fig. 2 for parameters.

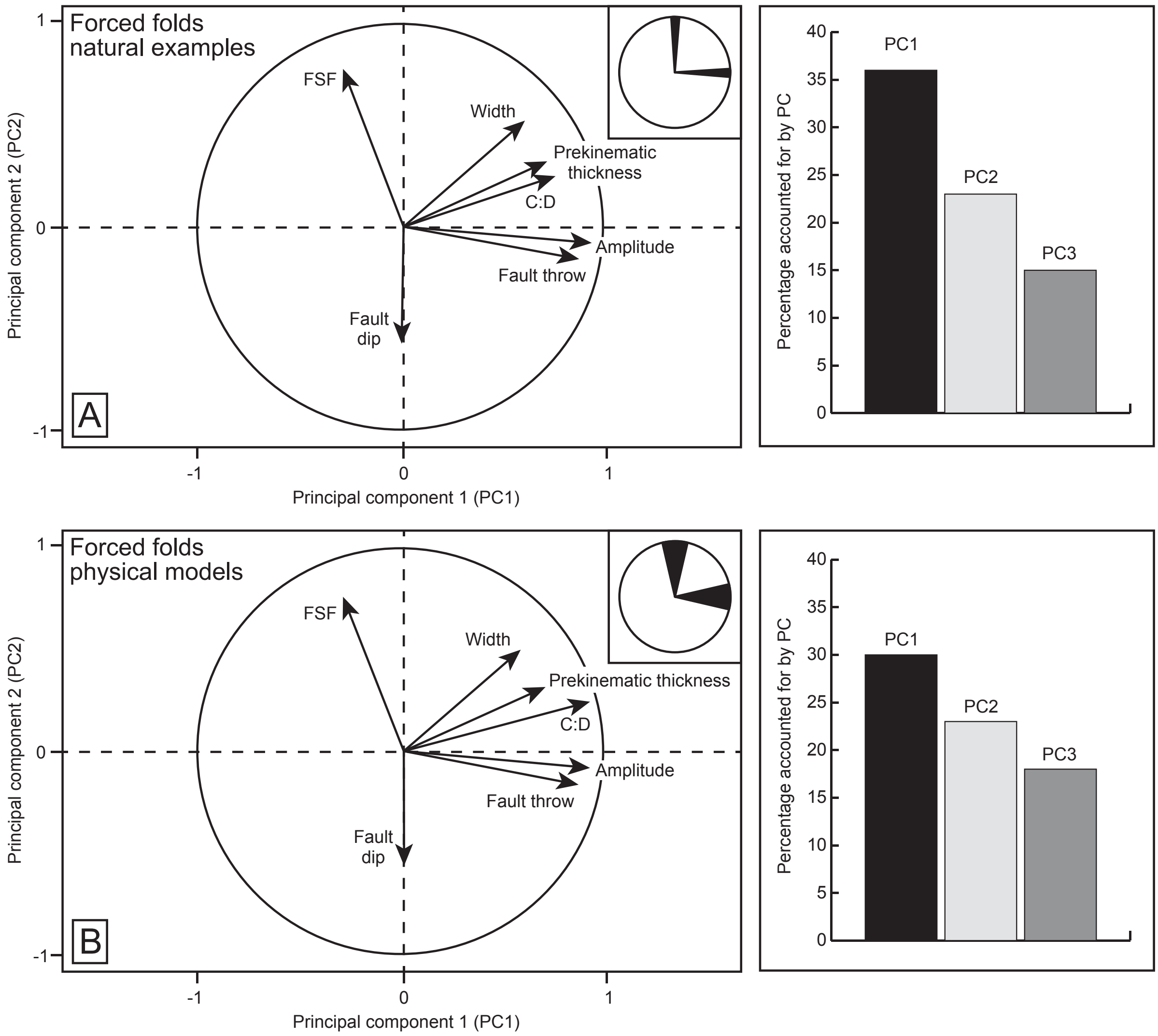

Figure 14 - Principal component analysis (PCA) for forced folds in nature (A) and physical models (B). The percentage of the data variation accounted for by each principal component (PC) and uncertainty associated with missing values is shown in each case. PCA was not undertaken for numerical models as there only Hardy (2018) explicitly model a forced fold. See Fig. 2 for parameters.

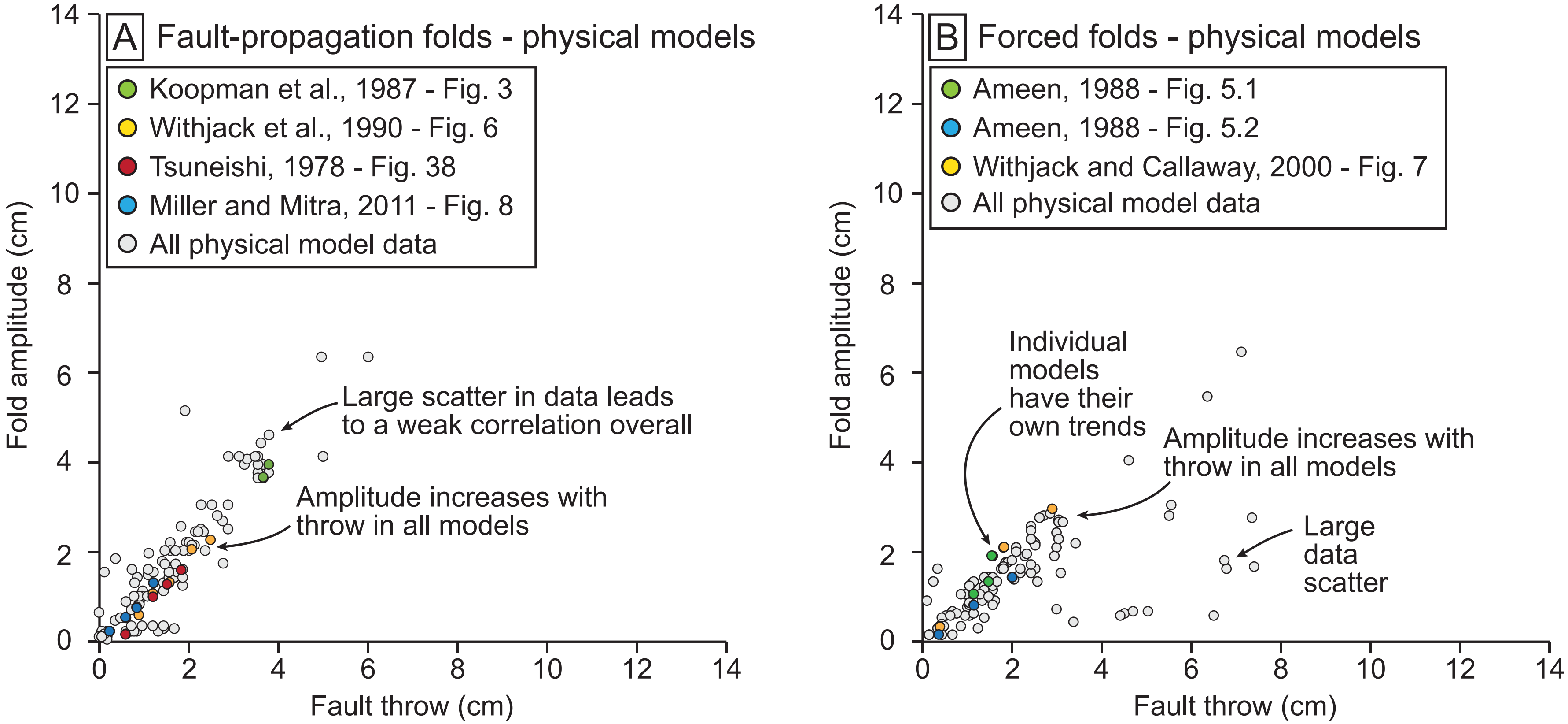

Figure 15 - Physical models of fault-propagation and forced folds show an overall weak-to-moderate correlation. However, individual models in isolation, show similar trends as observed in nature e.g. increased amplitude with throw. These relationships are often hidden within the data are likely due to the large amount of variance introduced by different model setups and material properties.

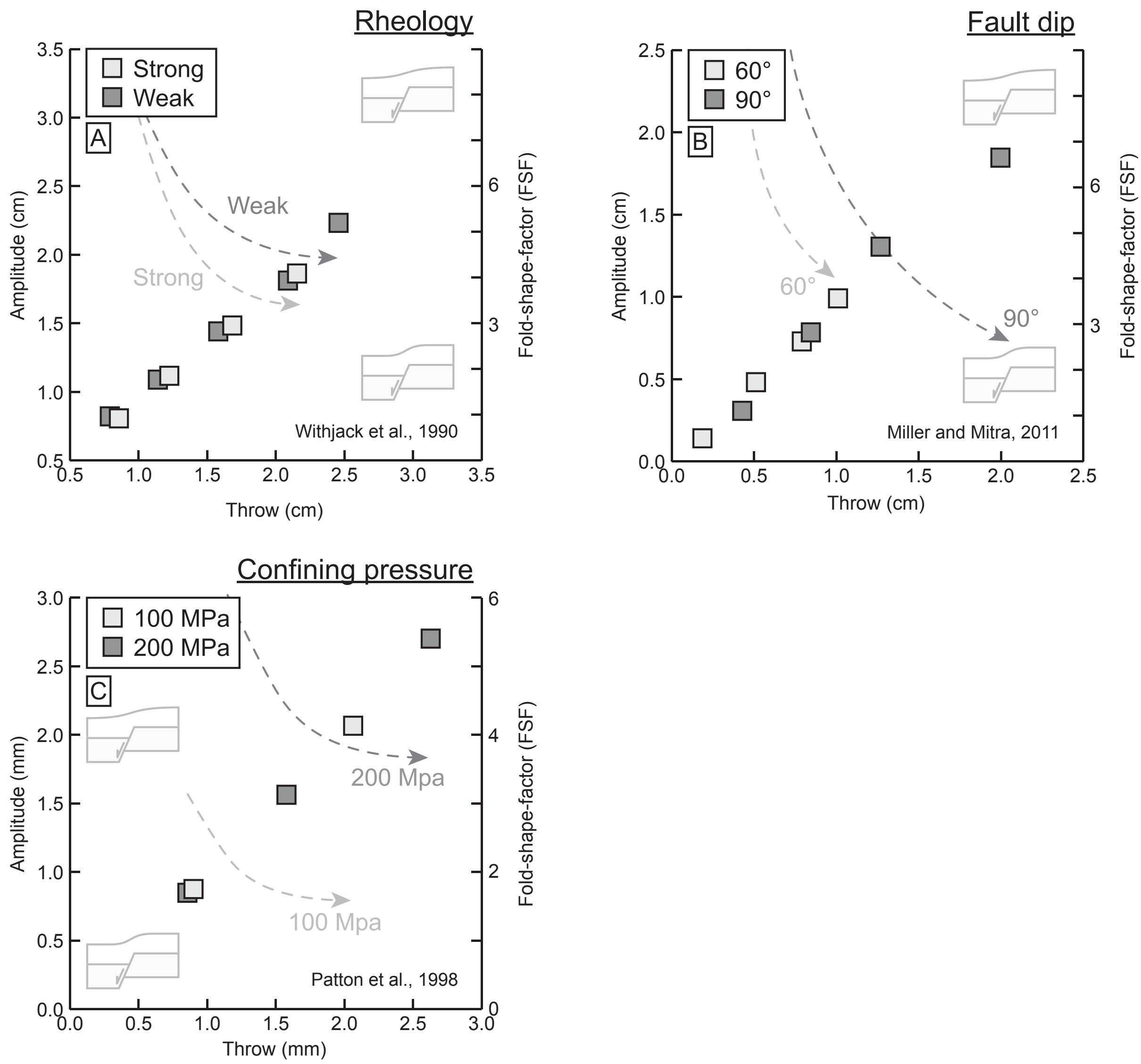

Figure 16 - Predictions of fault-propagation fold growth from physical models due to changes in (A) cover rheology, (B) fault dip, and (C) confining pressure. Fold-shape-factor (FSF) is represented by the dashed line and decreases with increased throw. A schematic of the fold shape is also shown. Amplitude is on the left-y-axis, while FSF is on the right-y-axis for panels A - C. Only in-tact fault-propagation fold measurements are plotted. FSF and amplitude values are taken from the same model at the same time. The reference for each plot is also shown.

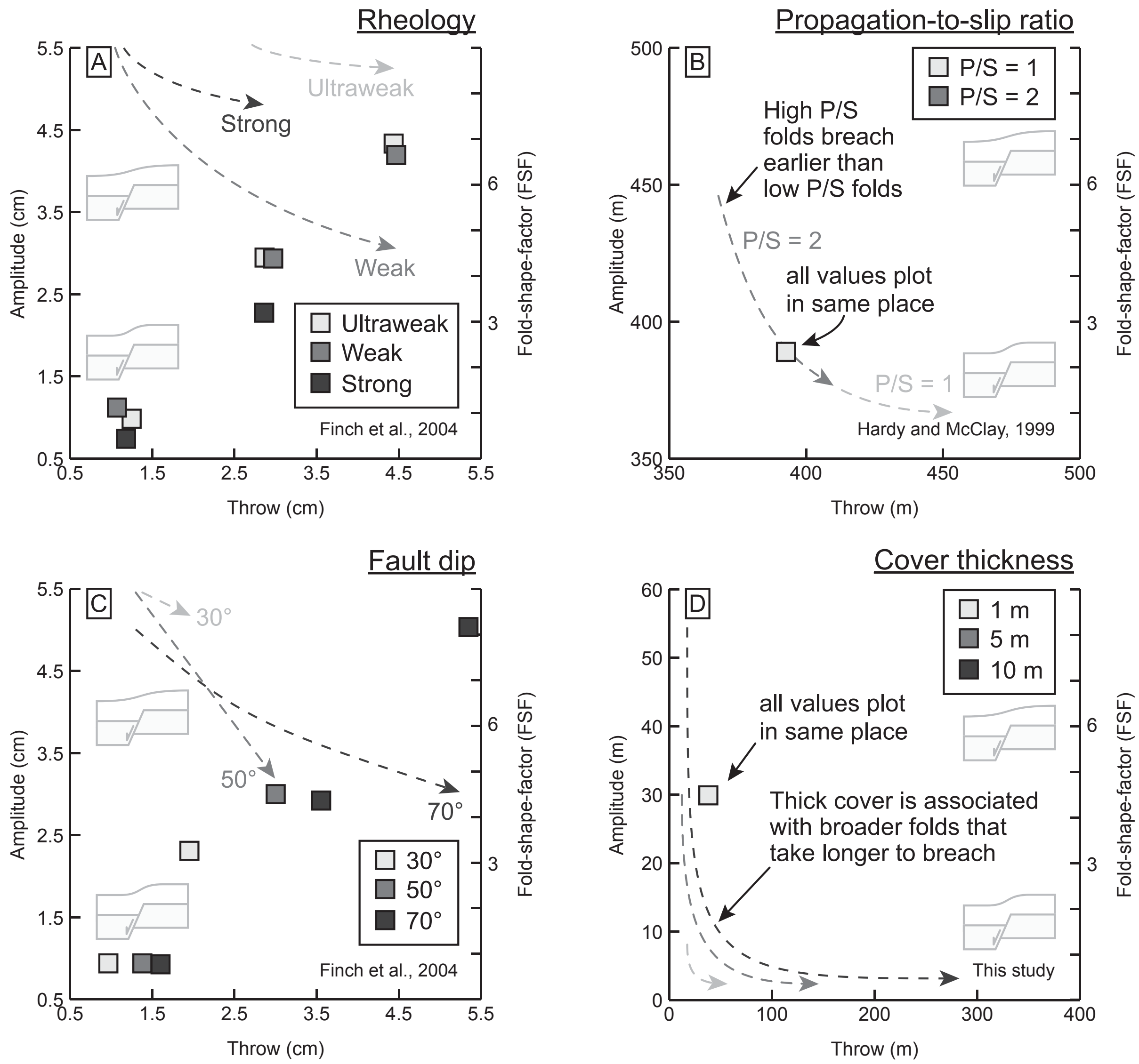

Figure 17 - Predictions of fault-propagation fold growth from numerical models due to changes in (A) cover rheology, (B) propagation-to-slip ratio, (C) fault dip, (D) cover thickness. Fold-shape-factor (FSF) is represented by the dashed line and decreases with increased throw. Amplitude is on the left-y-axis, while FSF is on the right-y-axis for panels A - D. Only in-tact forced fold measurements are plotted. The reference for each plot is also shown. Cover thickness (D) was calculated in this study using forward trishear models (after Allmendinger, 1998).

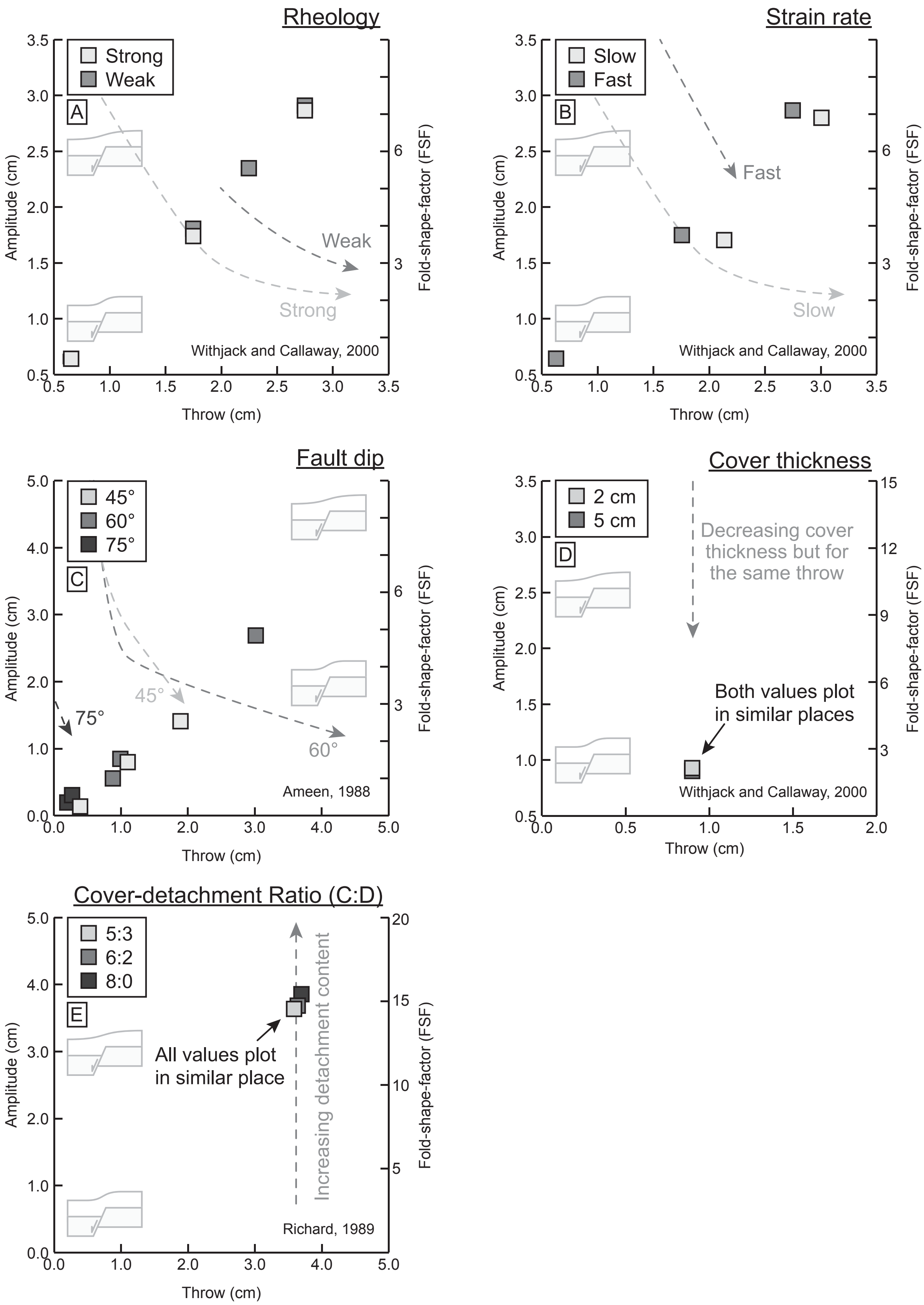
Rheology
Strong
Weak
A
Weak
Strong
Withjack and Callaway, 2000
Amplitude (cm)
Throw (cm)
Fold-shape-factor (FSF)
Strain rate
Slow
Fast
B
Fast
Slow
Withjack and Callaway, 2000
Amplitude (cm)
Throw (cm)
Fold-shape-factor (FSF)
Fault dip
45°
60°
75°
C
75°
45°
60°
Ameen, 1988
Amplitude (cm)
Throw (cm)
Fold-shape-factor (FSF)
Cover thickness
2 cm
5 cm
D
Decreasing cover thickness but for the same throw
Both values plot in similar places
Withjack and Callaway, 2000
Amplitude (cm)
Throw (cm)
Fold-shape-factor (FSF)
Cover-detachment Ratio (C:D)
5:3
6:2
8:0
E
All values plot in similar place
Increasing detachment content
Richard, 1989
Amplitude (cm)
Throw (cm)
Fold-shape-factor (FSF)

Figure 18 (previous page) - Predictions of forced fold growth from physical models due to changes in (A) cover rheology, (B) strain rate, (C) fault dip, (D) cover thickness, and (E) cover-detachment ratio. Fold-shape-factor (FSF) is represented by the dashed line and decreases with increased throw. A schematic of the fold shape is also shown. Amplitude is on the left-y-axis, while FSF is on the right-y-axis for panels A - E. Fold amplitude data on panels D – E are largely similar but the fold width and hence the FSF, is different. Only in-tact forced fold measurements are plotted. References for each plot are also shown. FSF and amplitude values are taken from the same model at the same time. Note that the strain rate and displacement rate are linked in Withjack and Callaway (2000).

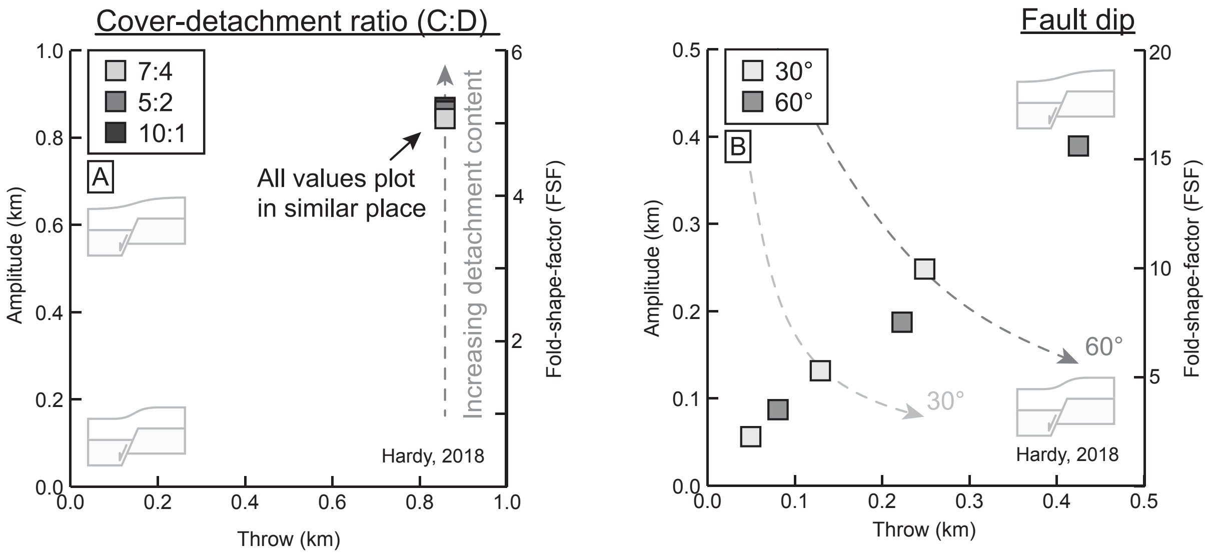

Figure 19 - Predictions of forced fold growth from numerical models (from Hardy, 2018) due to changes in (A) cover-detachment ratio, (B) fault dip. Fold-shape-factor (FSF) is represented by the dashed line and decreases with increased throw. Amplitude is on the left-y-axis, while FSF is on the right-y-axis for panels A - B. Only in-tact forced fold measurements are plotted.

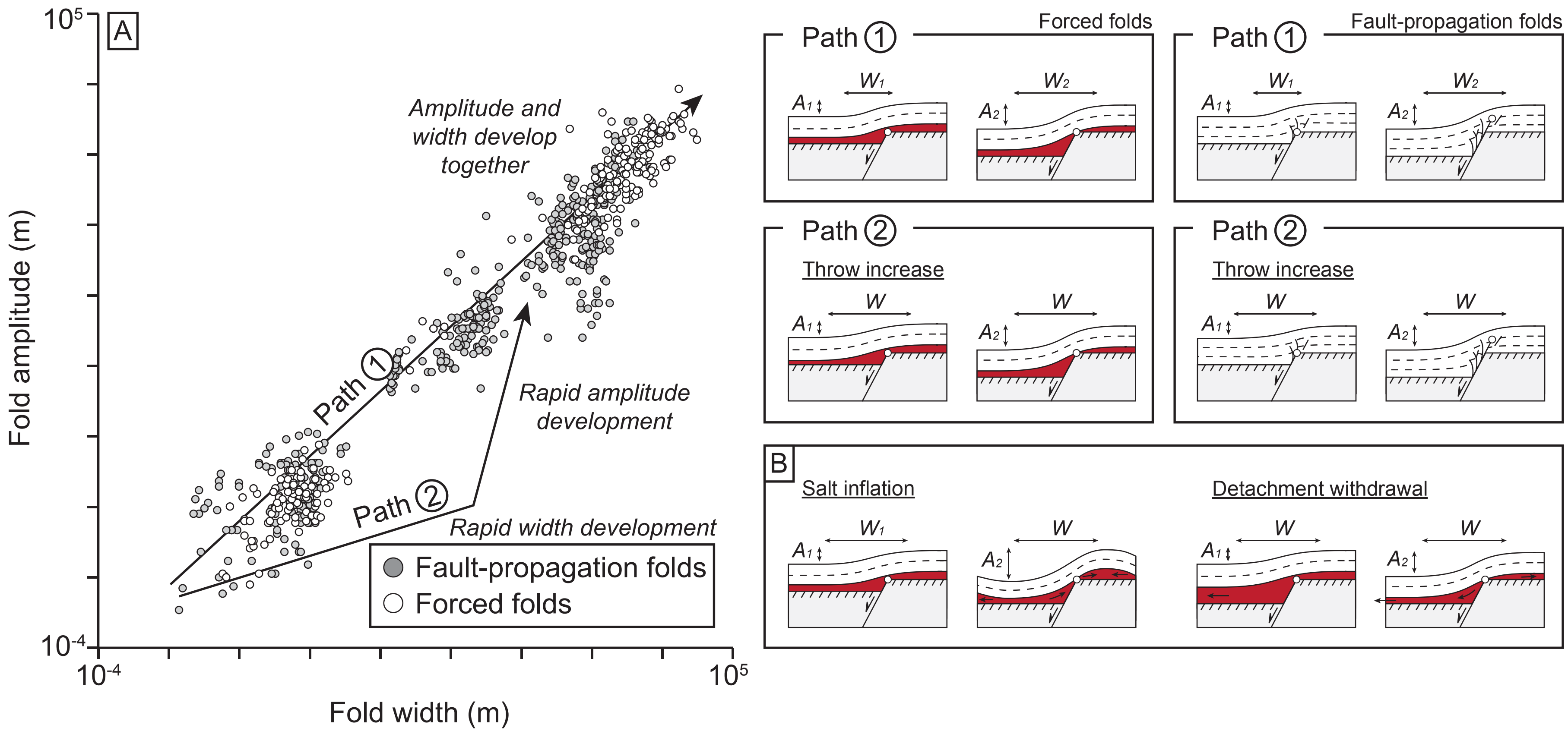

Figure 20. Growth of fault-propagation and forced folds (A). Two schematic paths for the growth fold evolution are plotted (path 1 and path 2). Folds following path 1 amplify and widen at a similar, gradual rate. Folds following path 2 widen early and amplify relatively late during fold growth. Amplitude and width variations due to salt flow are also shown (B).

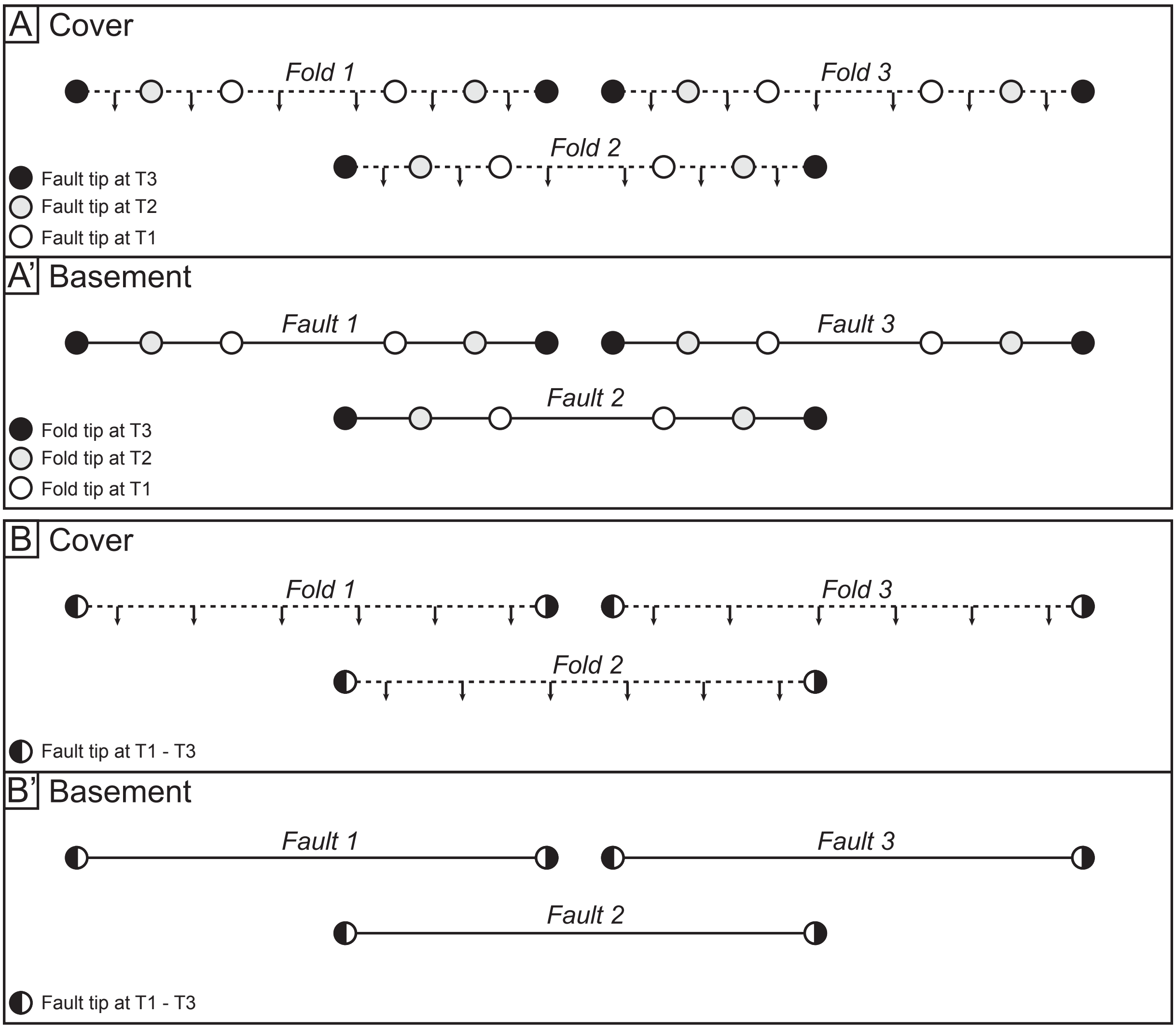

Figure 21. - Evolution of cover growth folds above growing basement-involved normal faults. (A) Isolated fault growth model. The basement normal faults get incrementally longer through time and accumulate displacement gradually; growth folds develop their along-strike width gradually and attain their amplitude as displacement is accrued. (B) Coherent fault growth model. The basement normal faults establish their lengths very rapidly before attaining displacement gradually; growth folds attain their along-strike width rapidly and then amplify as displacement is accrued. The across-strike width of fold is established early during fold growth in both models, and increases very slowly. Modified from Jackson and Rotevatn, 2013; Jackson et al. 2017. The direction of the dipping growth fold limb is indicated by the direction of the black arrows in (A) and (B).

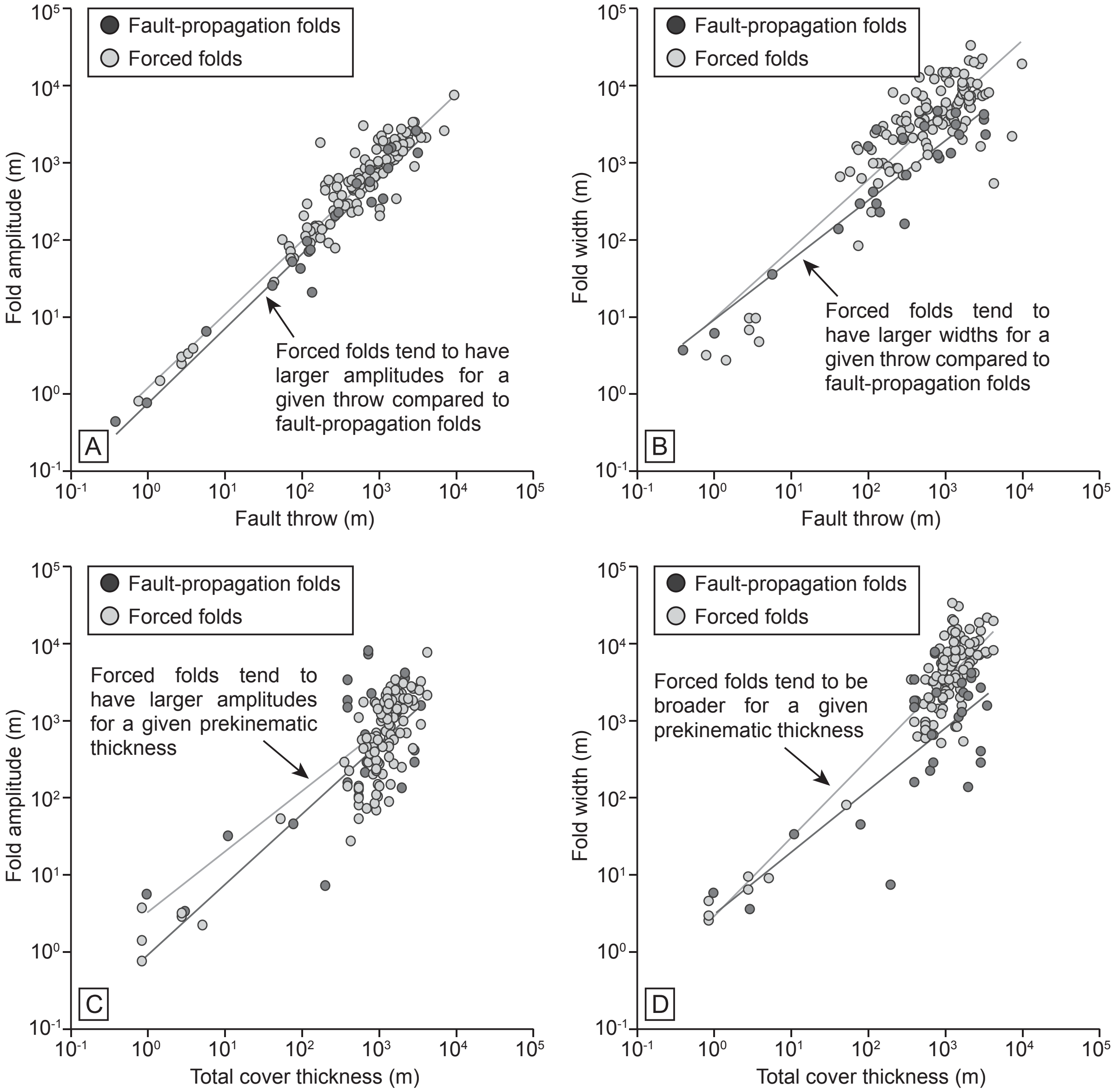

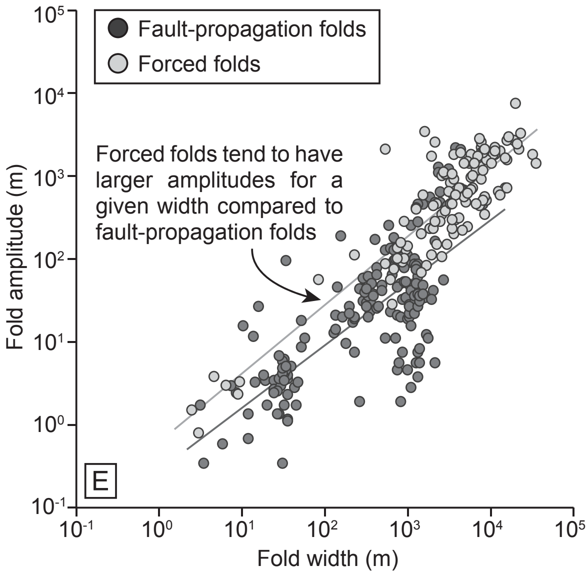

Figure 22. - Comparison of moderate-to-strong correlations (R_2 > 0.5) for fault-propagation (dark filled circles) and forced folds (lightly filled circles) in nature with the associated best-fit regressions from Figs. 11 and 12. See Fig. 2 for parameters.

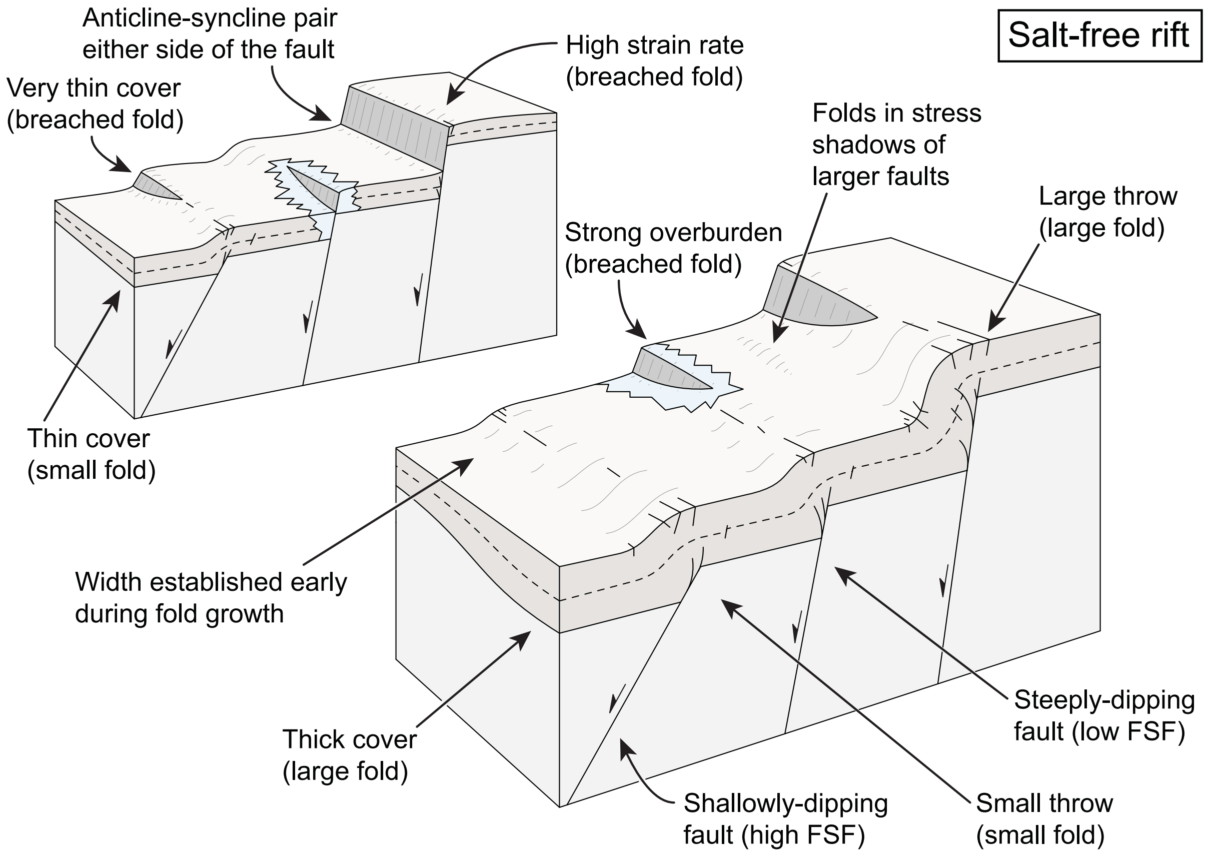

Salt-free rift
Anticline-syncline pair either side of the fault
High strain rate (breached fold)
Very thin cover (breached fold)
Folds in stress shadows of larger faults
Large throw (large fold)
Strong overburden (breached fold)
Thin cover (small fold)
Width established early during fold growth
Thick cover (large fold)
Steeply-dipping fault (low FSF)
Shallowly-dipping fault (high FSF)
Small throw (small fold)

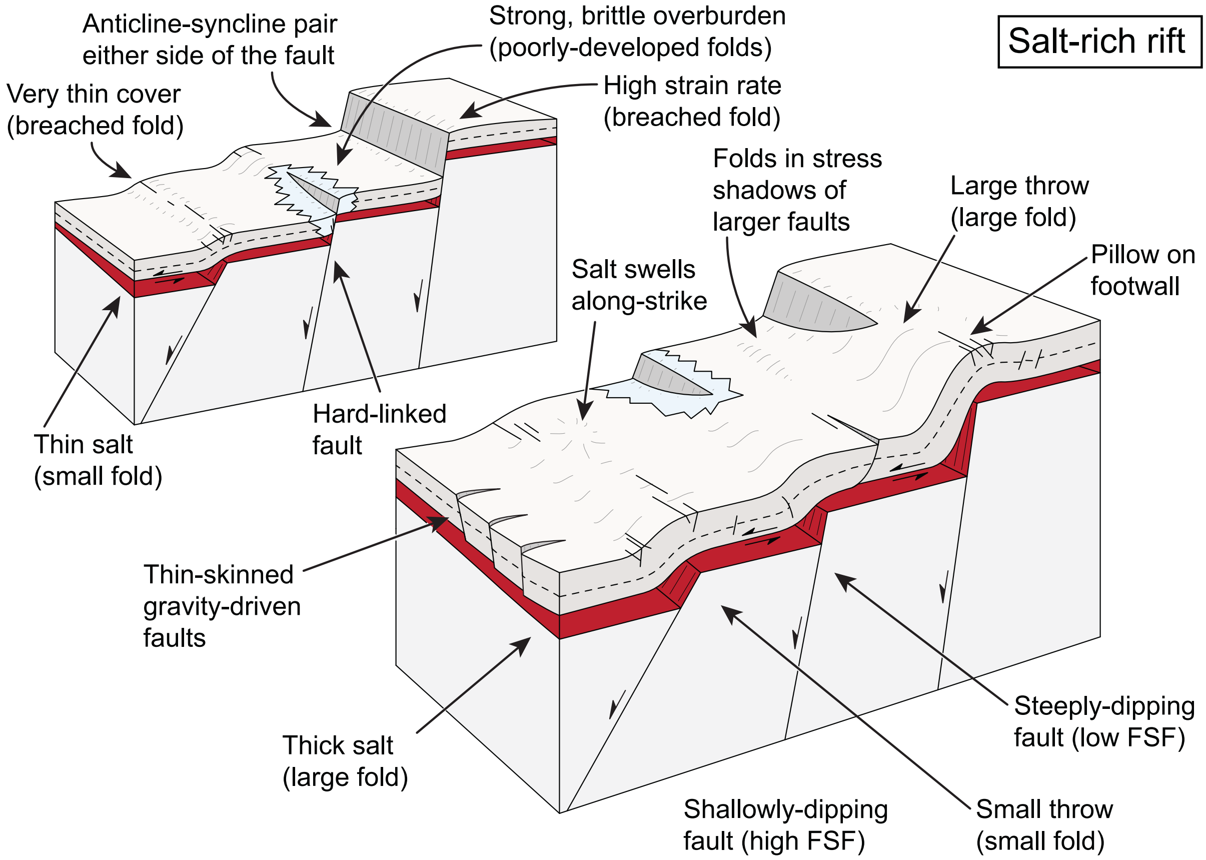

Salt-rich rift
Anticline-syncline pair either side of the fault
Strong, brittle overburden (poorly-developed folds)
Very thin cover (breached fold)
High strain rate (breached fold)
Folds in stress shadows of larger faults
Large throw (large fold)
Salt swells along-strike
Pillow on footwall
Thin salt (small fold)
Hard-linked fault
Thin-skinned gravity-driven faults
Thick salt (large fold)
Steeply-dipping fault (low FSF)
Shallowly-dipping fault (high FSF)
Small throw (small fold)

Figure 23. (previous page) - Growth fold geometry in salt-free (top) and salt-rich (bottom) sedimentary basins. Brittle, rheologically strong cover is shown in blue. Note how the width and amplitude of growth folds in salt-rich settings may be considerably different to those developed in salt-free settings. Salt may also create additional fault and fracture populations related to diapirism, independent of regional extension. Cover thickness decreases towards the background in both salt-free and salt-rich settings, which in turn, affects fold geometry.

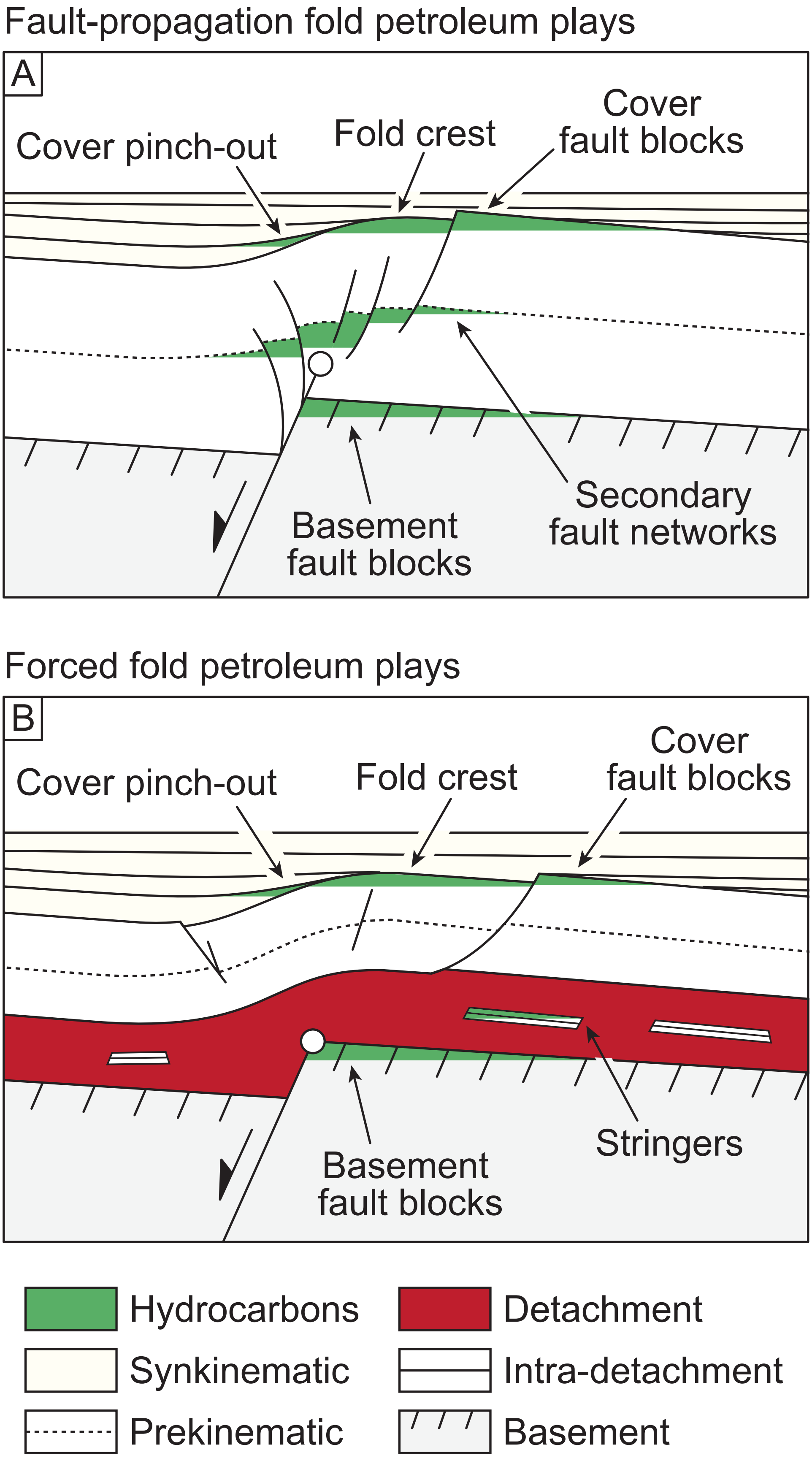

Fault-propagation fold petroleum plays
A
Cover pinch-out
Fold crest
Cover fault blocks
Basement fault blocks
Secondary fault networks
Forced fold petroleum plays
B
Cover pinch-out
Fold crest
Cover fault blocks
Basement fault blocks
Stringers
Hydrocarbons
Synkinematic
Prekinematic
Detachment
Intra-detachment
Basement

Figure 24. (previous page) - Petroleum plays associated with fault-propagation folds (A) and forced folds (B). Hydrocarbons may be trapped at all stratigraphic levels creating vertically stacked hydrocarbon play potential. Given that the plays are not necessarily formed at the same time, the hydrocarbon composition and hydrocarbon-water contacts within individual compartments may be different. As the fold grows different compartments may be charged and the volume may change as the shape and size changes.

Parameter	Fault-propagation folds (FPF)			Forced folds (FF)		
	Natural examples	**Physical models**	**Numerical models**	**Natural examples**	**Physical models**	**Numerical models**
Fold amplitude (A)	10 cm – 2.5 km	3 mm – 8.6 cm	4 mm – 965 m	75 cm – 3.2 km	7 mm – 6.6 cm	50 m – 820 m
Fold width (W)	10 cm – 7.5 km	1.5 mm – 16 cm	7 mm – 4.6 km	2.4 m – 20 km	6 mm – 38 cm	2 km – 3.4 km
Fold-shape-factor (FSF)	0.3 – 357	0.2 – 79	1.2 – 50	0.25 - 24	0.93 - 25	2.8 – 14
Fault throw (TH)	41 cm – 3.3 km	6 mm – 12 cm	4 mm – 1km	81 cm – 9.8 km	1 mm – 7 cm	50 m – 910 m
Fault dip (fd)	45° - 85°	45° - 90°	30° - 90°	13° – 90°	30° - 90°	30° – 65°
Prekinematic thickness (T_P)	2.8 m – 3.5 km	1 cm – 26 cm	6 cm – 9.7 km	43 cm – 2.3 km	3.5 mm – 7 cm	1.75 km – 2.75 km
Detachment thickness (T_D)	-	-	-	42 cm – 2.1 km	5 mm – 7 cm	250 m – 1 km
Cover-detachment ratio (C:D)	-	-	-	0.6 - 9	0.9 - 26	1.5 - 10

Table 1 – Ranges for the growth fold parameters identified in Fig. 2 Values are approximate based on measurements from global data compilation in Appendix D and E.

Correlation	Fault-propagation folds (FPF)			Forced folds (FF)	
	Natural examples	Physical models	Numerical models	Natural examples	Physical models
Fold amplitude vs fold width	$A=22.319(W)^{0.7659}$ *[$R^2 = 0.63$]*	No correlation *[$R^2 < 0.1$]*	$A=6.5446(W)^{1.0078}$ *[$R^2 = 0.8941$]*	$A=0.6116(W)^{0.8356}$ *[$R^2 = 0.7965$]*	*Weak correlation* *[$R^2 = 0.3451$]*
Fold amplitude vs fault dip	*Weak correlation* *[$R^2 = 0.1024$]*	No correlation *[$R^2 < 0.1$]*	*Weak correlation* *[$R^2 = 0.2566$]*	No correlation *[$R^2 < 0.1$]*	No correlation *[$R^2 < 0.1$]*
Fold amplitude vs fault throw	$A=8.0074(TH)^{0.8.021}$ *[$R^2 = 0.63$]*	$A=0.3536(TH)^{0.7647}$ *[$R^2 = 0.72$]*	$A=0.9585(TH)^{0.9219}$ *[$R^2 = 0.8912$]*	$A=1.2063(TH)^{0.9513}$ *[$R^2 = 0.8912$]*	*Weak correlation* *[$R^2 = 0.4355$]*
Fold amplitude vs prekinematic thickness	$A=0.7508(T_P)^{0.85}$ *[$R^2 = 0.71$]*	*Weak correlation* *[$R^2 = 0.1658$]*	$A=0.2152(T_P)^{0.8076}$ *[$R^2 = 0.8652$]*	$A=2.4864(T_P)^{0.8271}$ *[$R^2 = 0.6996$]*	*Weak correlation* *[$R^2 = 0.1032$]*
Fold width vs fault dip	*Weak correlation* *[$R^2 = 0.1063$]*	No correlation *[$R^2 < 0.1$]*	*Weak correlation* *[$R^2 = 0.1125$]*	No correlation *[$R^2 < 0.1$]*	No correlation *[$R^2 < 0.1$]*
Fold width vs fault throw	$W=7.5487(TH)^{0.7922}$ *[$R^2 = 0.835$]*	No correlation *[$R^2 < 0.1$]*	$W=6.4602(T_P)^{0.9246}$ *[$R^2 = 0.9038$]*	$W=8.8228(TH)^{0.9178}$ *[$R^2 = 0.7229$]*	*Weak correlation* *[$R^2 = 0.3061$]*
Fold width vs prekinematic thickness	$W=3.5994(T_P)^{0.7879}$ *[$R^2 = 0.7226$]*	*Weak correlation* *[$R^2 = 0.1567$]*	$W=0.2883(T_P)^{0.8501}$ *[$R^2 = 0.8303$]*	$W=7.7147(T_P)^{0.9318}$ *[$R^2 = 0.7784$]*	*Weak correlation* *[$R^2 = 0.2485$]*
Fold-shape-factor vs fault dip	No correlation *[$R^2 < 0.1$]*	No correlation *[$R^2 < 0.1$]*	No correlation *[$R^2 < 0.1$]*	No correlation *[$R^2 < 0.1$]*	No correlation *[$R^2 < 0.1$]*

Table 2 - Correlations for for fault-propagation and forced folds in nature, physical models and numerical models. Where Moderate-to-strong correlations ($R_2 > 0.5$) are present, the best-fit parametric equation has been provided. The R_2 value is shown in all cases. A = fold amplitude. W = fold width. TH = fault throw. T_P = prekinematic cover thickness. T_D = detachment thickness. Regression analysis was not undertaken for numerical models of forced folds.

Correlation	Fault-propagation folds (FPF)			Forced folds (FF)	
	Natural examples	Physical models	Numerical models	Natural examples	Physical models
Fold-shape-factor vs fault throw	*Weak correlation* *[$R^2 = 0.1214$]*	*Weak correlation* *[$R^2 = 0.3898$]*	No correlation *[$R^2 < 0.1$]*	No correlation *[$R^2 < 0.1$]*	No correlation *[$R^2 < 0.1$]*
Fold-shape-factor vs prekinematic thickness	*Weak correlation* *[$R^2 = 0.1488$]*	No correlation *[$R^2 < 0.1$]*	No correlation *[$R^2 < 0.1$]*	No correlation *[$R^2 < 0.1$]*	No correlation *[$R^2 < 0.1$]*
Detachment thickness vs fold amplitude	-	-	-	$A=2.6853(T_D)^{0.9065}$ *[$R^2 = 0.6226$]*	*Weak correlation* *[$R^2 = 0.1179$]*
Detachment thickness vs fold width	-	-	-	$W=8.914(T_D)^{1.0151}$ *[$R^2 = 0.7248$]*	*Weak correlation* *[$R^2 = 0.4058$]*
Detachment thickness vs fold-shape-factor	-	-	-	No correlation *[$R^2 < 0.1$]*	*Weak correlation* *[$R^2 = 0.133$]*
Cover-detachment ratio vs fold amplitude	-	-	-	No correlation *[$R^2 < 0.1$]*	No correlation *[$R^2 < 0.1$]*
Cover-detachment ratio vs fold width	-	-	-	No correlation *[$R^2 < 0.1$]*	No correlation *[$R^2 < 0.1$]*
Cover-detachment ratio vs fold-shape-factor	-	-	-	No correlation *[$R^2 < 0.1$]*	No correlation *[$R^2 < 0.1$]*

Table 2 continued - Correlations for for fault-propagation and forced folds in nature, physical models and numerical models. Where Moderate-to-strong correlations ($R_2 > 0.5$) are present, the best-fit parametric equation has been provided. The R_2 value is shown in all cases. A = fold amplitude. W = fold width. TH = fault throw. T_P = prekinematic cover thickness. T_D = detachment thickness. Regression analysis was not undertaken for numerical models of forced folds.

Appendix A - Genesis of fault-related folds

Forced fold – As a fault propagates towards the surface, folding occurs above the upper fault. Deformation is principally faulted at depth, but abruptly transitions to folding at shallower levels. This abrupt change between faulting below and folding above is facilitated due to a detachment or ductile lithology, such as salt or overpressured shale (e.g. Laubscher, 1982; Withjack and Callaway, 2000; Ford et al., 2007; Duffy et al., 2013; Lewis et al., 2013; Jackson and Lewis, 2016; Coleman et al., 2017). A breached forced fold resembles that of a breached fault-propagation fold.

Fault-propagation fold – As a fault propagates towards the surface, folding occurs above the upper fault tip. Deformation is manifested as faulting at depth but gradually transitions to folding at shallow levels (e.g. Withjack et al., 1990; Gawthorpe et al., 1997; Sharp et al., 2000; Jackson et al., 2006; Lewis et al., 2015).

Fault-propagation folds (breached) – Following fault-propagation folding, the underlying fault may propagate through its cover and folding ceases. The fold may then be preserved in the footwall and hangingwall, typically as an anticline and syncline, respectively (e.g. Withjack et al., 1990; Gawthorpe et al., 1997; Lewis et al., 2015). Forced folds that are breached appear similar to breached fault-propagation folds (e.g. Withjack and Callaway, 2000; Ford et al., 2007; Lewis et al., 2013).

Compactional drape – Differential compaction either side of a fault plane creates folding with sub-vertical fold axes (e.g. Thomson and Underhill, 1993; Skuce, 1996; Faerseth and Lien, 2002).

Withdrawal drape – Prekinematic strata may become folded above a pre-existing basement fault step as an underlying mobile unit, such as salt or shale, is evacuated. The withdrawal drape fold is geometrically similar to a forced fold, however, is *not* due to a propagating upper fault tip (e.g. Withjack and Callaway, 2000). Withdrawal drape folds are typically associated with nearby 'leakage points' such as salt or shale diapirs.

Frictional drag – The deflection of beds adjacent to a fault into folds that are convex in the direction of relative slip due to frictional sliding along a fault and progressive tilting of beds with increased amount of sliding along a fault (e.g. Billings, 1972; Resor, 2008; Spahic et al., 2013). Their origin has been recently called into question (cf. Reches and Eidelman, 1995; Graseman et al., 2005; Ferril et al., 2012).

Inversion – The compressional reactivation of pre-existing extensional structures, so that an initial structural low is uplifted, and subsequently inverted, to form a structural high (e.g. Badley et al., 1989; Mitra, 1993; Mitra and Islam, 1994; Turner and Williams, 2004; Jackson et al., 2013).

Fault-line deflection (recess) – Folding due to along-strike corrugations in fault plane geometry. Recess features are created at concave fault segments (e.g. Wheeler, 1939; Stewart and Hancock, 1991; Ehrlich and Gabrielsen, 2004).

Fault-line deflection (salient) – Folding due to along-strike corrugations in fault plane geometry. Salient features are created at convex fault segments (e.g. Wheeler, 1939; Machette et al., 1991; Stewart and Hancock, 1991; Ehrlich and Gabrielsen, 2004; cf. Claringbould et al., 2017).

References for Appendix A

BADLEY, M. E., PRICE, J. D. and BACKSHALL, L. C. 1989. Inversion, reactivated faults and related structures: seismic examples from the southern North Sea. Geological Society, London, Special Publications, 44, 201-219.

BILLINGS, M. P. and BILLINGS, M. 1972. Structural geology, Prentice-Hall Englewood Cliffs, NJ.

CLARINGBOULD, J. S., BELL, R. E., JACKSON, C. A. L., GAWTHORPE, R. L. and ODINSEN, T. 2017. Pre-existing normal faults have limited control on the rift geometry of the northern North Sea. Earth and Planetary Science Letters, 475, 190-206.

COLEMAN, A. J., JACKSON, C. A. L. and DUFFY, O. B. 2017. Balancing sub- and supra-salt strain in salt-influenced rifts: Implications for extension estimates. Journal of Structural Geology, 102, 208-225..

DUFFY, O. B., GAWTHORPE, R. L., DOCHERTY, M. and BROCKLEHURST, S. H. 2013. Mobile evaporite controls on the structural style and evolution of rift basins: Danish Central Graben, North Sea. Basin Research, 25, 310-330.

EHRLICH, R. and GABRIELSEN, R. H. 2004. The complexity of a ramp–flat–ramp fault and its effect on hanging-wall structuring: an example from the Njord oil field, offshore mid-Norway. Petroleum Geoscience, 10, 305-317.

FÆRSETH, R. B. and LIEN, T. 2002. Cretaceous evolution in the Norwegian Sea—a period characterized by tectonic quiescence. Marine and Petroleum Geology, 19, 1005-1027.

FERRILL, D. A., MORRIS, A. P. and MCGINNIS, R. N. 2012. Extensional fault-propagation folding in mechanically layered rocks: The case against the frictional drag mechanism. Tectonophysics, 576-577, 78-85.

FORD, M., LE CARLIER DE VESLUD, C. and BOURGEOIS, O. 2007. Kinematic and geometric analysis of fault-related folds in a rift setting: The Dannemarie basin, Upper Rhine Graben, France. Journal of Structural Geology, 29, 1811-1830.

GAWTHORPE, R. L., SHARP, I., UNDERHILL, J. R. and GUPTA, S. 1997. Linked sequence stratigraphic and structural evolution of propagating normal faults. Geology, 25, 795.

GRASEMANN, B., MARTEL, S. and PASSCHIER, C. 2005. Reverse and normal drag along a fault. Journal of Structural Geology, 27, 999-1010.

JACKSON, C. A. L., CHUA, S. T., BELL, R. E. and MAGEE, C. 2013. Structural style and early stage growth of inversion structures: 3D seismic insights from the Egersund Basin, offshore Norway. Journal of Structural Geology, 46, 167-185.

JACKSON, C. A. L. and LEWIS, M. M. 2016. Structural style and evolution of a salt-influenced rift basin margin; the impact of variations in salt composition and the role of polyphase extension. Basin Research, 28, 81-102.

LAUBSCHER, H. 1982. Die Sudostecke des Rheingrabens-ein kinematisches und dynamisches problem. Eclogae Geologicae Helvetiae, 75, 101-116.

LEWIS, M. M., JACKSON, C. A., GAWTHORPE, R. L. and WHIPP, P. S. 2015. Early synrift reservoir development on the flanks of extensional forced folds: A seismic-scale outcrop analog from the Hadahid Fault System, Suez Rift, Egypt. AAPG Bulletin.

LEWIS, M. M., JACKSON, C. A. L. and GAWTHORPE, R. L. 2013. Salt-influenced normal fault growth and forced folding: The Stavanger Fault System, North Sea. Journal of Structural Geology, 54, 156-173.

MITRA, S. 1993. Geometry and kinematic evolution of inversion structures. AAPG Bulletin, 77, 1159-1191.

MITRA, S. and ISLAM, Q. T. 1994. Experimental (clay) models of inversion structures. Tectonophysics, 230, 211-222.

RECHES, Z. E. and EIDELMAN, A. 1995. Drag along faults. Tectonophysics, 247, 145-156.

RESOR, P. G. 2008. Deformation associated with a continental normal fault system, western Grand Canyon, Arizona. Geological Society of America Bulletin, 120, 414-430.

SHARP, I. R., GAWTHORPE, R. L., UNDERHILL, J. R. and GUPTA, S. 2000. Fault-propagation folding in extensional settings: Examples of structural style and synrift sedimentary response from the Suez rift, Sinai, Egypt. Geological Society of America Bulletin, 112, 1877-1899.

SKUCE, A. G. 1996. Forward modelling of compaction above normal faults: an example from the Sirte Basin, Libya. Geological Society, London, Special Publications, 99, 135-146.

SPAHIĆ, D., GRASEMANN, B. and EXNER, U. 2013. Identifying fault segments from 3D fault drag analysis (Vienna Basin, Austria). Journal of Structural Geology, 55, 182-195.

STEWART, I. S. and HANCOCK, P. L. 1991. Scales of structural heterogeneity within neotectonic normal fault zones in the Aegean region. Journal of Structural Geology, 13, 191-204.

THOMSON, K. and UNDERHILL, J. Controls on the development and evolution of structural styles in the Inner Moray Firth Basin. Geological Society, London, Petroleum Geology Conference series, 1993. Geological Society of London, 1167-1178.

TURNER, J. P. and WILLIAMS, G. A. 2004. Sedimentary basin inversion and intra-plate shortening. Earth-Science Reviews, 65, 277-304.

WHEELER, G. 1939. Triassic fault-line deflections and associated warping. The Journal of Geology, 337-370.

WITHJACK, M. O., OLSON, J. and PETERSON, E. 1990. Experimental models of extensional forced folds. AAPG Bulletin, 74, 1038-1054.

WITHJACK, M. O. and CALLAWAY, S. 2000. Active normal faulting beneath a salt layer: an experimental study of deformation patterns in the cover sequence. AAPG bulletin, 84, 627-651.

Appendix B - Fault-propagation fold locations

Locality	Country	Fault System	Basin	Reference(s)	Published	Confidence
1	Libya		Sirte Basin	Fodor et al., 2005; Skuce, 1996	Yes	High
2	Egypt		Gulf of Suez	Jackson et al., 2006; Khalil and McClay, 2002; Khalil and McClay, 2016	Yes	High
3	US		Newark Basin	Olsen et al., 1996; Schlische et al., 1992	Yes	Low
4	Egypt		Northern Gulf of Suez	Jackson et al., 2006; Sharp et al., 2000a; b; Garfunkel and Bartov, 1977; Moustafa, 1993	Yes	High
5	Egypt		Central Gulf of Suez	Sharp et al., 2000b; Garfunkel and Bartov, 1977; Moustafa, 1993	Yes	High
6	Egypt		Southern Gulf of Suez	Sharp et al., 2000a; Garfunkel and Bartov, 1977; Moustafa, 1993	Yes	High
7	US	Balcones Fault System	Gulf Coast Basin	Ferrill et al., 2011; Ferril et al., 2012	Yes	High
8	US	Nopolo Fault	Loreto Basin	Willsey et al., 2002	Yes	High
9	Iceland		Vogar	Grant and Kattenhorn, 2004; Hardy et al., 2013; Trippanera et al., 2015	Yes	High
10	Iceland		Grindavik	Grant and Kattenhorn, 2004; Hardy et al., 2013	Yes	High
11	Iceland		Thingvellir	Grant and Kattenhorn, 2004; Hardy et al., 2013; Trippanera et al., 2015; Smart and Ferrill, 2018	Yes	High
12	Spain		Jiloca Graben	Lafuente et al., 2011	Yes	High

13	US		Canyonlands Graben	Cartwright and Mansfield, 1998	Yes	High
14	US	Koa’e Fault System	Kilauea Southwest and East Rift Zone	Martel and Langley, 2006; Kaven and Martel, 2007; Bubeck et al., 2018	Yes	High
15	US	Hat Creek System	Hat Creek Graben	Blakeslee and Kattenhorn, 2013	Yes	High
16	Israel	Galilee and Zurim Escarpment	Dead Sea	Matmon et al., 2010	Yes	High
17	US	White Rabbit Fault System	Kilauea Southwest Rift Zone	Podolsky and Roberts, 2008	Yes	High
18	Taiwan	Shanchiao Fault System	Taipei Basin	Chu et al., 2015	Yes	High
19	Saudi Arabia		Jebel Hafeet	van Gent et al., 2010	Yes	High
20	Norway	Oseburg East	Horda Platform	Finch et al., 2004; Jackson et al., 2018	Yes/No	High
21	Norway	Smorbukk	Halten Terrace	Corfield and Sharp, 2000; Bell et al., 2014; Færseth and Lien, 2002	Yes	High
22	Norway	Fjerritslev Fault System	Farsund Basin	Phillips et al., 2018	No	High
23	Israel		Levant Basin	Baudon and Cartwright, 2008a; b; c	Yes	Low
24	Norway	Strathspey-Brent-Statfjord Fault Zone	Eastern Shetland Basin	McLeod et al., 2000	Yes	Mid
25	US		Modoc Plateau	White and Crider, 2006	Yes	High
26	Gabon	Mikouloungou; Kiene; Mounana; Kaya; Magna faults	Franceville Basin	Ndongo et al., 2016	Yes	High
27	Norway		Vøring Basin	Færseth and Lien, 2002	Yes	Mid

28	Norway		Møre Basin	Færseth and Lien, 2002	Yes	Mid
29	Brazil		Espirito Santo Basin	Omosanya and Alves, 2014	Yes	High
30	Turkey	Yavansu Fault Zone	Menderes Graben	Hancock and Barka, 1987	Yes	High
31	UK	East Pennine Coalfield	Welbeck Low	Walsh and Watterson, 1987	Yes	High
32	Greece	Southern Corinth Fault System	Corinth Rift	Vita-Finzi and King, 1985	Yes	High
33	Israel		Levant Basin	Ghalayini et al., 2016	Yes	High
34	US	Sandy Creek Fault System	Cat Creek	Mitra, 1993	Yes	High
35	Java	Java	Kangean Basin	Mitra, 1993; Badley, 1989	Yes	High
36	UK		South Hewett Zone	Badley et al., 1989; Mitra, 1993	Yes	Mid
37	New Zealand	Manaia Fault System, Kupe Structure	Southern Taranaki Basin	Mitra, 1993; Knox, 1982; Conneally, 2017	Yes	High
38	UK	Heather; Ninian Structure	North Viking Graben	Paul and Mitra, 2015	Yes	High
39	Morocco		Anti-Atlas Basin	Robert-Charrue and Burkhard, 2008	Yes	Low
40	Nigeria		Maiduguri Basin	Avbovbo et al., 1986	Yes	Mid
41	US	Central Transform Fault	Guaymas Basin	Lonsdale and Lawver, 1980	Yes	High
42	US	Robinson's Bend Coalbed; Taylor Creek	Black Warrior Basin	Groshong et al., 2010	Yes	High
43	UK		Inner Moray Firth	Lapadat et al., 2016; http://www.seismicatlas.org/uploaded/image/ 200802/ e1d2ebbb-18d7	Yes	High

				-4f9f-a677-7511d521e 7aa.jpg		
44	Greece	Western Corinth Canal	Isthmia Graben	Sletten, 2016	No	High
45	Denmark	Coffee-Soil Fault	Tail-End Graben	Duffy et al., 2013	Yes	High
46	Greece	Milos Fault Zone	Southern Aegian Sea	Angelier, 1979	Yes	Mid
47	Greece	Karpathos Fault Zone	Southern Aegian Sea	Angelier, 1979	Yes	Mid
48	Greece	Samos Fault Zone	Southern Aegian Sea	Angelier, 1979	Yes	Mid
49	Argentina	Tres Cruces	Salta Rift	Monaldi et al., 2008	Yes	Mid
50	US	Slaughter Canyon	Permian Basin	Kosa et al., 2005	Yes	High
51	Bulgaria	Emine Fault System	Burgas Basin	Doglioni et al., 1996	Yes	High
52	Ethiopia	Fantale Magmatic System	Ethiopian Rift	Trippanera et al., 2015	Yes	High
53	Ethiopia	Manda Hararo Rift	Ethiopian Rift	Trippanera et al., 2015	Yes	High
54	Iceland	Eldgjá	Erdja Fissure Swarm	Trippanera et al., 2015	Yes	High
55	Iceland	Sveinar-Sveinagja	Sveinar Graben	Trippanera et al., 2015	Yes	High
56	Faroe Islands		Faroe-Shetland Basin	Walker et al., 2012; Walker et al., 2013	Yes	High

References for Appendix B

ANGELIER, J. 1979. Recent quaternary tectonics in the hellenic arc: Examples of geological observations on land. Tectonophysics, 52, 267-275.

AVBOVBO, A., AYOOLA, E. & OSAHON, G. 1986. Depositional and structural styles in Chad Basin of Northeastern Nigeria. AAPG Bulletin, 70, 1787-1798.

BADLEY, M. E., PRICE, J. D. & BACKSHALL, L. C. 1989. Inversion, reactivated faults and related structures: seismic examples from the southern North Sea. Geological Society, London, Special Publications, 44, 201-219.

BAUDON, C. & CARTWRIGHT, J. 2008a. Early stage evolution of growth faults: 3D seismic insights from the Levant Basin, Eastern Mediterranean. Journal of Structural Geology, 30, 888-898.

BAUDON, C. & CARTWRIGHT, J. 2008b. The kinematics of reactivation of normal faults using high resolution throw mapping. Journal of Structural Geology, 30, 1072-1084.

BAUDON, C. & CARTWRIGHT, J. A. 2008c. 3D seismic characterisation of an array of blind normal faults in the Levant Basin, Eastern Mediterranean. Journal of Structural Geology, 30, 746-760.

BELL, R. E., JACKSON, C. A. L., ELLIOTT, G. M., GAWTHORPE, R. L., SHARP, I. R. & MICHELSEN, L. 2014. Insights into the development of major rift-related unconformities from geologically constrained subsidence modelling: Halten Terrace, offshore mid Norway. Basin Research, 26, 203-224.

BLAKESLEE, M. W. & KATTENHORN, S. A. 2013. Revised earthquake hazard of the Hat Creek fault, northern California: A case example of a normal fault dissecting variable-age basaltic lavas. Geosphere, 9, 1397-1409.

BUBECK, A., WALKER, R. J., IMBER, J., and MACLEOD, C. J., 2018, Normal fault growth in layered basaltic rocks: The role of strain rate in fault evolution. Journal of Structural Geology, 115, 103-120.

CARTWRIGHT, J. & MANSFIELD, C. 1998. Lateral displacement variation and lateral tip geometry of normal faults in the Canyonlands National Park, Utah. Journal of Structural Geology, 20, 3-19.

CHU, S.-S., LIN, M.-L., HUANG, W.-C., NIEN, W.-T., LIU, H.-C. & CHAN, P.-C. 2015. Simulation of growth normal fault sandbox tests using the 2D discrete element method. Computers & Geosciences, 74, 1-12.

CONNEALLY, J., CHILDS, C. & NICOL, A. 2017. Monocline formation during growth of segmented faults in the Taranaki Basin, offshore New Zealand. Tectonophysics, 721, 310-321.

CORFIELD, S. & SHARP, I. 2000. Structural style and stratigraphic architecture of fault propagation folding in extensional settings: a seismic example from the Smørbukk area, Halten Terrace, Mid-Norway. Basin Research, 12, 329-341.

DUFFY, O. B., GAWTHORPE, R. L., DOCHERTY, M. & BROCKLEHURST, S. H. 2013. Mobile evaporite controls on the structural style and evolution of rift basins: Danish Central Graben, North Sea. Basin Research, 25, 310-330.

DOGLIONI, C., BUSATTA, C., BOLIS, G., MARIANNA, L. & ZANELLA, M. 1996. Structural evolution of the eastern Balkans. Marine and Petroleum Geology, 13, 225 – 251.

FÆRSETH, R. B. & LIEN, T. 2002. Cretaceous evolution in the Norwegian Sea—a period characterized by tectonic quiescence. Marine and Petroleum Geology, 19, 1005-1027.

FERRILL, D. A., MORRIS, A. P. & MCGINNIS, R. N. 2012. Extensional fault-propagation folding in mechanically layered rocks: The case against the frictional drag mechanism. Tectonophysics, 576-577, 78-85.

FERRILL, D. A., MORRIS, A. P., MCGINNIS, R. N., SMART, K. J. & WARD, W. C. 2011. Fault zone deformation and displacement partitioning in mechanically layered carbonates: The Hidden Valley fault, central Texas. AAPG Bulletin, 95, 1383-1397.

FINCH, E., HARDY, S. & GAWTHORPE, R. 2004. Discrete-element modelling of extensional fault-propagation folding above rigid basement fault blocks. Basin Research, 16, 467-488.

FODOR, L., TURKI, S., DALUB, H. & AL GERBI, A. 2005. Fault-related folds and along-dip segmentation of breaching faults: syn-diagenetic deformation in the south-western Sirt basin, Libya. Terra Nova, 17, 121-128.

GARFUNKEL, Z. & BARTOV, Y. 1977. The tectonics of the Suez rift, Bull. Geol. Surv. Isr.

GHALAYINI, R., HOMBERG, C., DANIEL, J. M. & NADER, F. H. 2016. Growth of layer-bound normal faults under a regional anisotropic stress field. Geological Society, London, Special Publications, 439.

GRANT, J. V. & KATTENHORN, S. A. 2004. Evolution of vertical faults at an extensional plate boundary, southwest Iceland. Journal of Structural Geology, 26, 537-557.

GROSHONG, R. H., HAWKINS, W. B., PASHIN, J. C. & HARRY, D. L. 2010. Extensional structures of the Alabama promontory and Black Warrior foreland Basin: Styles and relationship to the Appalachian fold-thrust belt. Geological Society of America Memoirs, 206, 579-605.

HANCOCK, P. L. & BARKA, A. A. 1987. Kinematic indicators on active normal faults in Western Turkey. Journal of Structural Geology, 9, 573-584.

HARDY, S. 2013. Propagation of blind normal faults to the surface in basaltic sequences: Insights from 2D discrete element modelling. Marine and Petroleum Geology, 48, 149-159.

HARDY, S., 2018, Coupling a frictional-cohesive cover and a viscous substrate in a discrete element model: First results of application to thick- and thin-skinned extensional tectonics. Marine and Petroleum Geology, 97, 32-44.

JACKSON, C. A. L., GAWTHORPE, R. L. & SHARP, I. R. 2006. Style and sequence of deformation during extensional fault-propagation folding: examples from the Hammam Faraun and El-Qaa fault blocks, Suez Rift, Egypt. Journal of Structural Geology, 28, 519-535.

JACKSON, C. A. L., CORFIELD, S. & DREYER, T. 2017. Temporal evolution of extensional fault-propagation folds. EarthArXiv. Doi: 10.31223/osf.io/v9p8e.

KAVEN, J. O. & MARTEL, S. J. 2007. Growth of surface-breaching normal faults as a three-dimensional fracturing process. Journal of Structural Geology, 29, 1463-1476.

KHALIL, S. & MCCLAY, K. 2002. Extensional fault-related folding, northwestern Red Sea, Egypt. Journal of Structural Geology, 24, 743-762.

KHALIL, S. M. & MCCLAY, K. R. 2016. 3D geometry and kinematic evolution of extensional fault-related folds, NW Red Sea, Egypt. Geological Society, London, Special Publications, 439, 1-11.

KNOX, G. 1982. Taranaki Basin, structural style and tectonic setting. New Zealand journal of geology and geophysics, 25, 125-140.

KOSA, E. & HUNT, D. 2005. Growth of syndepositional faults in carbonate strata: Upper Permian Capitan platform, New Mexico, USA.

LAFUENTE, P., ARLEGUI, L., LIESA, C. & SIMÓN, J. 2011. Paleoseismological analysis of an intraplate extensional structure: the Concud fault (Iberian Chain, eastern Spain). International Journal of Earth Sciences, 100, 1713-1732.

LĂPĂDAT, A., IMBER, J., YIELDING, G., IACOPINI, D., MCCAFFREY, K. J. W., LONG, J. J. & JONES, R. R. 2016. Occurrence and development of folding related to normal faulting within a mechanically heterogeneous sedimentary sequence: a case study from Inner Moray Firth, UK. Geological Society, London, Special Publications, 439.

LONSDALE, P. & LAWVER, L. 1980. Immature plate boundary zones studied with a submersible in the Gulf of California. Geological Society of America Bulletin, 91, 555-569.

MARTEL, S. J. & LANGLEY, J. S. 2006. Propagation of normal faults to the surface in basalt, Koae fault system, Hawaii. Journal of Structural Geology, 28, 2123-2143.

MATMON, A., KATZ, O., SHAAR, R., RON, H., PORAT, N. & AGNON, A. 2010. Timing of relay ramp growth and normal fault linkage, Upper Galilee, northern Israel. Tectonics, 29, 2, 1-13.

MCLEOD, A. E., DAWERS, N. H. & UNDERHILL, J. R. 2000. The propagation and linkage of normal faults: insights from the Strathspey–Brent–Statfjord fault array, northern North Sea. Basin Research, 12, 263-284.

MITRA, S. 1993. Geometry and kinematic evolution of inversion structures. AAPG Bulletin, 77, 1159-1191.

MOUSTAFA, A. R. 1993. Structural characteristics and tectonic evolution of the east-margin blocks of the Suez rift. Tectonophysics, 223, 381-399.

NDONGO, A., GUIRAUD, M., VENNIN, E., MBINA, M., BUONCRISTIANI, J.-F., THOMAZO, C. & FLOTTÉ, N. 2016. Control of fluid-pressure on early deformation structures in the Paleoproterozoic extensional Franceville Basin (SE Gabon). Precambrian Research, 277, 1-25.

OLSEN, P. E., KENT, D. V., CORNET, B., WITTE, W. K. & SCHLISCHE, R. W. 1996. High-resolution stratigraphy of the Newark rift basin (early Mesozoic, eastern North America). Geological Society of America Bulletin, 108, 40-77.

OMOSANYA, K. D. O. & ALVES, T. M. 2014. Mass-transport deposits controlling fault propagation, reactivation and structural decoupling on continental margins (Espírito Santo Basin, SE Brazil). Tectonophysics, 628, 158-171.

PAUL, D. & MITRA, S. 2015. Fault patterns associated with extensional fault-propagation folding. Marine and Petroleum Geology, 67, 120-143.

PHILLIPS, T. B., JACKSON, C. A., BELL, R. E. & DUFFY, O. B. 2018. Oblique reactivation of lithosphere-scale lineaments controls rift physiography–the upper-crustal expression of the Sorgenfrei–Tornquist Zone, offshore southern Norway. Solid Earth, 9, 403.

PODOLSKY, D. M. & ROBERTS, G. P. 2008. Growth of the volcano-flank Koa’e fault system, Hawaii. Journal of Structural Geology, 30, 1254-1263.

ROBERT-CHARRUE, C. & BURKHARD, M. 2008. Inversion tectonics, interference pattern and extensional fault-related folding in the Eastern Anti-Atlas, Morocco. Swiss Journal of Geosciences, 101, 397-408.

SCHLISCHE, R. W. 1992. Structural and stratigraphic development of the Newark extensional basin, eastern North America: Evidence for the growth of the basin and its bounding structures. Geological Society of America Bulletin, 104, 1246-1263.

SHARP, I., GAWTHORPE, R., ARMSTRONG, B. & UNDERHILL, J. 2000a. Propagation history and passive rotation of mesoscale normal faults: implications for synrift stratigraphic development. Basin Research, 12, 285-305.

SHARP, I. R., GAWTHORPE, R. L., UNDERHILL, J. R. & GUPTA, S. 2000b. Fault-propagation folding in extensional settings: Examples of structural style and synrift sedimentary response from the Suez rift, Sinai, Egypt. Geological Society of America Bulletin, 112, 1877-1899.

SLETTEN, S. H. 2016. Normal fault growth and fault zone architecture of normal faults exposed in the Corinth Canal, central Greece. MSc thesis, University of Bergen. Available at http://bora.uib.no/handle/1956/12783.

SKUCE, A. G. 1996. Forward modelling of compaction above normal faults: an example from the Sirte Basin, Libya. Geological Society, London, Special Publications, 99, 135-146.

SMART, K. J., and FERRILL, D. A., 2018, Discrete element modeling of extensional fault-related monocline formation. Journal of Structural Geology, 115, 82-90.

TRIPPANERA, D., ACOCELLA, V., RUCH, J., and ABEBE, B., 2015, Fault and graben growth along active magmatic divergent plate boundaries in Iceland and Ethiopia. Tectonics, 34, 11, 2318-2348.

VAN GENT, H. W., HOLLAND, M., URAI, J. L. & LOOSVELD, R. 2010. Evolution of fault zones in carbonates with mechanical stratigraphy – Insights from scale models using layered cohesive powder. Journal of Structural Geology, 32, 1375-1391.

VITA-FINZI, C. & KING, G. 1985. The seismicity, geomorphology and structural evolution of the Corinth area of Greece. Philosophical Transactions of the Royal Society of London A: Mathematical, Physical and Engineering Sciences, 314, 379-407.

WALKER, R. J., HOLDSWORTH, R. E., IMBER, J., and ELLIS, D., 2012, Fault-zone evolution in layered basalt sequences: A case study from the Faroe Islands, NE Atlantic margin. Geological Society of America Bulletin, 124, 7-8, 1382-1393.

WALKER, R., HOLDSWORTH, R., IMBER, J., FAULKNER, D., and ARMITAGE, P., 2013, Fault zone architecture and fluid flow in interlayered basaltic volcaniclastic-crystalline sequences. Journal of Structural Geology, 51, 92-104.

WALSH, J. J. & WATTERSON, J. 1987. Distributions of cumulative displacement and seismic slip on a single normal fault surface. Journal of Structural Geology, 9, 1039-1046.

WILLSEY, S. P., UMHOEFER, P. J. & HILLEY, G. E. 2002. Early evolution of an extensional monocline by a propagating normal fault: 3D analysis from combined field study and numerical modeling. Journal of Structural Geology, 24, 651-669.

Appendix C - Forced fold locations

Locality	Country	Fault System	Basin	Reference(s)	Published	Confidence
1	Norway	Revfallet	Halten Terrace	Dooley et al., 2003; Dooley et al., 2005; Pascoe et al., 1999; Faerseth and Lien, 2002; Gabrielsen et al., 1999; Grunnaleite and Gabrielsen, 1995	Yes	High
2	Norway	Bremstein	Halten Terrace	Wilson et al., 2013; Wilson et al., 2015; Coleman et al. 2017; Faerseth and Lien, 2002; Gabrielsen et al., 1999; Grunnaleite and Gabrielsen, 1995	Yes	High
3	France	Illfurth	Dannemarie Basin, Rhine Graben	Ford et al., 2007; Maurin and Niviere, 1999	Yes	High
4	Norway	Stavanger	Egersund Basin	Jackson and Lewis, 2016	Yes	High
5	Norway	Sele High	Egersund Basin	Lewis et al., 2013	Yes	High
6	UK	Dowsing Fault Zone	Sole Pit Trough	Coward and Stewart, 1995	Yes	High
7	Belguim	Southern Roer Valley	Roer Valley, Rhine Graben	Deckers, 2015; Deckers et al., 2014	Yes	High
8	US	Jackpot - Tamurian Block	Basin and Range	Howard and John, 1997	Yes	High
9	UK	Buchan Graben	Buchan Graben	Stewart and Clark, 1999; Stewart, 2014	Yes	High
10	Egypt	Ramadan Oil Field	Gulf of Suez	Brown, 1980; Abdine et al., 1992; Withjack et al., 2000	Yes	High
11	Denmark	Horn Graben	Horn Graben	Stewart and Clark, 1999	Yes	High
12	UK	Wright-Bray	Channel Basin	Harvey and Stewart, 1998	Yes	High

13	Canada	Creignish; Hollow Fault	Maritimes Basin	Keller and Lynch, 1999; Lynch et al., 1998	Yes	High
14	Spain	Ubierna; Saltacaballos	Basque-Cantabrian Basin	Tavani et al., 2018; Tavani et al., 2011; 2013; Tavani and Granado, 2014; Quintana et al., 2006	Yes	High
15	Israel	Ma'aleh Gerofit	Central Dead Sea Rift	Gross et al., 1997	Yes	High
16	US	Balcones	Gulf of Mexico Basin	Ferrill et al., 2012; Ferrill and Morris, 2008	Yes	High
17	US	Balcones	Gulf of Mexico Basin	Ferrill and Morris, 2008	Yes	High
18	US	Big Brushy Canyon	Big Brushy Canyon	Ferrill et al., 2007	Yes	High
19	Norway	Nordkapp Basin	Nordkapp Basin	Nilsen et al., 1995; Koyi et al., 1993; Koyi et al., 1995; Gudlaugson et al., 1998	Yes	High
20	UK	Keys Graben	Keys Graben	Jackson and Mulholland, 1993; Stewart et al., 1997; Penge et al., 1999	Yes	High
21	Denmark	East North Sea High	Norwegian-Danish Basin	Geil, 1991; Petersen et al., 1992; Stewart et al., 1996	Yes	High
22	Norway	Sleipner Basin	South Viking Graben	Kane et al., 2010	Yes	High
23	UK	Fisher Bank Basin	Fisher Bank Basin	Penge et al., 1999	Yes	High
24	UK	Forties-Montrose High	Forties-Montrose High	Penge et al., 1999	Yes	High
25	UK	East Deemster Graben	East Deemster Graben	Penge et al., 1999	Yes	High
26	UK	Dowsing Fault Zone	Swarte Bank Hinge	Stewart and Coward, 1995; Stewart et al., 1996	Yes	High

27	UK	Machar and Median Diapirs	East Central Trough	Stewart et al., 1996	Yes	High
28	UK	Cleaver Bank High	Cleaver Bank High	Oudmayer and de Jager, 1992	Yes	High
29	Denmark	Hyllebjerg Basin	Hyllebjerg Basin	Koyi and Petersen, 1993	Yes	High
30	Denmark	RÃ¸ddung Graben	RÃ¸ddung Graben	Koyi and Petersen, 1993	Yes	High
31	UK	Lagman Fault	Lagman Basin	Jackson and Mulholland, 1993	Yes	High
32	UK	Tynwald Fault	Tynwald Basin	Jackson and Mulholland, 1993	Yes	High
33	Denmark	Coffee-Soil Fault	Tail-End Graben	Duffy et al., 2013	Yes	High
34	Portugal		Northern Lusitanian Basin	Alves et al., 2002; Alves et al., 2003	Yes	High
35	Portugal	Arruda subbasin and Bombarral-Alcobaca subbasin	Central Lusitanian Basin	Alves et al., 2002; Alves et al., 2003	Yes	High
36	Canada		Whale Basin	Balkwill and Legall, 1987; Vendeville et al., 1995; Withjack and Callaway, 2000	Yes	High
37	Canada		Jeanne D'Arc Basin	Sinclair, 1995; Withjack and Callaway, 2000; Serano-Saurez et al., 2013	Yes	High
38	Portugal	Porto Basin	Porto Basin	Alves et al., 2006	Yes	High
39	Portugal	Alentejo Basin	Alentejo Basin	Alves et al., 2006	Yes	High
40	Spain	Zarate Fault	Lasarte Basin	Bodego and Agirrezabala, 2013	Yes	High
41	France	Aquitaine Basin	Aquitaine Basin	Bourrouilh et al., 1995	Yes	High

42	France	Parentis Basin	Parentis Basin	Ferrer et al., 2012; Ferrer et al., 2014	Yes	High
43	Ukraine		Dniepr-Donets Basin	Stovba and Stephenson, 2002; Brown et al., 2012	Yes	Low
44	Poland		Mid Polish Trough	Burliga et al., 2012; Krzywiec, 2010; Lamarche and Scheck-Wenderoth, 2005	Yes	High
45	Canada		Orpheus Basin	Durcanin et al., 2009; Zulfitriadi et al., 2011; Hanafi et al., 2013	No	High
46	Norway		Haapet Dome		No	High
47	Canada		Sverdrup Basin	Harrison and Jackson, 2014	Yes	Low
48	Morocco		Essaquira Basin	Tari et al., 2000; Tari et al., 2013	Yes	Low
49	Morocco		Agadir Basin	Tari et al., 2000; Tari et al., 2013	Yes	Low
50	Morocco		Safi Basin	Tari et al., 2000; Tari et al., 2013	Yes	Low
51	Israel	Sedom Fault	Southern Dead Sea Rift	Smit et al., 2008	Yes	High
52	Spain		Ebro Basin	Salas and Casas, 1993; Alvaro et al., 1979	Yes	Low
53	Canada		Carson Basin	Enachescu, 1992.	Yes	Low
54	Italy		Po Basin	Cardello et al., 2015	Yes	High
55	Norway		Feda Graben	Ge et al., 2016	Yes	High
56	Norway		Steinbit Terrace	Ge et al., 2016	Yes	High
57	Norway		Breiflabb Graben	Ge et al., 2016	Yes	High
58	Norway		Cod Terrace	Ge et al., 2016	Yes	High
59	UK		Josephine High	Ge et al., 2016; Vendeville et al., 1995	Yes	High
60	Norway		Sorvestlandet High	Ge et al., 2016; Stewart et al., 1992; Vendeville et al., 1995	Yes	High
61	Norway		Hidra High	Ge et al., 2016	Yes	High

62	Poland		Lower Silesian Basin	Mejia-Herrera et al., 2015	Yes	Mid
63	Italy		Radicondoli Radicondoli Basin	Brogi and Liotta, 2008	Yes	Low
64	Czech Republic		Most Basin	Rajchl and Uličný, 2001; 2008; Rajchl et al., 2009	Yes	High
65	Spain	Gargallo Fault	Maestrazgo Basin	Rodriguez-Lopez et al., 2007	Yes	High
66	France	Rhenish Fault	Soult-sous-Forets Area	Place et al., 2010	Yes	High
67	US	Moab Fault Splay	Paradox Basin	Berg and Skar, 2005	Yes	High
68	Iran		Southern Salt Basin	Perotti et al., 2016	Yes	Low
69	UK	Beatrice Fault System	Inner Moray Firth	Lapadat et al., 2016	Yes	High
70	Norway		Hammerfest Basin	Gabrielsen et al., 2016	Yes	High
71	Israel		Levant Basin	Reiche et al., 2014	Yes	Low
72	Russia		Pripyat Basin	Garetskii et al., 2004	Yes	High
73	Saudi Arabia		Rub' Al-Khali Basin	Stewart et al., 2016	Yes	Low
74	US		Rattlesnake Mountain	Stearns, 1978; Weinberg, 1979	Yes	High
75	Norway	Fjerritslev Fault System	Farsund Basin	Phillips et al., 2018	No	High
76	Ireland		Central Ireland Carboniferous Basin	Lewis and Couples, 1999	Yes	Low
77	US		Uinta Mountains	Stearns, 1978	Yes	High
78	US		West Powder River Basin	Sacrison, 1978; Stearns, 1978	Yes	High
79	US		Brady Structure	Sacrison, 1978	Yes	High

80	US		Carter Lake Anticline	Matthews and Work, 1978	Yes	Low
81	US		Bellview Dome	Matthews and Work, 1978	Yes	Mid
82	US		Milner Mountain Anticline	Matthews and Work, 1978	Yes	Mid
83	US		Dowe Pass Anticline	Matthews and Work, 1978	Yes	Mid
84	US	Horn Fault; Tensleep-Beaver Creek Fault	Horn Block	Palmquist, 1978	Yes	Mid
85	US		Piney Creek	Palmquist, 1978	Yes	Low
86	US		Fanny Peak Monocline	Lisenbee, 1978	Yes	Low
87	US		Rapid City Structure	Lisenbee, 1978	Yes	Low
88			Rockerville Quadrangle Area	Lisenbee, 1978	Yes	Low
89	US		Cascade Springs Anticline	Lisenbee, 1978	Yes	Mid
90	US		Stockade Beaver Creek Monocline	Lisenbee, 1978	Yes	Mid
91	US		Red Rock Fold	Cook, 1978	Yes	Low
92	Italy	Zuccale Fault	Elba Basin	Smith et al., 2007	Yes	High
93	Spain		Prebetic Basin	Rubinat et al., 2013	Yes	High
94	France	St Benoit Fault	Annot Basin	Tomasso and Sinclair, 2004	Yes	Mid
95	Borneo		East Barito Fordeep	Satyana and Silitonga, 1994	Yes	Mid
96	New Zealand		Taupo Volcanic Zone	Milner et al., 2002	Yes	Low

97	Germany		Gluckstadt Graben	Best et al., 1983; Warsitzka et al., 2017	Yes	Mid
98	Denmark		Step Graben	Remmelts, 1995	Yes	High
99	Denmark	Rifgronden Fault Zone	Terschelling Basin	Remmelts, 1995	Yes	Low
100	UK		West Central Graben	Weston et al., 1993; Hossack, 1995	Yes	High
101	Morocco		Essaouira Basin	Hafid et al., 2000	Yes	Mid
102	Mexico	Rincon de Parangueo Maar	Rincon de Parangueo	Aranda-Gomez et al., 2017	Yes	High
103	Tanzania	Lokichar	Usangu Basin	Morley, 2002	Yes	High

References for Appendix C

ABDINE, A. S., MESHREF, W., SHAHIN, A. N., GAROSSINO, P. & SHAZLY, S. 1992. Ramadan Field--Egypt Gulf of Suez Basin.

ALVARO, M., CAPOTE, R. & VEGAS, R. 1979. Un modelo de evolución geotectónica para la Cadena Celtibérica. Acta Geológica Hispánica, 14, 172-177.

ALVES, T. M., GAWTHORPE, R. L., HUNT, D. W. & MONTEIRO, J. H. 2002. Jurassic tectono-sedimentary evolution of the Northern Lusitanian Basin (offshore Portugal). Marine and Petroleum Geology, 19, 727-754.

ALVES, T. M., MANUPPELLA, G., GAWTHORPE, R. L., HUNT, D. W. & MONTEIRO, J. H. 2003. The depositional evolution of diapir- and fault-bounded rift basins: examples from the Lusitanian Basin of West Iberia. Sedimentary Geology, 162, 273-303.

ALVES, T. M., MOITA, C., SANDNES, F., CUNHA, T., MONTEIRO, J. H. & PINHEIRO, L. M. 2006. Mesozoic–Cenozoic evolution of North Atlantic continental-slope basins: The Peniche basin, western Iberian margin. AAPG bulletin, 90, 31-60.

ARANDA-GÓMEZ, J. J., CERCA, M., ROCHA-TREVIÑO, L., CARRERA-HERNÁNDEZ, J. J., LEVRESSE, G., PACHECO, J., YUTSIS, V., ARZATE-FLORES, J. A., CHACÓN, E. & BERALDI-CAMPESI, H. 2017. Structural evidence of enhanced active subsidence at the bottom of a maar: Rincón de Parangueo, México. Geological Society, London, Special Publications, 446, 225-254.

BALKWILL, H. & LEGALL, F. 1989. Whale Basin, Offshore Newfoundland: Extension and Salt Diapirism: Chapter 15: North American Margins.

BEST, G., KOCKEL, F. & SCHÖNEICH, H. 1983. Geological history of the southern Horn Graben. Petroleum Geology of the Southeastern North Sea and the Adjacent Onshore Areas in: Kaasschieter, J. P. H., and Reijers, T. J. A., eds., Petroleum geology of the southeastern North Sea and the adjacent onshore areas, Geol. Mijnbouw 62, 25-33.

BODEGO, A. & AGIRREZABALA, L. M. 2013. Syn-depositional thin- and thick-skinned extensional tectonics in the mid-Cretaceous Lasarte sub-basin, western Pyrenees. Basin Research, 25, 594-612.

BOURROUILH, R., RICHERT, J.-P. & ZOLNAI, G. 1995. The north Pyrenean Aquitaine basin, France: evolution and hydrocarbons. AAPG Bulletin, 79, 831-853.

BROGI, A. & LIOTTA, D. 2008. Highly extended terrains, lateral segmentation of the substratum, and basin development: The middle-late Miocene Radicondoli Basin (inner northern Apennines, Italy). Tectonics, 27, n/a-n/a.

BROWN, J., BOWYER, M. & ZOLOTARENKO, V. 2012. Wedges and buffers: some new structural observations from the Dnieper–Donets Basin, onshore Ukraine. Geological Society, London, Special Publications, 363, 431-448.

BROWN, R. N. 1980. History of exploration and discovery of Morgan, Ramadan and July oilfields, Gulf of Suez, Egypt.

BROWN, W. G. 1988. Deformational style of Laramide uplifts in the Wyoming foreland. Interaction of the Rocky Mountain foreland and the Cordilleran thrust belt: Geological Society of America Memoir, 171, 1-25.

BURLIGA, S., KOYI, H. A. & CHEMIA, Z. 2012. Analogue and numerical modelling of salt supply to a diapiric structure rising above an active basement fault. Geological Society, London, Special Publications, 363, 395-408.

CARDELLO, G. L. & DOGLIONI, C. 2015. From Mesozoic rifting to Apennine orogeny: The Gran Sasso range (Italy). Gondwana Research, 27, 1307-1334.

COLEMAN, A. J., JACKSON, C. A. L. & DUFFY, O. B. 2017. Balancing sub- and supra-salt strain in salt-influenced rifts: Implications for extension estimates. Journal of Structural Geology, 102, 208-225.

COOK, R. A. 1978. A relationship between strike-slip faults and the process of drape folding of layered rocks. Laramide folding associated with basement block faulting in the western United States, ed. Vincent Matthews III. GSA Memoir, 197-214.

COWARD, M. & STEWART, S. 1995. Salt-influenced structures in the Mesozoic-Tertiary cover of the southern North Sea, UK, In: Jackson, M.P.A., Roberts, D.G., Snelson, S., eds., Salt Tectonics: A Global Perspective, AAPG Memoir, 65, 229-250.

DECKERS, J. 2015. Decoupled extensional faulting and forced folding in the southern part of the Roer Valley Graben, Belgium. Journal of Structural Geology, 81, 125-134.

DECKERS, J., BROOTHAERS, M., LAGROU, D. & MATTHIJS, J. 2014. The late Maastrichtian to Late Paleocene tectonic evolution of the southern part of the Roer Valley Graben (Belgium). Netherlands Journal of Geosciences, 93, 83-93.

DOOLEY, T., MCCLAY, K. & PASCOE, R. 2003. 3D analogue models of variable displacement extensional faults: applications to the Revfallet Fault system, offshore mid-Norway. Geological Society, London, Special Publications, 212, 151-167.

DOOLEY, T., MCCLAY, K. R., HEMPTON, M. & SMIT, D. 2005. Salt tectonics above complex basement extensional fault systems: results from analogue modelling. Geological Society, London, Petroleum Geology Conference series, 6, 1631-1648.

DURCANIN, M. A. 2009. Influence of synrift salt on rift-basin development. MSc Thesis. Rutgers University. doi:10.7282/T39P31T3.

FÆRSETH, R. B. & LIEN, T. 2002. Cretaceous evolution in the Norwegian Sea—a period characterized by tectonic quiescence. Marine and Petroleum Geology, 19, 1005-1027.

FERRILL, D. A. & MORRIS, A. P. 2008. Fault zone deformation controlled by carbonate mechanical stratigraphy, Balcones fault system, Texas. AAPG bulletin, 92, 359-380.

FERRILL, D. A., MORRIS, A. P. & MCGINNIS, R. N. 2012. Extensional fault-propagation folding in mechanically layered rocks: The case against the frictional drag mechanism. Tectonophysics, 576-577, 78-85.

FERRILL, D. A., MORRIS, A. P. & SMART, K. J. 2007. Stratigraphic control on extensional fault propagation folding: Big Brushy Canyon monocline, Sierra Del Carmen, Texas. Geological Society, London, Special Publications, 292, 203-217.

FORD, M., LE CARLIER DE VESLUD, C. & BOURGEOIS, O. 2007. Kinematic and geometric analysis of fault-related folds in a rift setting: The Dannemarie basin, Upper Rhine Graben, France. Journal of Structural Geology, 29, 1811-1830.

GABRIELSEN, R. H., ODINSEN, T. & GRUNNALEITE, I. 1999. Structuring of the Northern Viking Graben and the Møre Basin; the influence of basement structural grain, and the particular role of the Møre-Trøndelag Fault Complex. Marine and Petroleum Geology, 16, 443-465.

GABRIELSEN, R. H., SOKOUTIS, D., WILLINGSHOFER, E. & FALEIDE, J. I. 2016. Fault linkage across weak layers during extension: an experimental approach with reference to the Hoop Fault Complex of the SW Barents Sea. Petroleum Geoscience.

GARETSKII, R., AISBERG, R. & STARCHIK, T. 2004. Pripyat Trough: Tectonics, geodynamics, and evolution. Russian Journal of Earth Sciences, 6, 217-250.

GE, Z., GAWTHORPE, R. L., ROTEVATN, A. & THOMAS, M. B. 2016. Impact of normal faulting and pre-rift salt tectonics on the structural style of salt-influenced rifts: The Late Jurassic Norwegian Central Graben, North Sea. Basin Research, n/a-n/a.

GEIL, K. 1991. The development of salt structures in Denmark and adjacent areas: the role of basin floor dip and differential pressure. First Break, 9, 467-483.

GROSS, M. R., BECKER, A. & GUTIÉRREZ-ALONSO, G. 1997. Transfer of displacement from multiple slip zones to a major detachment in an extensional regime: Example from the Dead Sea rift, Israel. Geological Society of America Bulletin, 109, 1021-1035.

GRUNNALEITE, I. & GABRIELSEN, R. H. 1995. Structure of the Møre basin, mid-Norway continental margin. Tectonophysics, 252, 221-251.

GUDLAUGSSON, S. T., FALEIDE, J. I., JOHANSEN, S. E. & BREIVIK, A. J. 1998. Late Palaeozoic structural development of the South-western Barents Sea. Marine and Petroleum Geology, 15, 73-102.

HAFID, M. 2000. Triassic–early Liassic extensional systems and their Tertiary inversion, Essaouira Basin (Morocco). Marine and Petroleum Geology, 17, 409-429.

HANAFI, B. R. 2013. The influence of basin architecture and synrift salt on structural evolution during and after rifting. MSc Thesis. Rutgers University. doi:10.7282/T37943C2.

HARRISON, J. C. & JACKSON, M. P. A. 2014. Exposed evaporite diapirs and minibasins above a canopy in central Sverdrup Basin, Axel Heiberg Island, Arctic Canada. Basin Research, 26, 567-596.

HOWARD, K. A. & JOHN, B. E. 1997. Fault-related folding during extension: Plunging basement-cored folds in the Basin and Range. Geology, 25, 223-226.

JACKSON, C. A. L. & LEWIS, M. M. 2016. Structural style and evolution of a salt-influenced rift basin margin; the impact of variations in salt composition and the role of polyphase extension. Basin Research, 28, 81-102.

JACKSON, D. I. & MULHOLLAND, P. 1993. Tectonic and stratigraphic aspects of the East Irish Sea Basin and adjacent areas: contrasts in their post-Carboniferous structural styles. Geological Society, London, Petroleum Geology Conference series, 4, 791-808.

KANE, K. E., JACKSON, C. A. L. & LARSEN, E. 2010. Normal fault growth and fault-related folding in a salt-influenced rift basin: South Viking Graben, offshore Norway. Journal of Structural Geology, 32, 490-506.

KOYI, H. & PETERSEN, K. 1993. Influence of basement faults on the development of salt structures in the Danish Basin. Marine and Petroleum Geology, 10, 82-94.

KOYI, H., TALBOT, C. J. & TORUDBAKKEN, B. 1995. Analogue models of salt diapirs and seismic interpretation in the Nordkapp Basin, Norway. Petroleum geoscience, 1, 185-192.

KOYI, H., TALBOT, C. J. & TØRUDBAKKEN, B. O. 1993. Salt diapirs of the southwest Nordkapp Basin: analogue modelling. Tectonophysics, 228, 167-187.

KRZYWIEC, P. 2010. Triassic evolution of the Kłodawa salt structure: basement-controlled salt tectonics within the Mid-Polish Trough (Central Poland). 2010, 48, 12.

LAMARCHE, J. & SCHECK-WENDEROTH, M. 2005. 3D structural model of the Polish Basin. Tectonophysics, 397, 73-91.

LĂPĂDAT, A., IMBER, J., YIELDING, G., IACOPINI, D., MCCAFFREY, K. J. W., LONG, J. J. & JONES, R. R. 2016. Occurrence and development of folding related to normal faulting within a mechanically heterogeneous sedimentary sequence: a case study from Inner Moray Firth, UK. Geological Society, London, Special Publications, 439.

LEWIS, H. & COUPLES, G. D. 1999. Carboniferous basin evolution of central Ireland — simulation of structural controls on mineralization. Geological Society, London, Special Publications, 155, 277-302.

LEWIS, M. M., JACKSON, C. A. L. & GAWTHORPE, R. L. 2013. Salt-influenced normal fault growth and forced folding: The Stavanger Fault System, North Sea. Journal of Structural Geology, 54, 156-173.

LISENBEE, A. L. 1978. Laramide structure of the Black Hills uplift, South Dakota-Wyoming-Montana. In: MATTHEWS, I. I. I. V. (ed.) Laramide Folding Associated with Basement Block Faulting in the Western United States. Geological Society of America.

MATTHEWS III, V. & WORK, D. F. 1978. Laramide folding associated with basement block faulting along the northeastern flank of the Front Range, Colorado. Laramide folding associated with basement block faulting in the western United States: Geological Society of America Memoir, 151, 101-124.

MAURIN, J. C. & NIVIERE, B. 1999. Extensional forced folding and decollement of the pre-rift series along the Rhine graben and their influence on the geometry of the syn-rift sequences. Geological Society, London, Special Publications, 169, 73-86.

MEJÍA-HERRERA, P., ROYER, J.-J., CAUMON, G. & CHEILLETZ, A. 2015. Curvature Attribute from Surface-Restoration as Predictor Variable in Kupferschiefer Copper Potentials. Natural Resources Research, 24, 275-290.

MILNER, D., COLE, J. & WOOD, C. 2002. Asymmetric, multiple-block collapse at Rotorua Caldera, Taupo Volcanic Zone, New Zealand. Bulletin of Volcanology, 64, 134-149.

MORLEY, C. K. 2002. Evolution of large normal faults: Evidence from seismic reflection data. AAPG bulletin, 86, 961-978.

NILSEN, K. T., VENDEVILLE, B. C. & JOHANSEN, J.-T. 1995. Influence of regional tectonics on halokinesis in the Nordkapp Basin, Barents Sea.

OUDMAYER, B. C. & DE JAGER, J. 1993. Fault reactivation and oblique-slip in the Southern North Sea. Geological Society, London, Petroleum Geology Conference series, 4, 1281-1290.

PALMQUIST, J. C. 1978. Laramide structures and basement block faulting: Two examples from the Big Horn Mountains, Wyoming. In: MATTHEWS, I. I. I. V. (ed.) Laramide Folding Associated with Basement Block Faulting in the Western United States. Geological Society of America.

PASCOE, R., HOOPER, R., STORHAUG, K. & HARPER, H. 1999. Evolution of extensional styles at the southern termination of the Nordland Ridge, Mid-Norway: a response to variations in coupling above Triassic salt. Petroleum Geology Conference Series, 5, 83-90.

PENGE, J., MUNNS, J. W., TAYLOR, B. & WINDLE, T. M. F. 1999. Rift–raft tectonics: examples of gravitational tectonics from the Zechstein basins of northwest Europe. Geological Society, London, Petroleum Geology Conference series, 5, 201-213.

PETERSEN, K., CLAUSEN, O. & KORSTGÅRD, J. 1992. Evolution of a salt-related listric growth fault near the D-1 well, block 5605, Danish North Sea: displacement history and salt kinematics. Journal of Structural Geology, 14, 565-577.

PHILLIPS, T. B., JACKSON, C. A., BELL, R. E. & DUFFY, O. B. 2018. Oblique reactivation of lithosphere-scale lineaments controls rift physiography–the upper-crustal expression of the Sorgenfrei–Tornquist Zone, offshore southern Norway. Solid Earth, 9, 403.

PLACE, J., DIRAISON, M., NAVILLE, C., GÉRAUD, Y., SCHAMING, M. & DEZAYES, C. 2010. Decoupling of deformation in the Upper Rhine Graben sediments. Seismic reflection and diffraction on 3-component Vertical Seismic Profiling (Soultz-sous-Forêts area). Comptes Rendus Geoscience, 342, 575-586.

QUINTANA, L., ALONSO, J. L., PULGAR, J. A. & RODRÍGUEZ-FERNÁNDEZ, L. R. 2006. Transpressional inversion in an extensional transfer zone (the Saltacaballos fault, northern Spain). Journal of Structural Geology, 28, 2038-2048.

RAJCHL, M. & ULIČNÝ, D. 2001. Response of a Fluvial Depositional System to Unequal Com-paction of Underlying Peat (Neogene, Most Basin, Czech Re-public). GeoLines, 13, 105.

RAJCHL, M., ULIČNÝ, D., GRYGAR, R. & MACH, K. 2009. Evolution of basin architecture in an incipient continental rift: the Cenozoic Most Basin, Eger Graben (Central Europe). Basin Research, 21, 269-294.

RAJCHL, M., ULIČNÝ, D. & MACH, K. 2008. Interplay between tectonics and compaction in a rift-margin, lacustrine delta system: Miocene of the Eger Graben, Czech Republic. Sedimentology, 55, 1419-1447.

REICHE, S., HÜBSCHER, C. & BEITZ, M. 2014. Fault-controlled evaporite deformation in the Levant Basin, Eastern Mediterranean. Marine Geology, 354, 53-68.

REMMELTS, G. 1995. Fault-related salt tectonics in the southern North Sea, the Netherlands.

RODRÍGUEZ-LÓPEZ, J. P., LIESA, C. L., MELÉNDEZ, N. & SORIA, A. R. 2007. Normal fault development in a sedimentary succession with multiple detachment levels: the Lower Cretaceous Oliete sub-basin, Eastern Spain. Basin Research, 19, 409-435.

RUBINAT, M., ROCA, E., ESCALAS, M., QUERALT, P., FERRER, O. & LEDO, J. 2013. The influence of basement structure on the evolution of the Bicorb-Quesa Diapir (eastern Betics, Iberian Peninsula): contractive thin-skinned deformation above a pre-existing extensional basement fault. International Journal of Earth Sciences, 102, 25-41.

SACRISON, W. 1978. Seismic interpretation of basement block. Laramide folding associated with basement block faulting in the western United States, 151, 39.

SALAS, R. & CASAS, A. 1993. Mesozoic extensional tectonics, stratigraphy and crustal evolution during the Alpine cycle of the eastern Iberian basin. Tectonophysics, 228, 33-55.

SATYANA, A. H. & SILITONGA, P. D. 1994. Tectonic reversal in East Barito Basin, South Kalimantan: consideration of the types of inversion structures and petroleum system significance. Proceedings of the Indonesian Petroleum Association, 23rd Annual Convention, 57-74.

SINCLAIR, I. K. 1995. Transpressional inversion due to episodic rotation of extensional stresses in Jeanne d'Arc Basin, offshore Newfoundland. Geological Society, London, Special Publications, 88, 249-271.

SMIT, J., BRUN, J. P., FORT, X., CLOETINGH, S. & BEN-AVRAHAM, Z. 2008. Salt tectonics in pull-apart basins with application to the Dead Sea Basin. Tectonophysics, 449, 1-16.

SMITH, S. A. F., HOLDSWORTH, R. E., COLLETTINI, C. & IMBER, J. 2007. Using footwall structures to constrain the evolution of low-angle normal faults. Journal of the Geological Society, 164, 1187-1191.

STEARNS, D. W. 1978. Faulting and forced folding in the Rocky Mountains foreland. Geological Society of America Memoirs, 151, 1-38.

STEWART, S. A. 2014. Detachment-controlled triangle zones in extension and inversion tectonics. Interpretation, 2, SM29-SM38.

STEWART, S. A. 2016. Structural geology of the Rub' Al-Khali Basin, Saudi Arabia. Tectonics, 35, 2417-2438.

STEWART, S. A. & CLARK, J. A. 1999. Impact of salt on the structure of the Central North Sea hydrocarbon fairways. Geological Society, London, Petroleum Geology Conference Series, 5, 179-200.

STEWART, S. A. & COWARD, M. P. 1995. Synthesis of salt tectonics in the southern North Sea, UK. Marine and Petroleum Geology, 12, 457-475.

STEWART, S. A., HARVEY, M. J., OTTO, S. C. & WESTON, P. J. 1996. Influence of salt on fault geometry: examples from the UK salt basins. Geological Society, London, Special Publications, 100, 175-202.

STEWART, S. A., RUFFELL, A. H. & HARVEY, M. J. 1997. Relationship between basement-linked and gravity-driven fault systems in the UKCS salt basins. Marine and Petroleum Geology, 14, 581-604.

STOVBA, S. M. & STEPHENSON, R. A. 2002. Style and timing of salt tectonics in the Dniepr-Donets Basin (Ukraine): implications for triggering and driving mechanisms of salt movement in sedimentary basins. Marine and Petroleum Geology, 19, 1169-1189.

SERANO-SUAREZ, B. E. 2013. Evolution of the Jeanne d’Arc basin, offshore Newfoundland, Canada. MSc Thesis. Rutgers University. doi:10.7282/T3V123DK.

TARI, G. & JABOUR, H. 2013. Salt tectonics along the Atlantic margin of Morocco. Geological Society, London, Special Publications, 369, 337-353.

TARI, G., MOLNAR, J., ASHTON, P. & HEDLEY, R. 2000. Salt tectonics in the Atlantic margin of Morocco. The Leading Edge, 19, 1074-1078.

TAVANI, S., BALSAMO, F. & GRANADO, P. 2018. Petroleum system in supra-salt strata of extensional forced-folds: A case-study from the Basque-Cantabrian basin (Spain). Marine and Petroleum Geology, 96, 315–330.

TAVANI, S., CAROLA, E., GRANADO, P., QUINTÀ, A. & MUÑOZ, J. A. 2013. Transpressive inversion of a Mesozoic extensional forced fold system with an intermediate décollement level in the Basque-Cantabrian Basin (Spain). Tectonics, 32, 146-158.

TAVANI, S. & GRANADO, P. 2014. Along-strike evolution of folding, stretching and breaching of supra-salt strata in the Plataforma Burgalesa extensional forced fold system (northern Spain). Basin Research, 1-13.

TAVANI, S., QUINTÀ, A. & GRANADO, P. 2011. Cenozoic right-lateral wrench tectonics in the Western Pyrenees (Spain): The Ubierna Fault System. Tectonophysics, 509, 238-253.

TOMASSO, M. & SINCLAIR, H. D. 2004. Deep-water sedimentation on an evolving fault-block: the Braux and St Benoit outcrops of the Gres d'Annot. Geological Society, London, Special Publications, 221, 267-283.

VENDEVILLE, B. C., GE, H. & JACKSON, M. P. A. 1995. Scale models of salt tectonics during basement-involved extension. Petroleum Geoscience, 1, 179-183.

WARSITZKA, M., KLEY, J., JÄHNE-KLINGBERG, F. & KUKOWSKI, N. 2017. Dynamics of prolonged salt movement in the Glückstadt Graben (NW Germany) driven by tectonic and sedimentary processes. International Journal of Earth Sciences, 106, 131-155.

WEINBERG, D. M. 1979. Experimental folding of rocks under confining pressure: Part VII. Partially scaled models of drape folds. Tectonophysics, 54, 1-24.

WILSON, P., ELLIOTT, G. M., GAWTHORPE, R. L., JACKSON, C. A.-L., MICHELSEN, L. & SHARP, I. R. 2013. Geometry and segmentation of an evaporite-detached normal fault array: 3D seismic analysis of the southern Bremstein Fault Complex, offshore mid-Norway. Journal of Structural Geology, 51, 74-91.

WILSON, P., ELLIOTT, G. M., GAWTHORPE, R. L., JACKSON, C. A., MICHELSEN, L. & SHARP, I. R. 2015. Lateral variation in structural style along an evaporite-influenced rift fault system in the Halten Terrace, Norway: Influence of basement structure and evaporite facies. Journal of Structural Geology, 79, 110-123.

WITHJACK, M. O. & CALLAWAY, S. 2000. Active normal faulting beneath a salt layer: an experimental study of deformation patterns in the cover sequence. AAPG bulletin, 84, 627-651.

ZULFITRIADI, Z. 2011. The Mesozoic Orpheus rift basin, offshore Nova Scotia and Newfoundland, Canada. MSc Thesis. Rutgers University. doi:10.7282/T3WD404M.

Appendix D – Fault-propagation fold database

Fault-propagation fold database may be downloaded here:

https://figshare.com/s/c6663901f6ca8c6f6fe4

Appendix E – Forced fold database

Forced fold database may be downloaded here:

https://figshare.com/s/c6663901f6ca8c6f6fe4

Appendix F – Uncertainties

This study measures growth fold parameters (Fig. 2) from a series of published examples in nature, physical, mechanical and kinematic models. Here, we illustrate using a series of examples how growth fold parameters were measured and their associated errors. As all of the errors are relatively minimal and the data points would still plot in similar locations (for example, on Figs. 11 – 12; 21), the general relationships/trends would remain largely the same. Changes in the measured values would inevitably shift the best-fit regressions and alter the derived parametric equations, but the trends would remain the same. References for each example are also shown.

Parameter	Values
Amplitude	10 - 13 mm
Width	96 - 100 mm
Prekinematic	40 - 41 mm
Fault throw	10 - 11 mm
Fault dip	45°
FSF	7 - 10

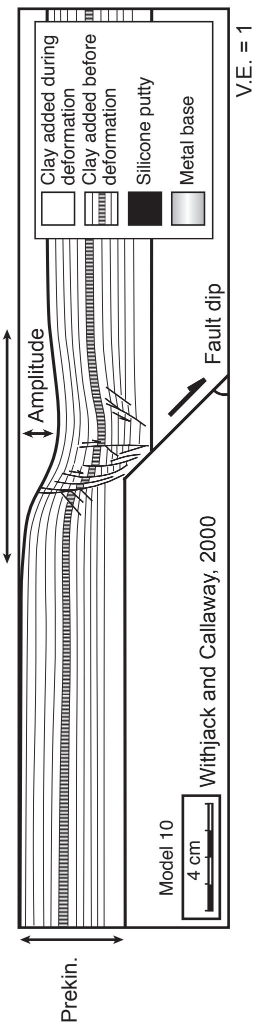

Parameter	Values
Amplitude	9 - 11 mm
Width	117 - 133 mm
Prekinematic	38 - 40 mm
Fault throw	9 - 11 mm
Fault dip	45°
FSF	11 - 15
Detachment	9 - 12 mm
C:D	3 - 4

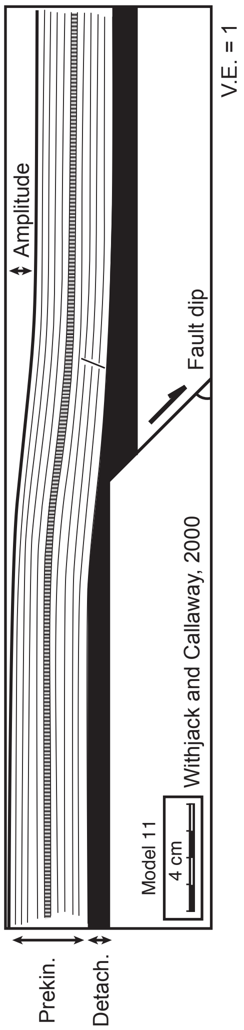

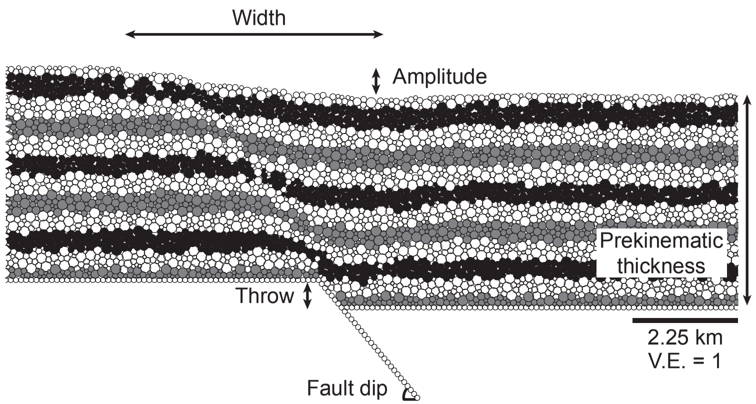

Parameter	Values
Amplitude	0.6 - 0.65 km
Width	7.6 - 7.8 km
Prekinematic	5.4 - 5.5 km
Fault throw	0.6 - 0.65 km
Fault dip	50°
FSF	11.6 - 13

Mechanical model of a fault-propagation fold from Finch et al., 2004.

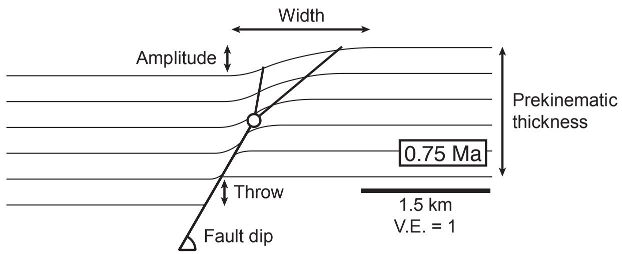

Parameter	Values
Amplitude	0.55 - 0.6 km
Width	1.4 - 1.55 km
Prekinematic	1.49 - 1.5 km
Fault throw	0.55 - 0.6 km
Fault dip	60°
FSF	2.3 - 2.8

Trishear fault-propagation fold from Hardy and McClay, 1999

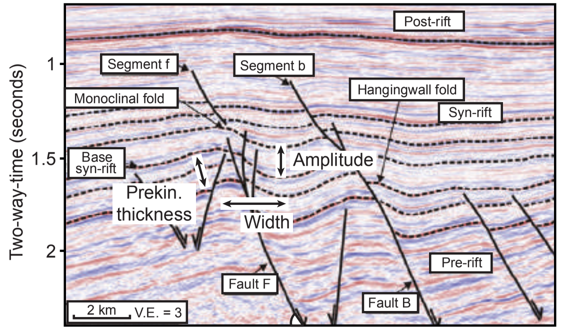

Parameter	Values
Amplitude	0.3 - 0.4 km
Width	2 - 2.1 km
Prekinematic	0.4 - mm
Fault throw	0.4 - 0.6 km
Fault dip	42 - 45°
FSF	5 - 7

FPF above Fault F from Lapadat et al., 2016

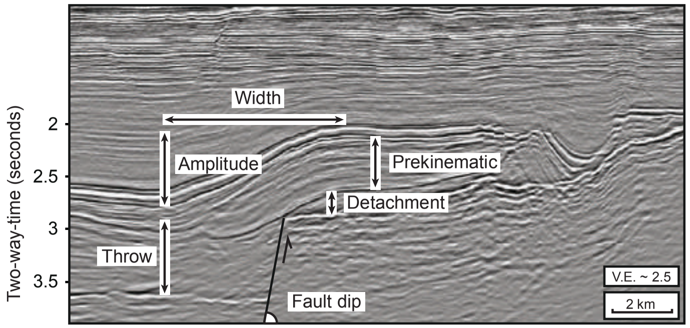

Parameter	Values
Amplitude	0.9 - 1 km
Width	5.5 - 5.6 km
Prekinematic	0.5 - 0.7 km
Fault throw	1.2 - 1.25 km
Fault dip	66 - 68°
FSF	5.5 - 6.2
Detachment	0.3 - 0.36 km
C:D	1.4 - 2.3

Forced fold from Lewis et al., 2013 using velocity of 2.8 km/s from Jackson and Lewis, 2012

Appendix G - Principal Component Analysis (PCA) Explanation

To demonstrate how PCA works we first consider the following scenario: envision a multi-variate dataset consisting of three measured variables (or 'dimensions'), x, y and z. If the x- and y- variables are plotted, we can see that they are highly correlated (Fig. G.1A). PCA allows us to represent these data along a best-fit, single axis (PC1 - the black line on Fig. G.1A), termed a 'principal component' (PC). This principal axis explains the largest data variation and permits the simplification of two-dimensional data i.e., the x- and y- variables, in this case, to one dimension. By reducing the data to fewer dimensions, the relationship between the x- and y- variables can no longer be explicitly calculated (as in linear regression) but the relationships between the variables are maintained. In other words, when we plot the original data against the principal component, the data is spread along the length of the axis (Fig. G.1B). This suggests that the x- and y- variables are highly correlated, and the principal component explains a large proportion of the data variation, as shown in Fig. G.1A.

Given that we also have a third variable, z, we cannot explain all of the data variance with a single principal component, additional principal components may be calculated to explain further data variance (PC2 - grey line on Fig. G.1A). Each successive principal component introduced into the analysis explains a successively smaller portion of the data (data variance is larger on Fig. G.1B than Fig. G.1C) and is geometrically orthogonal to the others (e.g. Wold et al., 1987; Jolliffe, 1993; Ringner, 2008; Abdi and Williams, 2010; Lever et al., 2017), but together, these principal components cumulatively explain the data variance. The number of principal components can be as large as the number of samples or the number of components. As PC1 and PC2 explain the majority of the data variance, we may project the original data (consisting of the x-, y- and z- values) and their trends onto new axes, comprised of the principle components (black arrows on Fig. G.1D). If particular variables are correlated, they will plot close to one-another. It should be noted that the sign of any principal component, i.e. the direction of the arrows on Fig. G.1D, is completely arbitrary (e.g. Jolliffe, 1987). In our example case, the x- and y- variables plot very close to one-another and the PC1 axis, so are strongly correlated. The z-variable in contrast, is correlated with the PC2 axis, but is also relatively close to the y-variable. We can therefore interpret that the x- and z-variables are both correlated to y variable (Fig. G.1C), and there may be a reason for their correlation, such as the x- and z- variables control the y-variable. Furthermore, principal components identify major trends in highly-dimensional data and the correlated variables. If a data point only has missing values for particular variables i.e. the data point has an x-, and y- value but not a z-value, the position of the principal components that explains the most data variation may slightly change. Furthermore, the original data may be projected slightly differently.

The PCA method described above can also be applied to our growth fold dataset. However, instead of three variables (e.g. x, y and z), we have more variables or dimensions (e.g. fault dip, fault throw, fold amplitude, fold width etc.). Following the same method, we can thus, determine which parameters are correlated and speculate a geological reasoning for the relationship. Where missing values for particular parameters are missing (i.e. data gaps), then a best-fit, iterative value is used to fill in the record (as discussed in Appendix H). A full description of the PCA method is described in Josse and Husson (2016).

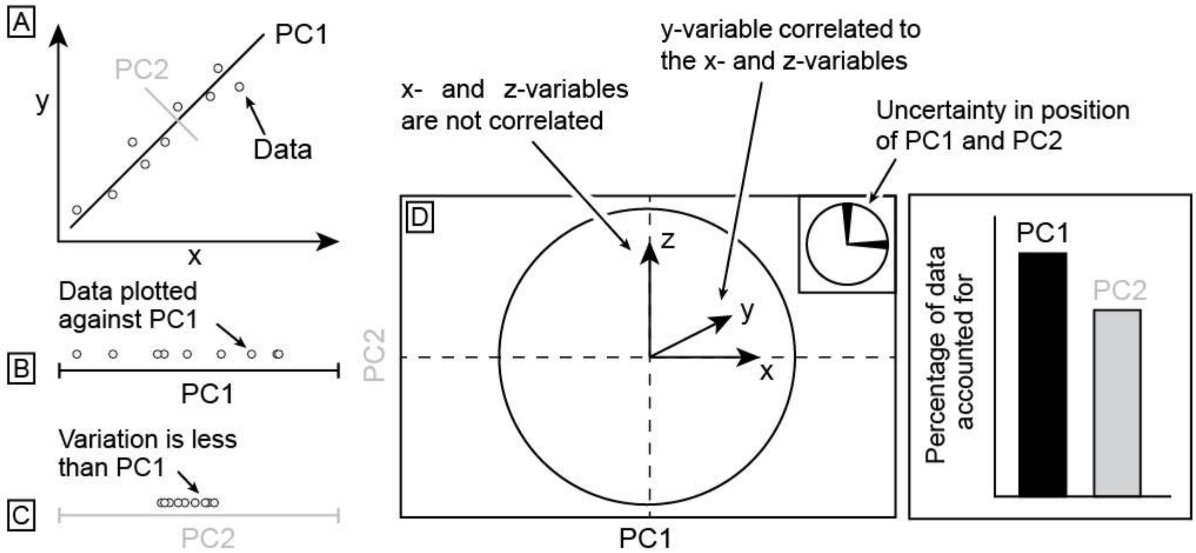

Figure G.1. – Summary of principal component analysis (PCA) method using example data with x-,y- and z-variables. The x-variable is plotted against the y-variable for the example data (A). The most and second-most data variation is described by PC1 and PC2, respectively. By projecting the data onto two new axes, PC1 (B) and PC2 (C), the data can be analysed for clustering and hidden trends. The x-, y- and z-variables are then plotted to see which variables are likely related (D). Where values are missing in the dataset, uncertainty is introduced in the analysis hence the trend and position of PC1 and PC2 (on panel A) may shift. PC1 and PC2 each account a certain amount of the data as shown in the bar chart.

References for Appendix G

ABDI, H. and WILLIAMS, L. J. 2010. Principal component analysis. Wiley interdisciplinary reviews: computational statistics, 2, 433-459.

JOLLIFFE, I. T. 1990. PRINCIPAL COMPONENT ANALYSIS: A BEGINNER'S GUIDE — I. Introduction and application. Weather, 45, 375-382.

JOLLIFFE, I. T. 1993. Principal component analysis: A beginner's guide — II. Pitfalls, myths and extensions. Weather, 48, 246-253.

JOLLIFFE, I. T. 2002. Principal component analysis, New York, Springer.

LEVER, J., KRZYWINSKI, M. and ALTMAN, N. 2017. Points of significance: Principal component analysis. Nature Publishing Group.

RINGNÉR, M. 2008. What is principal component analysis? Nature Biotechnology, 26, 303.

WOLD, S., ESBENSEN, K. and GELADI, P. 1987. Principal component analysis. Chemometrics and Intelligent Laboratory Systems, 2, 37-52.

Appendix H - Principal component analysis sensitivity

Principal component analysis (PCA) simplifies the complexity of high-dimensional multi-variate data, such as our growth fold dataset (Appendices D – E), while retaining trends and patterns (e.g. Jolliffe, 1993; Jolliffe, 2002; Lever et al., 2002). This allows us to identify possible relationships between parameters which are non-linear or very complex.
In an ideal scenario, all structural and stratigraphic parameters (cf. Fig. 2 in the main text) may be measured but this may not be possible in all cases. Therefore, the best-fit position of each principal component (PC) may vary, and an uncertainty is introduced. We explore this uncertainty using two examples: (i) a numerical model, and (ii) a real example from our growth fold database.

Example 1 – Numerical trishear forward model

To quantitatively investigate the effect of missing parameters within individual examples, we used FaultFold (Allmendinger, 1998) to generate a series of 2D trishear forward models for fault-propagation folds with different structural and stratigraphic parameter variations. As the initial parameters are known, and the fold geometry can be measured, none of the forward models are missing any values and there is no uncertainty in the PCA analysis – '*Dataset 1*', 491 records, each with 5 parameters. We then randomly removed 20% of the values (any parameter from any record) to reflect a dataset with missing values – '*Dataset 2*'. We then undertook PCA on *Dataset 2* with the missing values to see how uncertainty affected the strength, and thus, the interpretation of the PCA using three methods (Fig. H.1; cf. Josse and Husson, 2012; Josse et al., 2012; Audiger et al., 2016; Josse and Husson, 2016):

1) Ignore incomplete records (and reduce the sample size);
2) Replace missing values in individual records with the mean value for an appropriate parameter (sample size remains the same);
3) Replace missing values in individual records using a regularised iterative value for the appropriate parameter (sample size remains the same).

We can see that regardless of the PCA method used on *Dataset 2*, the correlations (the directions of the arrows and the relative positions of arrows) are very similar. In this example, we see a correlation between the prekinematic thickness, the total slip, the fold amplitude and to a lesser extent, the fold width. In addition, we see a correlation between the fold-shape-factor (FSF) and the fault dip, and to a lesser extent, the fold width. The PCA for *Dataset 2* (with missing values) is almost identical to *Dataset 1* (without missing values), suggesting PCA may be used even on incomplete datasets, at least with caution.

It is important to mention that these examples are similar sized, thus, replacing a data gap with a mean value has a negligible effect on the correlation. If the sample contained lots of different sized folds, the replaced variable may be unrealistic and a magnitude larger or smaller. Similarly, removing the record completely (and all of the other parameters, even if only one value is missing), may significantly reduce the sample size, making the dataset susceptible to extremes. An iterative approach tackles both of these issues, giving a parameter that is not out of character with the rest of the record values, and does not remove the record from the sample. This is our preferred method for PCA, but we include the uncertainty associated with the missing value so that correlations can be qualitatively checked in all cases.

Example 2 – Natural examples of fault-propagation folds

Now applying the same sensitivity test to the dataset of natural examples of fault-propagation folds (cf. Appendix D) that already contains missing values. We may compare the results of PCA using the same three methods (Fig. H.2; cf. Josse and Husson, 2012; Josse et al., 2012; Audiger et al., 2016; Josse and Husson, 2016):

1) Ignore incomplete records (and reduce the sample size);
2) Replace missing values in individual records with the mean value for an appropriate parameter (sample size remains the same);
3) Replace missing values in individual records using a regularised iterative value for the appropriate parameter (sample size remains the same).

Similar to Example 1, the PCA results for Example 2 are largely similar irrespective of the method. Our results show there is a correlation between the amplitude and width of the fold, the fault throw and the thickness of the prekinematic cover. The fold-shape-factor is seemingly uncorrelated to the other variables. However, we do see slight changes in the direction of the arrows. In order to not drastically reduce the number of sample records in our analysis, missing values have been replaced using iteration (method 3).

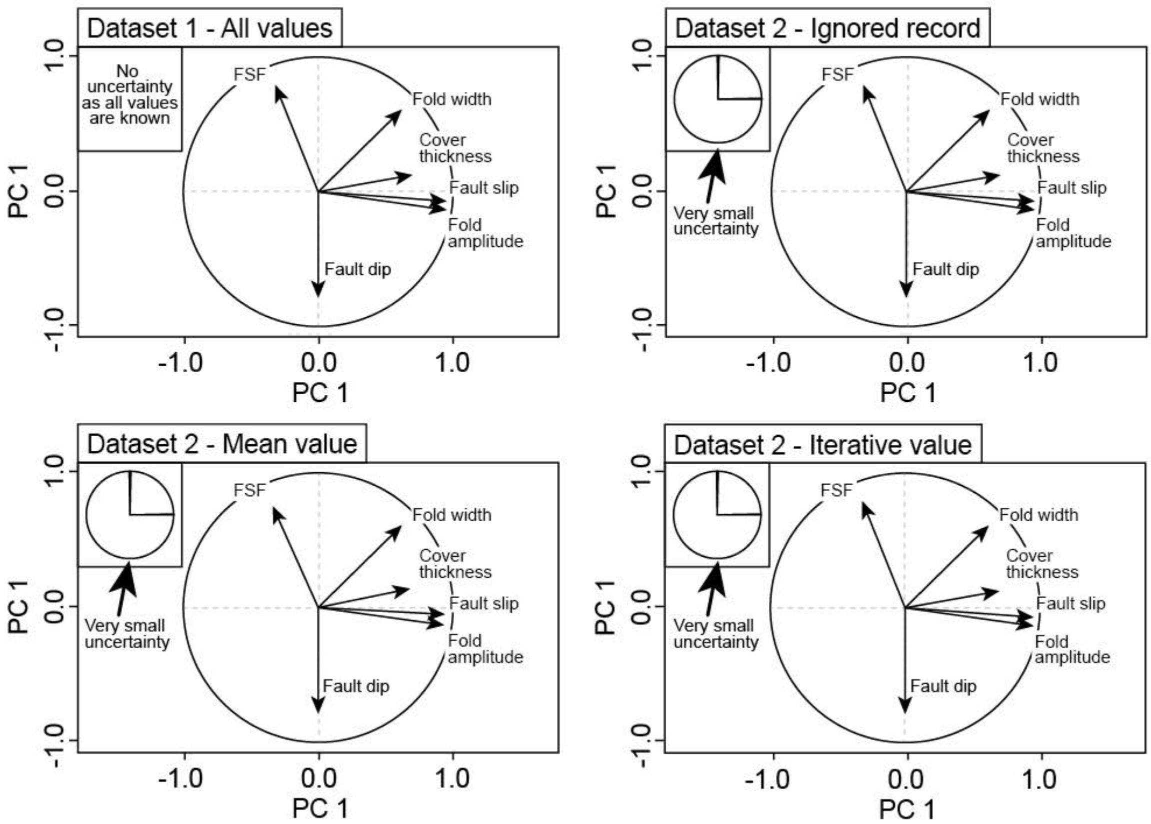

Figure H.1. – Summary of principal component analysis (PCA) sensitivity for the trishear forward model dataset. Top left – Dataset 1 (without missing values). Top right – Dataset 2 (with missing values), where records with missing values are ignored. Bottom left - Dataset 2 (with missing values), where records with missing values for a particular variable are replaced with the mean value for that variable of the entire data. Bottom right - Dataset 2 (with missing values), where records with missing values for a particular variable are replaced with a regularized iterative value for that variable in that record.

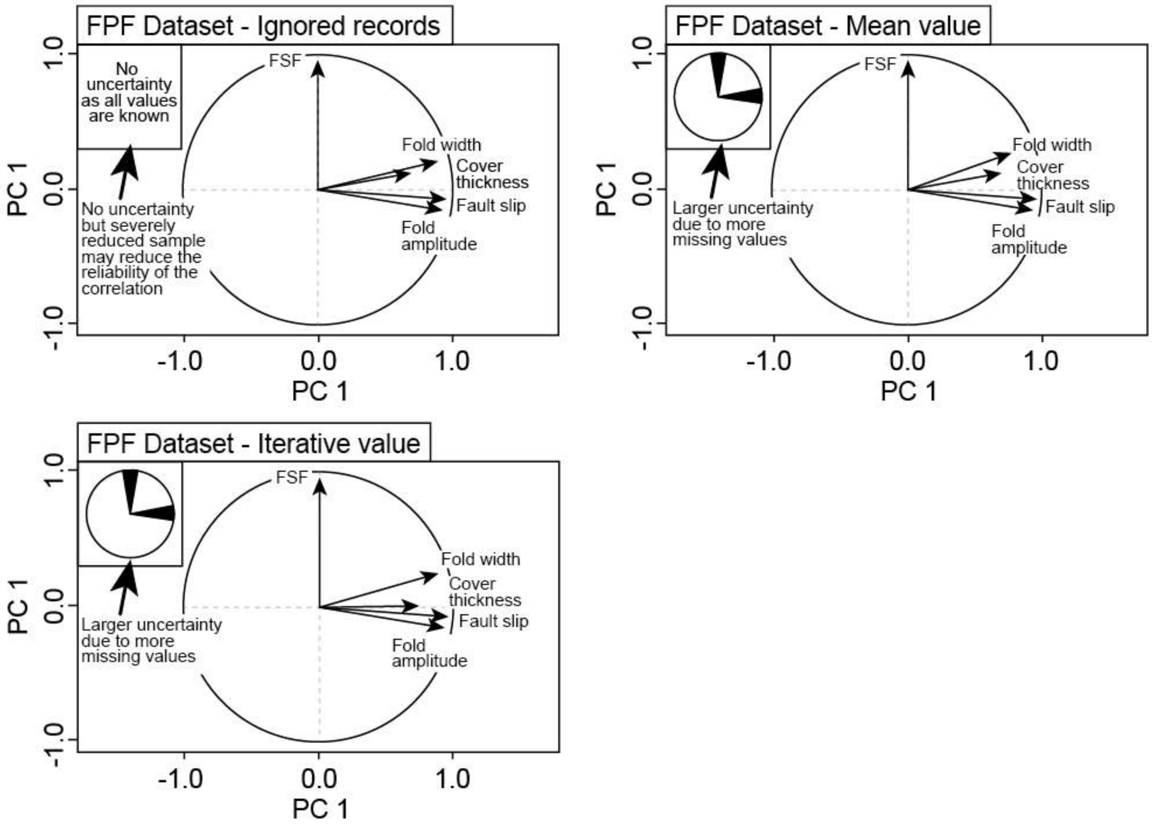

Figure H.2. – Summary of principal component analysis (PCA) sensitivity for the fault-propagation fold dataset of natural examples. Top left – Original dataset of real examples (with missing values). Top right – Dataset 2, where missing values are replaced by the mean value for that particular parameter. Bottom left - Dataset 2 where missing values replaced with a regularized iterative value for that variable in that record.

References for Appendix H

ALLMENDINGER, R. W. 1998. Inverse and forward numerical modeling of trishear fault-propagation folds. Tectonics, 17, 640-656.

AUDIGIER, V., HUSSON, F. and JOSSE, J. 2016. A principal component method to impute missing values for mixed data. Advances in Data Analysis and Classification, 10, 5-26.

JOLLIFFE, I. T. 1993. Principal component analysis: A beginner's guide — II. Pitfalls, myths and extensions. Weather, 48, 246-253.

JOLLIFFE, I. T. 2002. Principal component analysis, New York, Springer.

JOSSE, J., CHAVENT, M., LIQUET, B. and HUSSON, F. 2012. Handling missing values with regularized iterative multiple correspondence analysis. Journal of classification, 29, 91-116.

JOSSE, J. and HUSSON, F. 2012. Selecting the number of components in principal component analysis using cross-validation approximations. Computational Statistics and Data Analysis, 56, 1869-1879.

JOSSE, J. and HUSSON, F. 2016. missMDA: a package for handling missing values in multivariate data analysis. Journal of Statistical Software, 70, 1-31.

LEVER, J., KRZYWINSKI, M. and ALTMAN, N. 2017. Points of significance: Principal component analysis. Nature Methods, 14, 641-642.